Nonlinear optical trapping of metallic nanoparticles

Zhu, Z.

DOI
10.4233/uuid:a3ec5690-8c78-4920-8c50-c986c09566a0

Publication date
2025

Document Version
Final published version

Citation (APA)
Zhu, Z. (2025). *Nonlinear optical trapping of metallic nanoparticles*. [Dissertation (TU Delft), Delft University of Technology]. https://doi.org/10.4233/uuid:a3ec5690-8c78-4920-8c50-c986c09566a0

Important note
To cite this publication, please use the final published version (if applicable).
Please check the document version above.

NONLINEAR OPTICAL TRAPPING OF METALLIC NANOPARTICLES

NONLINEAR OPTICAL TRAPPING OF METALLIC NANOPARTICLES

Dissertation

for the purpose of obtaining the degree of doctor
at Delft University of Technology
by the authority of the Rector Magnificus, prof. dr. ir. T.H.J.J. van der Hagen,
chair of the Board for Doctorates
to be defended publicly on
Wednesday, the 19th of March, 2025 at 12:30 o'clock

by

Zheng ZHU

Master in Optical Engineering,
China university of petroleum (east China), China
born in Shandong, China

This dissertation has been approved by the promoters.

Composition of the doctoral committee:

Rector Magnificus,	chairperson
Em. Prof. dr. H. P. Urbach,	Delft University of Technology, *promotor*
Prof. dr. X.C. Yuan,	Shenzhen University, China, *promotor*
Dr. A. J. L. Adam,	Delft University of Technology, *copromotor*
Independent members:	
Prof. dr. S. M. Witte,	Delft University of Technology
Dr. O. EI Gawhary,	Delft University of Technology
Prof. dr. K. Boller,	University of Twente
Dr. N. Bhattacharya,	Delft University of Technology
Reserve members:	
Prof. dr. S. Stallinga,	Delft University of Technology

Prof. dr. M. C. Jun and Prof. dr. Y. Q. Zhang of Shenzhen University have contributed greatly to the preparation of this dissertation.

Keywords: metallic nanoparticle, nonlinear optical force, nonlinear effect

Printed by: Ridderprint

Front & Back: The design features the **Taichi** symbol on both cover pages, embodying the Daoist principle of 'one generates two,' where the dual forces of **Yin** and **Yang** emerge from the 'Supreme Origin.' This thesis also discusses the "one generates two" problem but in optics. We will describe how an original optical potential well can give rise to two separate wells through the emergence of opposing forces.

ISBN 978-94-6522-072-7 An electronic version of this dissertation is available at http://repository.tudelft.nl/.

Dedicated to my parents, Anqi, and all others who supported me.

CONTENTS

ACRONYM

SP Surface Plasmon

SA Saturable absorption

RSA Reverse Saturable Absorption

STED Stimulated Emission Depletion

SAM Spin Angular Momentum

OAM Orbital Angular Momentum

NA Numerical Aperture

MG Maxwell-Garnett

HSA Human Serum Albumin

LSPR Localized Surface Plasmon Resonance

NP Nano-Particle

SUMMARY

Optical trapping of metallic nanoparticles has diverse applications because metallic nanoparticles have unique properties. One significant advantage is that the optical force exerted on metallic nanoparticles is considerably larger than that on dielectric nanoparticles of the same size and shape. This results in a significantly deeper optical potential well compared to the optical trapping of dielectric nanoparticles.

In this thesis, our central objective is to delve into the underlying physical mechanisms behind an exceptional and enhanced optical trapping phenomenon that is referred to as"nonlinear optical trapping". To achieve this, we extensively investigated the third-order nonlinear effects that come into play in this intriguing optical trapping behavior. This investigation aimed to shed light on the underlying principles and mechanisms that enable the manipulation of nanoparticles beyond the diffraction limit, opening up exciting possibilities for various applications in nanotechnology and beyond.

First, we analytically calculated the time-averaged optical force exerted on a metallic nanoparticle using the dipole approximation theory. Besides the usual variables that had an influence on stable optical trapping, we considered the volume fraction of the samples in our simulation model. This study highlighted the critical role of the volume fraction of the sample for the stability of optical trapping of a gold nanoparticle in various solutions, including gold nanoparticle solutions, human serum albumin solutions, and HIV-1 virus solutions. Our calculations show that the optical force on the trapped gold nanoparticle weakens and the depth of the potential well reduces as the volume fraction of the corresponding sample increases. These results provide valuable insights for optimizing the stability of optical trapping in various applications.

In the subsequent exploration of the nonlinear regime, our research centered on uncovering the intricate nonlinear optical trapping of gold nanoparticles. During our investigation, it became increasingly clear that the conventional approach using the scalar polarizability of the nanoparticle, was insufficient for accurately depicting the optical response of the nanoparticle to the tightly focused external field. Consequently, we expanded upon the traditional scalar method, introducing a vectorial approach to better analyze the nonlinear optical forces at play. Upon comparing the outcomes of both the scalar and vectorial methods, we arrived at the conclusion that, particularly in scenarios involving nonlinear effects induced by tightly focused fields, the vectorial polarizability agrees more closely with experimental observations and results.

We have discussed changes in optical forces in the context of nonlinear optical trapping. However, the intricate interactions between the nonlinear optical effect and optical trapping are still unsolved. To address this issue, we have deeply investigated the saturable absorption effect on the gold nanoparticle caused by the circular-polarized femtosecond laser beam. Thus, based on the saturable absorption (SA) effect, the nonlinear refractive index of the gold nanoparticle and its extinction cross-sections were calculated as a function of the incident power. Furthermore, at higher peak power, the nonlinear

effect of gold nanoparticles changed from saturable absorption to reverse saturable absorption (RSA). The changes in the nonlinear absorption coefficient of the gold nanoparticle altered the nonlinear optical trapping in the SA and RSA regime. As a result of the SA effect, a distinct potential energy barrier forms within a circular energy ravined. During the initial phase of the RSA regime, the structure of the nonlinear optical potential remained consistent with that observed in the SA regime, but an interesting alteration occured in the deep RSA regime. A novel nonlinear optical trapping emerged in which gold nanoparticles are trapped at the center, encircled by the original circumgyrating nanoparticles. This experimental result confirmed our theoretical prediction proposed in our thesis.

The findings presented here contributed to bridging gaps in our knowledge of nonlinear optical trapping, thus enhancing our understanding of this phenomenon and providing a more comprehensive understanding of the underlying physical principles. This research also opened doors to further exploration of nonlinear metallic materials. Additionally, the discovery of novel nonlinear optical trapping effects had the potential to synergize with various structured light beams and other nonlinear materials, including quantum dots and nonlinear nanocrystals. We anticipated that these works can lead to the discovery of new trapping phenomena and their integration with other nanotechnologies, expanding the scope of nonlinear optical trapping and facilitating advancements in practical applications.

SAMENVATTING

Het optisch vangen van metalen nanopartikels heeft diverse toepassingen vanwege hun unieke eigenschappen. Een significant voordeel is dat de optische kracht uitgeoefend op gouden nanopartikels aanzienlijk groter is dan die op dielectric nanopartikels. Dit resulteert in een aanzienlijk diepere optische potentiaalput in vergelijking met de optische vangst van dielectric nanopartikels.

In deze thesis is ons centrale doel om de onderliggende fysische mechanismen achter een uitzonderlijk en verbeterd optisch vangstverschijnsel dat wordt aangeduid als "niet-lineaire optische vangst"te onderzoeken. Om dit te bereiken, onderzoeken we uitgebreid de niet-lineaire effecten van de derde orde die een rol spelen in dit intrigerende optische vangstgedrag. Via rigoureuze analyse en experiment is ons doel om de fundamentele principes en mechanismen te verduidelijken die de manipulatie van nanopartikels mogelijk maken buiten de beperkingen van de diffractiegrens. Dit onderzoek beoogt inzicht te verschaffen in de onderliggende principes en mechanismen die de manipulatie van nanopartikels mogelijk maken buiten de diffractiegrens, en opent spannende mogelijkheden voor diverse toepassingen in nanotechnologie en daarbuiten.

Eerst berekenen we analytisch de tijdgemiddelde optische kracht uitgeoefend op het metalen nanopartikel met behulp van de dipoolbenaderingstheorie. Naast de gebruikelijke variabelen die invloed hebben op stabiele optische vangst, hebben we aanvankelijk de volumefractie van de monsters in ons simulatiemodel overwogen. Dit onderzoek benadrukt de cruciale rol van de volumefractie van het monster in de stabiliteit van de optische vangst van een gouden nanopartikel in verschillende oplossingen, waaronder gouden nanopartikeloplossingen, menselijk serumalbumine-oplossingen en HIV-1-virusoplossingen. Onze berekeningen tonen aan dat de optische kracht op het gevangen gouden nanopartikel afneemt en de diepte van de potentiaalput afneemt naarmate de volumefractie van het overeenkomstige monster toeneemt. Deze resultaten bieden waardevolle inzichten voor het optimaliseren van de stabiliteit van optische vangst in diverse toepassingen.

In het daaropvolgende onderzoek naar het niet-lineaire regime concentreert ons onderzoek zich op het ontrafelen van de ingewikkelde niet-lineaire optische vangst van gouden nanopartikels. Tijdens ons onderzoek werd steeds duidelijker dat de conventionele benadering, die afhankelijk is van scalaire polariseerbaarheid, onvoldoende is om de optische respons van het nanopartikel op het sterk gefocuste externe veld nauwkeurig te beschrijven. Daarom hebben we de traditionele scalaire methode uitgebreid en een vectoriële benadering geïntroduceerd om de niet-lineaire optische krachten beter te analyseren. Door de resultaten van zowel de scalaire als de vectoriële methoden te vergelijken, zijn we tot de conclusie gekomen dat, met name in situaties met niet-lineaire effecten veroorzaakt door sterk gefocuste velden, de vectoriële polariseerbaarheid nauwer aansluit bij experimentele waarnemingen en resultaten.

We hebben de veranderingen in optische krachten besproken in het kader van niet-lineaire optische vangst. Echter, de complexe interacties tussen het niet-lineaire optische effect en optische vangst zijn nog gedeeltelijk onbekend. Om dit probleem aan te pakken, onderzoeken we diepgaand het verzadigbare absorptie-effect op het gouden nanopartikel gestimuleerd door de circulair-gepolariseerde femtoseconde laser. Daarom wordt op basis van het verzadigbare absorptie (SA) effect de niet-lineaire brekingsindex van het gouden nanopartikel en zijn doorsnede berekend als een functie van het ingestraalde vermogen. Bovendien verandert het niet-lineaire effect van gouden nanopartikels bij hoger piekvermogen van verzadigbare absorptie naar omgekeerde verzadigbare absorptie (RSA). De veranderingen in de niet-lineaire absorptiecoëfficiënt van het gouden nanopartikel veranderen de niet-lineaire optische vangst in de SA- en RSA-regio. Als gevolg van het SA-effect vormt zich een duidelijke potentiële energiebarrière binnen een cirkelvormige energiegeul. Tijdens de initiële fase van het RSA-regime blijft de structuur van het niet-lineaire optische potentiaal consistent met die waargenomen in het SA-regime, maar er treedt een interessante verandering op in het diepe RSA-regime. Een nieuw niet-lineaire optische vangsteffect ontstaat waarbij een gouden nanopartikel wordt gevangen in het midden, omringd door het oorspronkelijke cirkelvormige nanopartikel. Dit experimentele resultaat toont perfect de theoretische voorspelling die in onze thesis is voorgesteld.

De bevindingen die hier worden gepresenteerd dragen bij aan het overbruggen van lacunes in onze kennis van niet-lineaire optische vangst, waardoor ons begrip van dit fenomeen wordt verbeterd en een meer alomvattend begrip van de onderliggende fysische principes wordt geboden. Dit onderzoek opent ook de deuren naar verder onderzoek van niet-lineaire metalen materialen. Bovendien heeft de ontdekking van nieuwe niet-lineaire optische vangsteffecten het potentieel om te synergiseren met verschillende gestructureerde lichtbundels en andere niet-lineaire materialen, waaronder quantumdots en niet-lineaire nanokristallen. We verwachten dat dit zal leiden tot de ontdekking van nieuwe vangstfenomenen en hun integratie met andere nanotechnologieën, waardoor het bereik van niet-lineaire optische vangst wordt uitgebreid en vooruitgang in praktische toepassingen wordt vergemakkelijkt.

1

INTRODUCTION

"Well, this is my life's work. It has to do with radiation pressure, the pressure of light. I'm going to give you a little lecture. When light shines on you, it pushes on you. Everybody knows that light has heat. The sun is hot. But the fact is, the sun pushes on you. And with lasers, if you focus the light down to very small spots, you can actually push things or pull, it turns out. Push, pull, and make what they call optical traps. So I am the inventor of the optical trap, and it sort of started in that very strange way. Just by accident."

—— Arthur Ashkin

1

The central topic of this thesis is the nonlinear optical trapping of metallic nanoparticles. This thesis provides a mathematical description of the nonlinear optical trapping model, along with experimental demonstrations and discussions of potential applications.

In this chapter, we begin with a brief review of optical trapping, including its history, evolution, and various applications in scientific research. Then, we also introduce the motivation and the latest advance of the research in “nonlinear optical trapping” presented in this dissertation. Finally, we conclude the chapter by descrbing the scope of the thesis and providing an overview of the link between the chapters.

1.1. OPTICAL TRAPPING

As far back as the 16th century, Johannes Kepler speculated that sunlight would exert a certain pressure because the tails of the comets he observed were always pointing away from Sun[1]. James Clerk Maxwell predicted that the electromagnetic field carries with its momentum and that "optical radiation pressure" is exerted on illuminated objects in 1873[2]. Until 1901, the optical radiation force was observed by Nichols[3] and Lebedev[4]. Radiation pressure has since played an important role mainly in astron-

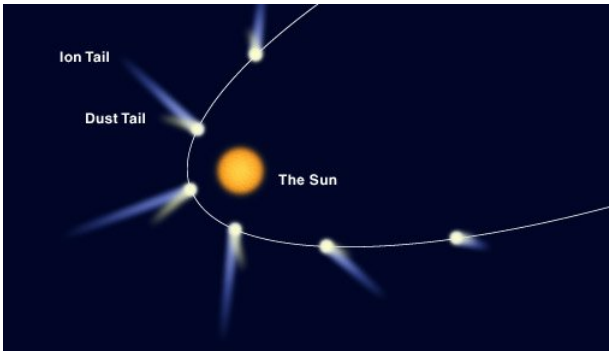

Figure 1.1: The diagram of a comet showing the dust tail and iron gas tail[5].

omy, where light intensities and distances are vast. However, the invention of lasers in the early 1970s paved the way for the manipulation of micrometer-sized objects, as first demonstrated by Arthur Ashkin's group at the Bell Laboratory in New Jersey [6–8]. Fig. 1.2 shows excerpts of the original design of optical trapping from A. Ashkin's archives at Bell Labs in 1969. By striking a focused continuous visible laser with a power of 1 W at a dielectric sphere with a radius of 1 wavelength, a radiation pressure of $F_{rad} = 10^{-10}N$ [7] was produced, causing the particle to be accelerated inwards and forwards, as published in 1970. The team demonstrated stable optical potential wells through their experiment on optical levitation of small glass spheres in the following year[8]. This micromanipulation of small objects opened up diverse potential applications, such as optical power and pressure measurements. At the time, Ashkin believed that trapping atoms using this technique was impossible. However, only a few years later, the analysis and methods of atomic trapping were carried out by Ashkin in 1978[9] and Letokhov in the USSR[10]. In 1986, the first demonstration of a three-dimensional stable atom trap was achieved using

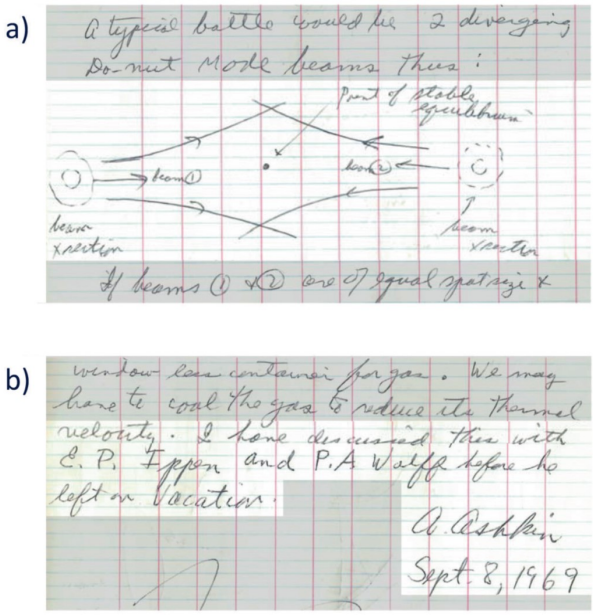

Figure 1.2: Two excerpts from A. Ashkin's archives at Bell Labs in 1969. It presents the original design of optical trapping[6].

a single tightly focused Gaussian beam by Steve Chu at Bell Labs[11]. For the development of methods to cool and trap atoms with laser light, Steve Chu[12], Claude Cohen-Tannoudji[13], and William D. Phillips[14] were awarded the Nobel prizes in Physics 1997. The development of laser cooling and trapping[15, 16] has enabled groundbreaking advances in physics, including Bose-Einstein condensation[17–19], quantum computation with neutral atoms[20, 21], and high precision optical clocks[22]. To date, optical trapping of diatomic molecules[23] and the poly-atomic molecules[24] already have been demonstrated successfully. Although optical trapping was originally designed for an atom trapping experiment, the first optical tweezers experiment was not applied to atoms [25]. Due to the difficulties of atomic trapping, the more straightforward dielectric particle was chosen to try the tweezer trap. Finally, in 1983, a transparent particle (silica nanosphere) was trapped by a single highly focused laser beam, and the single-beam trap was referred to as an "**optical tweezer**"[6]. On October 2, 2018, A. Askin was awarded the Nobel Prize in Physics. The Royal Swedish Academy of Sciences said " He was honored for his invention of 'optical tweezers' that grab particles, atoms, viruses, and other living cells with their laser beam fingers. With this, he was able to use the radiation pressure of light to move physical objects, 'an old dream of science fiction'."

Encouraged by the trapping of silica nanospheres [26], a new subfield of optical trapping emerged. Ashkin *et al.* employed an optical tweezer in cells[27], viruses, and bacteria[28], which marked the beginning of optical trapping in biology. Remarkable observation of cell reproduction was achieved within optical trapping. Using infrared lasers, optical trapping provided the ability to manipulate cells under damage-free conditions[27].

When probing the cytoplasmic flow of the organelles in the cell, one can detect the elastic and viscoelastic properties of the cytoplasm[29]. Manipulation of organelles in cells is also possible in vivo cells using the optical trap[30, 31]. The deformations and elastic behavior of cells were demonstrated by optical tweezers[32]. Optical tweezers in combination with the technique of pulsed laser can achieve cutting and moving cells and organelles, such as cutting and manipulating pieces of chromosomes for gene isolation[33].

One of the most profound advances in biological applications of optical tweezers is the study of objects of molecular scale. The feasibility of using optical tweezers as a force probe to measure the driving force of kinesin molecules was demonstrated by Block and Svoboda *et al.* in 90s[34, 35]. Another striking advance in this field was the detection of the overstretching forces exerted on DNA molecules, which is essential for understanding the kinetics of DNA[36]. The observation of single base-pair (0.34 nm) steps taken by RNA polymerase represents a milestone in precision measurements of optical trapping[37]. Integrating optical tweezers with spectroscopy and microscopy is vital in life science. Combined with single-fluorophore detection, even the angstrom-scale tether extension of labeled DNA suspended between two trapped beads was directly observed[38]. Direct observation of the folding transitions of a single calmodulin molecule can be achieved using single-molecule force spectroscopy[39]. Combined with multicolor confocal and stimulated emission depletion (STED) fluorescence microscopy, proteins on DNA are visualized at a resolution of 50 nm[40]. Optical tweezers can also be applied in protein synthesis by manipulating the ribosome[41]. Although originally designed for atom trapping, optical tweezers, as a powerful tool, have broad-reaching applications in biology.

Exciting applications of optical trapping also exist in other diverse areas of physics and chemistry. Optical levitation of nanoparticles has been used to demonstrate force sensing at the level of $10^{-21}N$, which is suitable for precise measurements[42]. Optical trapping of designed anisotropic microparticles with high-speed spin was demonstrated on a plane perpendicular to the optic axis[43]. Using a trapped particle as a tip, the scanning force microscope has a much lower spring constant than a mechanical cantilever[44]. Ablation[45] and microfabrication with optical tweezers[46] were demonstrat-ed with micro samples. Svoboda and Block found that metallic nanoparticles have polarizabilities larger than dielectric particles and can be stably trapped in three dimensions [47]. Measurements within optical tweezers show a phenomenon that strong attractive interactions can exist between colloidal particles in a metastable superheated state[48].

In recent years, optical tweezers have profited greatly from advances in other fields of nano-optics. Near-field optical techniques provide new possibilities to decrease the size of the trap into the sub-diffraction-limit scale[49, 50]. Unlike conventional far-field methods, the use of surface plasmon(SP) techniques enables the generation of sub-diffraction-limited spot sizes, which facilitate the high precision of optical trapping in various nanostructures and materials[51, 52]. Structured light beams as an advanced method have been widely used in optical manipulation[53]. The light fields shaped in amplitude, phase and polarization can boost the optical trapping schemes in two-dimensional and three-dimensional trapping[54]. In addition, acoustic and electron beam trapping have emerged as well[55, 56]. Since the invention of optical tweezers,

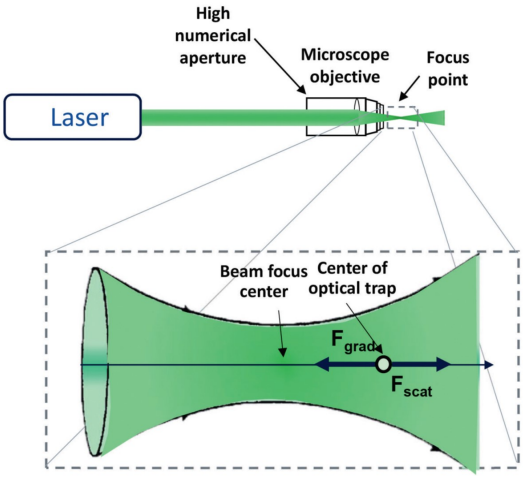

Figure 1.3: The first schematic of an optical tweezer designed by A. Ashkin[6] and an enlarged view near the beam focus.

this technique has been proven to be a powerful and indispensable tool in the study of the light-matter interactions at micro-, nano-, and angstrom-scales.

1.2. NONLINEAR OPTICAL TRAPPING

Optical trapping has proven to be a powerful tool with a wide range of applications. A conventional optical tweezers system is schematically shown in Fig. 1.3. A collimated Gaussian laser beam propagates through an objective lens and is tightly focused into a medium. Benefiting from the confinement of optical forces, a nanoparticle is trapped in the focal spot on the optical axis at the equilibrium point. It has been a consensus that only one optical potential well is observable when nanoparticles are trapped by a single Gaussian beam[26]. However, Jiang *et al.*[57] discovered a novel physical phenomenon of optical trapping in 2010. They found that the site of the stable trap of gold nanoparticles is split into two positions when utilizing a single focused femtosecond laser. The behavior of nonlinear trapping of gold nanoparticles has been studied. Using a linear-polarized femtosecond pulsed laser with a center wavelength of 800 nm, the minimal split distance between two trapped gold nanoparticles was measured as 100 nm in the experiment of Jiang *et al.*[57].

Generally, the size of the focal spot is determined by the diffraction limit of the optical system[52, 58], which restricts the precision of optical trapping. However, in nonlinear optical trapping, the distance between two spaced trapping positions depends on the intensity and can reach below the diffraction limit without the help of any other complex optical instruments. Jiang *et al.* proposed that the "trap split" effect can be explained by a nonlinear polarization mechanism but the exact physical mechanism is unknown. Their work advanced optical trapping from the linear regime into the nonlinear regime and started the study of nonlinear optical trapping.

Multiple traps often require either the fabrication of nanostructures or complex opti-

cal elements. Optical trapping from a single to multiple traps can be performed by optical manipulation techniques[53], such as laser scanning[59], diffractive optical element [60, 61], and SP tweezers[62]. Zhang *et al.* [63] demonstrated the nonlinear-induced multiplexed optical trapping through femtosecond cylindrical vector beams (CVBs). The required topological degree is produced by a simple vortex retard plate. The obtained vortex beam can determine the number of trap sites in nonlinear optical trapping.

In addition to pushing and pulling the nanoparticle, the ability to rotate objects is also highly demanded in micromachines[64] and metrology[65, 66]. Over past decades, an appealing way is to transfer angular momentum to particles to realize the rotation. The spin rotation of a trapped nanoparticle can be achieved by a circular polarization beam carrying spin angular momentum (SAM)[67, 68]. The orbital rotation can be obtained by transfer of orbital angular momentum (OAM) from a vortex beam[69, 70]. Qin *et al.* [71] experimentally demonstrated orbital manipulation of metallic nanoparticles in the nonlinear regime with only a single circular-polarized femtosecond Gaussian beam. The rotation frequency can be more than 1 kHz in water and the radius of rotation is at the sub-diffraction-limit scale.

There are several other publications that continue the exploration of nonlinear optical trapping. Huang and Jiang *et al.* [72] demonstrated a three dimensional spheroidal shell-like nonlinear optical trapping when the gold nanoparticles were trapped by a linearly polarized femtosecond laser beam. Their theoretical results can well describe the three dimensional nonlinear optical potential well. However, their qualitative analyses can not thoroughly explain the mechanism behind the nonlinear optical trapping process. Gong *et al.* [73] theoretically investigated the time averaged optical forces exerted on a nonlinear dielectric nanoparticle by a focused femtosecond laser pulse. The authors concluded that the splitting of the trap in two can be attributed to the self-defocusing effect of the particle. The self-focusing effect of the dielectric nanoparticle can only enhance the stability of optical trapping. Although their theoretical work can provide some support for the calculation of time averaged nonlinear optical forces and optical potential wells, they only show the trap splitting in one dimension while the experimental results demonstrate a three dimentional stable nonlinear optical trapping.

1.3. RESEARCH OBJECTIVE AND OUTLINE

From the above section, the most promising characteristic of nonlinear optical trapping is the ability to manipulate the nanoparticle below the diffraction limit scale. The lack of comprehensive and explicit theoretical work limits the development of nonlinear optical trapping. The details of light-matter interaction behind the nonlinear optical trapping process is still unknown. There are three aspects in the research of nonlinear optical trapping which have been and still are challenging:

1. Under the stimulation of a tightly focused laser pulse, the changing process of the physical properties of the nano-object needs to be investigated;
2. The intensity-dependent nonlinear optical forces exerted on the nanoparticle should be described clearly during the process of nonlinear optical trapping;
3. New applications of nonlinear optical trapping should be explored.

Hence, in this thesis, a quantitative analysis model is developed to achieve a deeper understanding of the physics relevant to nonlinear optical trapping. Based on a sound

theoretical model, more novel phenomena linked to nonlinear optical trapping are then demonstrated.

Before proceeding with an in depth study of nonlinear optical trapping research, the theoretical framework of optical trapping in the linear regime needs to be introduced following in the footsteps of predecessors[26, 47]. This is done in Chapter 2. Optical trapping is the consequence of the equilibrium of optical forces exerted on the nanoparticle. Under certain conditions, the optical response of a nanoparticle to the external optical field can be modeled as an electric dipole[74]. We derived equations for the time averaged optical forces using the dipole approximation theory[75–77]. The focused optical field is analytically described using vectorial diffraction theory[78]. While several factors have been proposed which influence the stability of optical traps, the volume fraction of the particles during optical trapping has often been neglected. To address this topic, we analyze the stability of optical trapping of a gold nanoparticle in human serum albumin solutions, HIV-1 virus solutions, and gold nanoparticle solutions using effective medium theory. Our analysis of the optical force on a single gold nanoparticle in solutions of varying volume fractions reveals that the optical force and the depth of optical potentials well decrease with increasing volume fraction.

In Chapter 3, almost all the nonlinear optical trapping experiments are performed with metallic nanoparticles[57, 63, 71, 72]. A metallic nanoparticle of gold[79–81], silver[82], or copper[83] can exhibit saturable absorption under a femtosecond pulsed illumination. The refractive index and permittivity of the nanoparticle change during this transient nonlinear process. These changes in the optical properties lead to a variation in the polarizability, scattering, and absorption cross-section of the nanoparticle. The interaction between the dipole and the optical field is determined by the dipolar polarizability[84]. However, the scalar polarizability, which is convenient and effective in traditional optical trapping, cannot adequately present the nonlinear response of the metal nanoparticle to the external optical fields. Hence, we propose a theoretical model to interpret the nonlinear optical trapping effect using the vector method. By combining the vector diffraction theory and the nonlinear optical effect, the polarizability vector of the metallic nanoparticle is derived. Analytical expressions are obtained for the optical force equations as well as for the optical potential well. We describe the experimental setup in detail and compare the experimental results with the theoretical model. The vectorial method yields good agreement with experimental observations.

In Chapter 4, based on the above-mentioned theoretical model, when the optical intensity is gradually increased, nonlinear effects from saturable absorption and reverse saturable absorption arise subsequently and thereby modulate the nonlinear properties of materials. However, in current non-linear optical traps, the underlying physical mechanism is mainly confined within the SA regime because threshold values required to excite the RSA regime are extremely high. In chapter 4, we demonstrate, both in theory and experiment, nonlinear optical tweezers within the RSA regime proving that a fascinating composite trapping state is achievable at ultra-high intensities through an optical force reversal induced through nonlinear absorption. Our research can help perfect the nonlinear optical trapping system, thereby providing beneficial guidance for wider applications of nonlinear optics.

1

REFERENCES

[1] L.-A. McFadden and D. T. Britt, *Primitive solar system objects: Asteroids and comets,* in *Encyclopedia of Physical Science and Technology (Third Edition)*, edited by R. A. Meyers (Academic Press, New York, 2003) third edition ed., pp. 73–85.

[2] J. C. Maxwell, *A treatise on electricity and magnetism*, Vol. 1 (Oxford: Clarendon Press, 1873).

[3] E. F. Nichols and G. F. Hull, *A preliminary communication on the pressure of heat and light radiation,* Physical Review (Series I) **13**, 307 (1901).

[4] P. Lebedew, *Experimental investigation of the pressure of light,* The Astrophysical Journal **15**, 60 (1902).

[5] L. Jiang, A. Shi, and Z. Qin, *Future prospect of solar sails by comparing two light propulsion sailing schemes,* in *21st AIAA International Space Planes and Hypersonics Technologies Conference* (2017).

[6] A. Ashkin, *Optical tweezers and their application to biological systems,* Nobel Lecture , 72 (2018).

[7] A. Ashkin, *Acceleration and trapping of particles by radiation pressure,* Phys. Rev. Lett. **24**, 156 (1970).

[8] A. Ashkin and J. M. Dziedzic, *Optical levitation by radiation pressure,* Applied Physics Letters **19**, 283 (1971).

[9] A. Ashkin, *Trapping of atoms by resonance radiation pressure,* Phys. Rev. Lett. **40**, 729 (1978).

[10] V. Letkhov and V. Minogin, *Trapping and storage of atoms in a laser field,* Applied physics **17**, 99 (1978).

[11] S. Chu, J. E. Bjorkholm, A. Ashkin, and A. Cable, *Experimental observation of optically trapped atoms,* Phys. Rev. Lett. **57**, 314 (1986).

[12] S. Chu, L. Hollberg, J. E. Bjorkholm, A. Cable, and A. Ashkin, *Three-dimensional viscous confinement and cooling of atoms by resonance radiation pressure,* Phys. Rev. Lett. **55**, 48 (1985).

[13] A. Aspect, J. Dalibard, A. Heidmann, C. Salomon, and C. Cohen-Tannoudji, *Cooling atoms with stimulated emission,* Phys. Rev. Lett. **57**, 1688 (1986).

[14] A. L. Migdall, J. V. Prodan, W. D. Phillips, T. H. Bergeman, and H. J. Metcalf, *First observation of magnetically trapped neutral atoms,* Phys. Rev. Lett. **54**, 2596 (1985).

[15] W. D. Phillips, *Nobel lecture: Laser cooling and trapping of neutral atoms,* Rev. Mod. Phys. **70**, 721 (1998).

[16] S. Chu, *Nobel lecture: The manipulation of neutral particles,* Rev. Mod. Phys. **70**, 685 (1998).

[17] K. B. Davis, M. O. Mewes, M. R. Andrews, N. J. van Druten, D. S. Durfee, D. M. Kurn, and W. Ketterle, *Bose-einstein condensation in a gas of sodium atoms,* Phys. Rev. Lett. **75**, 3969 (1995).

[18] M. H. Anderson, J. R. Ensher, M. R. Matthews, C. E. Wieman, and E. A. Cornell, *Observation of bose-einstein condensation in a dilute atomic vapor,* Science **269**, 198 (1995).

[19] E. A. Cornell and C. E. Wieman, *Nobel lecture: Bose-einstein condensation in a dilute gas, the first 70 years and some recent experiments,* Rev. Mod. Phys. **74**, 875 (2002).

[20] H. Bernien, S. Schwartz, A. Keesling, H. Levine, A. Omran, H. Pichler, S. Choi, A. S. Zibrov, M. Endres, M. Greiner, *et al.*, *Probing many-body dynamics on a 51-atom quantum simulator,* Nature **551**, 579 (2017).

[21] H. Levine, A. Keesling, G. Semeghini, A. Omran, T. T. Wang, S. Ebadi, H. Bernien, M. Greiner, V. Vuletić, H. Pichler, and M. D. Lukin, *Parallel implementation of high-fidelity multiqubit gates with neutral atoms,* Phys. Rev. Lett. **123**, 170503 (2019).

[22] A. D. Ludlow, M. M. Boyd, J. Ye, E. Peik, and P. O. Schmidt, *Optical atomic clocks,* Rev. Mod. Phys. **87**, 637 (2015).

[23] J., F., Barry, D., J., McCarron, E., B., Norrgard, and M., *Magneto - optical trapping of a diatomic molecule,* Nature (2014).

[24] N. B. Vilas, C. Hallas, L. Anderegg, P. Robichaud, A. Winnicki, D. Mitra, and J. M. Doyle, *Magneto-optical trapping and sub-doppler cooling of a polyatomic molecule,* Nature **606** (2022).

[25] A. Ashkin, *Optical trapping and manipulation of neutral particles using lasers,* Optics and Photonics News (1999).

[26] A. Ashkin, J. M. Dziedzic, J. E. Bjorkholm, and S. Chu, *Observation of a single-beam gradient force optical trap for dielectric particles,* Opt. Lett. **11**, 288 (1986).

[27] A. Ashkin, J. M. Dziedzic, and T. Yamane, *Optical trapping and manipulation of single cells using infrared laser beams,* Nature **330**, 769 (1987).

[28] A. Ashkin and J. M. Dziedzic, *Optical trapping and manipulation of viruses and bacteria,* Science **235**, 1517 (1987).

[29] A. Ashkin and J. M. Dziedzic, *Internal cell manipulation using infrared laser traps.* Proceedings of the National Academy of Sciences **86**, 7914 (1989).

[30] G. Weber and K. O. Greulich, *Manipulation of cells, organelles, and genomes by laser microbeam and optical trap,* International review of cytology **133**, 1 (1992).

[31] H. Felgner, F. Grolig, O. Müller, and M. Schliwa, *Chapter 11 in vivo manipulation of internal cell organelles,* (Academic Press, 1997) pp. 195–203.

[32] M. Dao, C. Lim, and S. Suresh, *Mechanics of the human red blood cell deformed by optical tweezers,* Journal of the Mechanics and Physics of Solids **51**, 2259 (2003).

[33] S. Seeger, S. Monajembashi, K.-J. Hutter, G. Futterman, J. Wolfrum, and K. O. Greulich, *Application of laser optical tweezers in immunology and molecular genetics,* Cytometry **12**, 497 (1991).

[34] S. M. Block, L. S. Goldstein, and B. J. Schnapp, *Bead movement by single kinesin molecules studied with optical tweezers,* Nature **348**, 348 (1990).

[35] K. Svoboda, C. F. Schmidt, B. J. Schnapp, and S. M. Block, *Direct observation of kinesin stepping by optical trapping interferometry,* Nature **365**, 721 (1993).

[36] S. B. Smith, Y. Cui, and C. Bustamante, *Overstretching b-dna: the elastic response of individual double-stranded and single-stranded dna molecules,* Science **271**, 795 (1996).

[37] E. A. Abbondanzieri, W. J. Greenleaf, J. W. Shaevitz, R. Landick, and S. M. Block, *Direct observation of base-pair stepping by rna polymerase,* Nature **438**, 460 (2005).

[38] M. J. Comstock, T. Ha, and Y. R. Chemla, *Ultrahigh-resolution optical trap with single-fluorophore sensitivity,* Nature methods **8**, 335 (2011).

[39] *The complex folding network of single calmodulin molecules,* Science **334**, 512 (2011).

[40] I. Heller, G. Sitters, O. D. Broekmans, G. Farge, C. Menges, W. Wende, S. W. Hell, E. J. Peterman, and G. J. Wuite, *Sted nanoscopy combined with optical tweezers reveals protein dynamics on densely covered dna,* Nature methods **10**, 910 (2013).

[41] D. H. Goldman, C. M. Kaiser, A. Milin, M. Righini, I. Tinoco, and C. Bustamante, *Mechanical force releases nascent chain–mediated ribosome arrest in vitro and in vivo,* Science **348**, 457 (2015).

[42] J. Ahn, Z. Xu, J. Bang, Y.-H. Deng, T. M. Hoang, Q. Han, R.-M. Ma, and T. Li, *Optically levitated nanodumbbell torsion balance and ghz nanomechanical rotor,* Phys. Rev. Lett. **121**, 033603 (2018).

[43] E. Higurashi, H. Ukita, H. Tanaka, and O. Ohguchi, *Optically induced rotation of anisotropic micro-objects fabricated by surface micromachining,* Applied Physics Letters **64**, 2209 (1994).

[44] L. P. Ghislain and W. W. Webb, *Scanning-force microscope based on an optical trap,* Opt. Lett. **18**, 1678 (1993).

[45] H. Misawa, M. Koshioka, K. Sasaki, N. Kitamura, and H. Masuhara, *Three-dimensional optical trapping and laser ablation of a single polymer latex particle in water,* Journal of applied physics **70**, 3829 (1991).

[46] X.-C. Yao and A. Castro, *Optical trapping microfabrication with electrophoretically delivered particles inside glass capillaries,* Opt. Lett. **28**, 1335 (2003).

[47] K. Svoboda and S. M. Block, *Optical trapping of metallic rayleigh particles,* Opt. Lett. **19**, 930 (1994).

[48] A. E. Larsen and D. G. Grier, *Like-charge attractions in metastable colloidal crystallites,* Nature **385**, 230 (1997).

[49] A. V. Zayats and I. I. Smolyaninov, *Near-field photonics: surface plasmon polaritons and localized surface plasmons,* Journal of Optics A: Pure and Applied Optics **5**, S16.

[50] D. Erickson, X. Serey, Y.-F. Chen, and S. Mandal, *Nanomanipulation using near field photonics,* Lab Chip **11**, 995 (2011).

[51] C. Min, Z. Shen, J. Shen, Y. Zhang, H. Fang, G. Yuan, L. Du, S. Zhu, T. Lei, and X. Yuan, *Focused plasmonic trapping of metallic particles,* Nature communications **4**, 2891 (2013).

[52] Y. Zhang, C. Min, X. Dou, X. Wang, H. P. Urbach, M. G. Somekh, and X. Yuan, *Plasmonic tweezers: for nanoscale optical trapping and beyond,* Light: Science & Applications **10**, 59 (2021).

[53] Y. Yang, Y. Ren, M. Chen, Y. Arita, and C. Rosales-Guzmán, *Optical trapping with structured light: a review,* Advanced Photonics **3**, 034001 (2021).

[54] E. Otte and C. Denz, *Optical trapping gets structure: Structured light for advanced optical manipulation,* Applied Physics Reviews **7**, 041308 (2020).

[55] J. Millen, T. S. Monteiro, R. Pettit, and A. N. Vamivakas, *Optomechanics with levitated particles,* Reports on Progress in Physics **83**, 026401 (2020).

[56] H. Zheng, U. M. Mirsaidov, L.-W. Wang, and P. Matsudaira, *Electron beam manipulation of nanoparticles,* Nano Letters **12**, 5644 (2012).

[57] Y. Jiang, T. Narushima, and H. Okamoto, *Nonlinear optical effects in trapping nanoparticles with femtosecond pulses,* Nature Physics **6**, 1005 (2010).

[58] M. Born and E. Wolf, *Principles of optics: electromagnetic theory of propagation, interference and diffraction of light* (Elsevier, 2013).

[59] K. Sasaki, M. Koshioka, H. Misawa, N. Kitamura, and H. Masuhara, *Pattern formation and flow control of fine particles by laser-scanning micromanipulation,* Opt. Lett. **16**, 1463 (1991).

[60] J. E. Curtis, B. A. Koss, and D. G. Grier, *Dynamic holographic optical tweezers,* Optics communications **207**, 169 (2002).

[61] J. Liesener, M. Reicherter, T. Haist, and H. Tiziani, *Multi-functional optical tweezers using computer-generated holograms,* Optics Communications **185**, 77 (2000).

[62] M. Righini, A. S. Zelenina, C. Girard, and R. Quidant, *Parallel and selective trapping in a patterned plasmonic landscape,* Nature Physics **3**, 477 (2007).

[63] Y. Zhang, J. Shen, C. Min, Y. Jin, Y. Jiang, J. Liu, S. Zhu, Y. Sheng, A. V. Zayats, and X. Yuan, *Nonlinearity-induced multiplexed optical trapping and manipulation with femtosecond vector beams,* Nano letters **18**, 5538 (2018).

[64] L. Paterson, M. P. MacDonald, J. Arlt, W. Sibbett, P. E. Bryant, and K. Dholakia, *Controlled rotation of optically trapped microscopic particles,* Science **292**, 912 (2001).

[65] Y. Arita, M. Mazilu, and K. Dholakia, *Laser-induced rotation and cooling of a trapped microgyroscope in vacuum,* Nature communications **4**, 2374 (2013).

[66] J. Ahn, Z. Xu, J. Bang, P. Ju, X. Gao, and T. Li, *Ultrasensitive torque detection with an optically levitated nanorotor,* Nature Nanotechnology **15**, 89 (2020).

[67] M. E. Friese, T. A. Nieminen, N. R. Heckenberg, and H. Rubinsztein-Dunlop, *Optical alignment and spinning of laser-trapped microscopic particles,* Nature **394**, 348 (1998).

[68] A. Lehmuskero, R. Ogier, T. Gschneidtner, P. Johansson, and M. Käll, *Ultrafast spinning of gold nanoparticles in water using circularly polarized light,* Nano Letters **13**, 3129 (2013).

[69] K. T. Gahagan and G. A. Swartzlander, *Optical vortex trapping of particles,* Opt. Lett. **21**, 827 (1996).

[70] J. E. Curtis and D. G. Grier, *Structure of optical vortices,* Phys. Rev. Lett. **90**, 133901 (2003).

[71] Y. Qin, L.-M. Zhou, L. Huang, Y. Jin, H. Shi, S. Shi, H. Guo, L. Xiao, Y. Yang, C.-W. Qiu, *et al.*, *Nonlinearity-induced nanoparticle circumgyration at sub-diffraction scale,* Nature Communications **12**, 3722 (2021).

[72] L. Huang, Y. Qin, Y. Jin, H. Shi, H. Guo, L. Xiao, and Y. Jiang, *Spheroidal trap shell beyond diffraction limit induced by nonlinear effects in femtosecond laser trapping,* Nanophotonics **9**, 4315 (2020).

[73] L. Gong, B. Gu, G. Rui, Y. Cui, Z. Zhu, and Q. Zhan, *Optical forces of focused femtosecond laser pulses on nonlinear optical rayleigh particles,* Photon. Res. **6**, 138 (2018).

[74] B. T. Draine, *The Discrete-Dipole Approximation and Its Application to Interstellar Graphite Grains,* Astrophys. J. **333**, 848 (1988).

[75] P. C. Chaumet and M. Nieto-Vesperinas, *Time-averaged total force on a dipolar sphere in an electromagnetic field,* Optics Letters **25**, 1065 (2000).

[76] J. R. Arias-Gonzalez and M. Nieto-Vesperinas, *Optical forces on small particles: attractive and repulsive nature and plasmon-resonance conditions,* Journal of the Optical Society of America A **20**, 1201 (2003).

[77] S. Albaladejo, M. I. Marqués, M. Laroche, and J. J. Sáenz, *Scattering forces from the curl of the spin angular momentum of a light field,* Phys. Rev. Lett. **102** (2009), 10.1103/PhysRevLett.102.113602.

[78] L. Novotny and B. Hecht, *Principles of nano-optics,* (Cambridge University Press, 2012) Chap. 3.

[79] Y. Gao, X. Zhang, Y. Li, H. Liu, Y. Wang, Q. Chang, W. Jiao, and Y. Song, *Saturable absorption and reverse saturable absorption in platinum nanoparticles,* Optics communications **251**, 429 (2005).

[80] L. De Boni, E. L. Wood, C. Toro, and F. E. Hernandez, *Optical saturable absorption in gold nanoparticles,* Plasmonics **3**, 171 (2008).

[81] D. Wu, J. Peng, Z. Cai, J. Weng, Z. Luo, N. Chen, and H. Xu, *Gold nanoparticles as a saturable absorber for visible 635 nm q-switched pulse generation,* Optics Express **23**, 24071 (2015).

[82] S. Luo, Y. Chen, G. Fan, F. Sun, and S. Qu, *Saturable absorption and reverse saturable absorption on silver particles with different shapes,* Applied Physics A: Materials Science & Processing **117**, 891 (2014).

[83] C.-B. Yao, X. Wen, Q.-H. Li, X.-Y. Yan, J. Li, K.-X. Zhang, W.-J. Sun, L.-N. Bai, and S.-B. Yang, *The saturable absorption and reverse saturable absorption properties of cu doped zinc oxide thin films,* Chemical Physics Letters **671**, 113 (2017).

[84] C. F. Bohren and D. R. Huffman, *Absorption and scattering of light by small particles* (John Wiley & Sons, 2008).

2

THE OPTICAL TRAPPING OF METALLIC NANOPARTICLES

"Facts do not cease to exist because they are ignored."

—— Aldous Huxley

Some original content of this chapter has been published in *Optics Communications*

2.1. INTRODUCTION

The research in the field of optical trapping can be categorized into three distinct areas, each focusing on specific research topics. First, the technology of laser cooling of atoms has paved the way for modern ultra-cold atom technology. Second, the manipulation of micrometer-sized particles stands as a versatile tool with a wide range of applications[1]. Last but certainly not least, the stable optical trapping of nanoparticles within the nano-scale size range is a primary area of interest in the field of nanotechnology. Our research scope reported in this thesis is mainly in the third sub-field in our thesis.

Metallic nanoparticles, especially gold nanoparticles, are efficient and natural probes, which can be used as a highly sensitive force transducer[2–4] to monitor forces in the pico-Newton regime and to measure distances in the nanometer range. Compared to other probes, such as quantum dots and organic dyes, gold nanoparticles can be biologically harmless when exposed to light for prolonged periods[5]. In addition, the optical forces exerted on gold nanoparticles are several times greater than those exerted on dielectric nanoparticles [6]. Gold nanoparticles have been widely used in biomedical experiments, for instance, in the diagnosis of cancer cells[5], the detection of DNA [7, 8], delivery of therapeutic drugs [9], and monitoring the motion of protein [10].

In this chapter, taking the gold nanoparticle as an example, we first give a theoretical framework for the description of optical trapping. For particles much smaller than the wavelength of incident light, the nanoparticle can often be modeled as an electric dipole[11]. The dipolar polarizability reflects the strength and method of interaction between the nanoparticle and the optical field[12]. We deduce the time-averaged optical force exerted on the particle using the dipole approximation theory and perform a quantitative analysis of the optical force and potentials on a single gold nanoparticle. In addition, we theoretically investigate the effect of the volume fraction on the optical trapping of gold nanoparticles. This finding can aid in more effective control of gold nanoparticles in various applications.

2.2. THE METHOD FOR OPTICAL TRAPPING OF METALLIC NANOPARTICLES

Optical trapping of nanoparticles is a subdivision of nano-optics. All the problems that need to be solved in this thesis belong to the light-matter interaction. It is necessary and convenient to express the basic theory in the subsequent chapters with uniform notation and convention. The notation introduced below is used throughout the rest of the thesis.

2.2.1. THE DEDUCTION OF THE TIME-AVERAGED OPTICAL FORCE EQUATION

The equations for optical forces exerted on the nanoparticle in electromagnetic fields are based on the conservation law of linear momentum. The light field can be described by two vectors: the electric field strength $\boldsymbol{\mathcal{E}}(\mathbf{r},t)$ and the magnetic field $\boldsymbol{\mathcal{H}}(\mathbf{r},t)$, respectively. The magnetic induction is $\boldsymbol{\mathcal{B}}=\mu_0\boldsymbol{\mathcal{H}}$. In vacuum, at every point and every time, the field vectors satisfy the Maxwell equations.:

$$\nabla\times\boldsymbol{\mathcal{E}}=-\frac{\partial\boldsymbol{\mathcal{B}}}{\partial t}, \tag{2.1}$$

$$\nabla\times\frac{\boldsymbol{\mathcal{B}}}{\mu_0}=\varepsilon_0\frac{\partial\boldsymbol{\mathcal{E}}}{\partial t}+\boldsymbol{\mathcal{J}}, \tag{2.2}$$

$$\nabla\cdot\varepsilon_0\boldsymbol{\mathcal{E}}=\rho, \tag{2.3}$$

$$\nabla\cdot\boldsymbol{\mathcal{B}}=0, \tag{2.4}$$

where ε_0 and μ_0 are the permittivity and permeability of the vacuum, $\boldsymbol{\mathcal{J}}$ and ρ denote current density and charge density, respectively.

A sufficiently small nanoparticle can be modeled as an electric dipole. We will derive the force an electromagnetic field exerts on an electric dipole. We start from the Lorentz force on a charge q, which moves with speed $\mathbf{v}(\mathbf{t})$ and is at the position $\mathbf{r}$:

$$\mathbf{F}=q(\boldsymbol{\mathcal{E}}(\mathbf{r},\mathbf{t})+\mathbf{v}(\mathbf{t})\times\boldsymbol{\mathcal{B}}(\mathbf{r},\mathbf{t})), \tag{2.5}$$

The conservation of the charge requires that the rate of increase of the charge inside a volume V must be equal to the flux of charges passing through its surface from outside of volume:

$$-\int_{\partial V}\boldsymbol{\mathcal{J}}\cdot\hat{\mathbf{n}}\,\mathrm{d}^2r=\frac{d}{dt}\int_V\rho\,\mathrm{d}^3r, \tag{2.6}$$

where the source has the charge density ρ and the current density $\boldsymbol{\mathcal{J}}$. We omit $(\mathbf{r},t)$ here. ∂V is the boundary of V with outwards pointing unit vector $\hat{\mathbf{n}}$. Using the divergence theorem, the differential form of the conservation law follows:

$$-\nabla\cdot\boldsymbol{\mathcal{J}}=\frac{\partial\rho}{\partial t}, \tag{2.7}$$

Because scattering is primarily by electric dipoles, we will assume that all charges and currents are due to variations of the polarisation density $\boldsymbol{\mathcal{P}}$. It means that only polarization current density $\partial\boldsymbol{\mathcal{P}}/\partial t$ occurs:

$$\boldsymbol{\mathcal{J}}=\frac{\partial\boldsymbol{\mathcal{P}}}{\partial t}. \tag{2.8}$$

The force on the moving charge can be expressed in terms of a volume integral over a force density $\mathbf{f}$,

$$\mathbf{F}=\int_V\mathbf{f}\,\mathrm{d}^3r. \tag{2.9}$$

Then for the force density, we have the expression:

$$\mathbf{f} = \rho\boldsymbol{\mathcal{E}} + \boldsymbol{\mathcal{J}} \times \boldsymbol{\mathcal{B}}, \tag{2.10}$$

By substituting Eq. (2.8) into Eq. (2.7), the charge density becomes $\rho = -\nabla \cdot \boldsymbol{\mathcal{P}}$. The force density Eq. (2.10) can then be rewritten as

$$\mathbf{f} = -\boldsymbol{\mathcal{E}}(\nabla \cdot \boldsymbol{\mathcal{P}}) + \frac{\partial \boldsymbol{\mathcal{P}}}{\partial t} \times \boldsymbol{\mathcal{B}}. \tag{2.11}$$

Considering the Cartesian component of $\mathbf{f}$ and denote it as f_i where $i = x, y, z$. Using Gauss's theorem, the first term of the force density f_i can be expressed as

$$\int_V -\mathscr{E}_i(\nabla \cdot \boldsymbol{\mathcal{P}})\mathrm{d}^3 r = \int_V (\boldsymbol{\mathcal{P}} \cdot \nabla)\mathscr{E}_i \, \mathrm{d}^3 r - \int_{\partial V} (\mathscr{E}_i \boldsymbol{\mathcal{P}}) \cdot \hat{\mathbf{n}} \, \mathrm{d}^2 r, \tag{2.12}$$

To derive the optical forces exerted on a dipole at point $\mathbf{r}_0$ inside V, we use the polarization density that is given by $\boldsymbol{\mathcal{P}} = \boldsymbol{p}\,\delta(\mathbf{r} - \mathbf{r}_0)$ where $\boldsymbol{p}$ denotes the dipole moment vector. We assume that the dipole is at a fixed position and its time dependence is solely due to the time dependence of the dipole moment $\boldsymbol{p}$. The second term at the right side of Eq. (2.12) vanishes if the dipole's position is not on the boundary of the volume. Only the first term of Eq.(2.12) contributes to the force density. We can write the force as follows:

$$\mathbf{F} = \int_V (\boldsymbol{\mathcal{P}} \cdot \nabla)\boldsymbol{\mathcal{E}} \, \mathrm{d}^3 r + \int_V \frac{\partial}{\partial t}\boldsymbol{\mathcal{P}} \times \boldsymbol{\mathcal{B}} \, \mathrm{d}^3\mathrm{r} \tag{2.13}$$

$$= \int_V (\boldsymbol{\mathcal{P}} \cdot \nabla)\boldsymbol{\mathcal{E}} \, \mathrm{d}^3 r + \int_V \frac{\partial}{\partial t}(\boldsymbol{\mathcal{P}} \times \boldsymbol{\mathcal{B}}) \, \mathrm{d}^3\mathrm{r} - \int_\mathrm{V} \boldsymbol{\mathcal{P}} \times \frac{\partial}{\partial t}\boldsymbol{\mathcal{B}} \, \mathrm{d}^3\mathrm{r}. \tag{2.14}$$

After integration and combing with Eq. (2.1), the expression for the force can be written as

$$\mathbf{F} = (\boldsymbol{p} \cdot \nabla)\boldsymbol{\mathcal{E}} + \boldsymbol{p} \times (\nabla \times \boldsymbol{\mathcal{E}}) + \frac{\partial}{\partial t}(\boldsymbol{p} \times \boldsymbol{\mathcal{B}}). \tag{2.15}$$

Combing with Eq. (A1), we have an identity:

$$\boldsymbol{p} \times (\nabla \times \boldsymbol{\mathcal{E}}) = \nabla(\boldsymbol{p} \cdot \boldsymbol{\mathcal{E}}) - (\boldsymbol{p} \cdot \nabla)\boldsymbol{\mathcal{E}}, \tag{2.16}$$

then Eq. (2.15) can be rewritten as

$$\mathbf{F} = \nabla(\boldsymbol{p} \cdot \boldsymbol{\mathcal{E}}) + \frac{\partial}{\partial t}(\boldsymbol{p} \times \boldsymbol{\mathcal{B}}) \tag{2.17}$$

$$= \sum_i p_i \nabla \boldsymbol{\mathcal{E}}_i + \frac{\partial}{\partial t}(\boldsymbol{p} \times \boldsymbol{\mathcal{B}}), \quad i = x, y, z. \tag{2.18}$$

Notice that optical force is additive. We can sum the forces acting on individual dipoles to obtain the net force acting on a macroscopic body. This thesis solely analyzes the force acting on a small object treated as a single dipole.

With a fixed frequency ω, we will now delve into time-harmonic sources and fields in more detail. If the electromagnetic field is time-harmonic, then the electric field strength $\boldsymbol{\mathcal{E}}$ and the magnetic field $\boldsymbol{\mathcal{H}}$ can be described with the complex time-harmonic factor $e^{-i\omega t}$ with $\omega > 0$:

$$\boldsymbol{\mathcal{E}}(\mathbf{r},t) = \mathrm{Re}\{\mathbf{E}(\mathbf{r})\mathrm{e}^{-\mathrm{i}\omega\mathrm{t}}\}, \tag{2.19}$$

$$\boldsymbol{\mathcal{H}}(\mathbf{r},t) = \mathrm{Re}\{\mathbf{H}(\mathbf{r})\mathrm{e}^{-\mathrm{i}\omega\mathrm{t}}\}, \tag{2.20}$$

where the **E** and **H** are the complex field amplitudes. The relationship between the dipole and field is linear and hence the dipole moment is a time-harmonic field as well

$$\boldsymbol{p}(t) = \mathrm{Re}\{\mathbf{p}\mathrm{e}^{-\mathrm{i}\omega\mathrm{t}}\}, \tag{2.21}$$

where **p** is the complex dipole vector. Combining with Eq. (2.18) and Eq. (2.21), the time-averaged force on a unit dipole can be rearranged as

$$\langle \mathbf{F} \rangle = \frac{1}{2}\sum_i \mathrm{Re}\left\{p_i^* \nabla E_i\right\}. \quad i = x, y, z, \tag{2.22}$$

where $\langle ... \rangle$ denotes the time average and the second term of the right side of Eq. (2.18) vanishes in the time average. We assume that the particle has no permanent dipole moment. The induced dipole moment is proportional to the external electric field at the position r_0,

$$\mathbf{p} = \alpha \mathbf{E}(r_0), \tag{2.23}$$

where α denotes the polarizability of the particle. Note that the α is the complex number. The optical forces exerted on the nanoparticle are usually separated into two components: gradient forces and radiation pressures. By inserting Eq. (2.23) into Eq. (2.22) and arranging the corresponding items, we obtain

$$\langle \mathbf{F} \rangle = \frac{1}{2}\sum_i \mathrm{Re}\left\{(\alpha E_i)^* \nabla E_i\right\} \tag{2.24}$$

$$= \frac{1}{2}\mathrm{Re}\{\alpha\}\sum_i \mathrm{Re}\{E_i^* \nabla E_i\} + \frac{1}{2}\mathrm{Im}\{\alpha\}\sum_i \mathrm{Im}\{E_i^* \nabla E_i\}, \quad i = x, y, z. \tag{2.25}$$

This result will be more intuitive if we can represent it in two separated parts: the gradient force part and the radiation pressure part. For the first term in Eq.(2.25), we have the

gradient force part:

$$\langle \mathbf{F} \rangle_{\text{grad}} = \frac{1}{2}\text{Re}\{\alpha\}\sum_i \text{Re}\{E_i^* \nabla E_i\} \tag{2.26}$$

$$= \frac{1}{4}\text{Re}\{\alpha\}(\sum_i \{E_i^* \nabla E_i\} + \sum_i \{E_i \nabla E_i^*\}) \tag{2.27}$$

$$= \frac{1}{4}\text{Re}\{\alpha\}\nabla(\sum_i \{E_i E_i^*\}) \tag{2.28}$$

$$= \frac{1}{4}\text{Re}\{\alpha\}\nabla|\mathbf{E}|^2. \tag{2.29}$$

This term is called the gradient force. The second term of Eq.(2.25) is called the radiation pressure. Maxwell showed that the radiation pressure can be regarded as a consequence of the momentum transfer from the radiation field to the particle and this force pushes the polarized particle in the direction of radiation. The radiation pressure is associated with the imaginary part of the complex polarizability and the gradients of the optical field. The radiation pressure part is:

$$\langle \mathbf{F} \rangle_{\text{rad}} = \frac{1}{2}\text{Im}\{\alpha\}\sum_i \text{Im}\{E_i^* \nabla E_i\}. \tag{2.30}$$

We consider the complex electric field vector $\mathbf{E}$ as a constant. $\mathbf{E} = \mathbf{p}/\alpha$. Then using the vector calculus identity Eq.(A1) we have:

$$\sum_i \{E_i^* \nabla E_i\} = \sum_i \frac{p_i^*}{\alpha^*}\nabla E_i \tag{2.31}$$

$$= \sum_i \nabla(\frac{p_i^*}{\alpha^*} \cdot E_i) \tag{2.32}$$

$$= \nabla(\frac{\mathbf{p}^*}{\alpha^*} \cdot \mathbf{E}) \tag{2.33}$$

$$= \frac{\mathbf{p}^*}{\alpha^*} \times (\nabla \times \mathbf{E}) + (\frac{\mathbf{p}^*}{\alpha^*} \cdot \nabla)\mathbf{E}, \tag{2.34}$$

and together with maxwell equations, the last term in Eq. (2.30) can be written as

$$\begin{aligned} \langle \mathbf{F} \rangle_{\text{rad}} &= \frac{1}{2}\text{Im}\{\alpha\}\text{Im}\{\mathbf{E}^* \times (\nabla \times \mathbf{E}) + (\mathbf{E}^* \cdot \nabla)\mathbf{E}\} \\ &= \frac{\omega\mu_0}{2}\text{Im}\{\alpha\}\text{Re}\left\{\mathbf{E} \times \mathbf{H}^*\right\} + \frac{1}{2}\text{Im}\{\alpha\}\text{Im}\left\{(\mathbf{E}^* \cdot \nabla)\mathbf{E}\right\}, \end{aligned} \tag{2.35}$$

where ω is the angular frequency of the light in the vacuum and μ_0 is the permeability in the vacuum. We will use the symbol σ for the extinction cross-section of the nanoparticle,

$$\sigma = \frac{n_h k_0}{\varepsilon_0}\text{Im}\{\alpha\} = n_h c\omega\mu_0\text{Im}\{\alpha\}. \tag{2.36}$$

where $n_h = 1$ and it is the refractive index of the medium, k_0 is the wavenumber in the vacuum and c is the speed of light in a vacuum. The *Poynting vector* $\boldsymbol{\mathcal{S}} = \boldsymbol{\mathcal{E}} \times \boldsymbol{\mathcal{H}}$, which represents the direction and magnitude of the rate of transfer of energy as a function of spaces and time. For an electromagnetic field with a given frequency ω, the time average of Poynting vector $\langle \boldsymbol{\mathcal{S}} \rangle$ is written as:

$$\langle \boldsymbol{\mathcal{S}} \rangle = \frac{1}{2} \mathrm{Re}\{\mathbf{E} \times \mathbf{H}^*\}. \tag{2.37}$$

We can rewrite the Eq.(2.35) as

$$\langle \mathbf{F} \rangle_{\mathrm{rad}} = \frac{\sigma}{c} \langle \boldsymbol{\mathcal{S}} \rangle + \frac{\sigma \varepsilon_0}{2k_0} \mathrm{Im}\left\{(\mathbf{E}^* \cdot \nabla)\mathbf{E}\right\}. \tag{2.38}$$

Then we can get a concise form of the force equation:

$$\langle \mathbf{F} \rangle_{\mathrm{total}} = \langle \mathbf{F} \rangle_{\mathrm{grad}} + \langle \mathbf{F} \rangle_{\mathrm{rad}} \tag{2.39}$$

$$= \underbrace{\frac{1}{4} \mathrm{Re}\{\alpha\} \nabla |\mathbf{E}|^2}_{\text{gradient force}} + \underbrace{\frac{\sigma}{c} \langle \boldsymbol{\mathcal{S}} \rangle + \frac{\sigma \varepsilon_0}{2k_0} \mathrm{Im}\left\{(\mathbf{E}^* \cdot \nabla)\mathbf{E}\right\}}_{\text{radiation pressure}} \tag{2.40}$$

This represents the final phase of the force equation, essential for accurately determining the total force acting on a dipole-like nanoparticle. Understanding this equation is crucial for advancing our research in nanotechnology. The total force consists of the gradient force on the nanoparticle and the radiation pressure acting on the dipole-like nanoparticle. The first term is known as the gradient force. The second term represents the radiation force from the Poynting vector. The last term is also a special component of the radiation pressure. We will discuss this term in more detail here. First, we can consider an identity:

$$2i\mathrm{Im}\{(\mathbf{E}^* \cdot \nabla)\mathbf{E}\} = (\mathbf{E}^* \cdot \nabla)\mathbf{E} - [(\mathbf{E}^* \cdot \nabla)\mathbf{E}]^* \tag{2.41}$$

$$= (\mathbf{E}^* \cdot \nabla)\mathbf{E} - (\mathbf{E} \cdot \nabla)\mathbf{E}^*. \tag{2.42}$$

Let us consider another identity Eq.(A2),

$$\begin{aligned} \nabla \times (\mathbf{E} \times \mathbf{E}^*) &= -(\mathbf{E} \cdot \nabla)\mathbf{E}^* + (\mathbf{E}^* \cdot \nabla)\mathbf{E} - \mathbf{E}^* \nabla \cdot \mathbf{E} + \mathbf{E} \nabla \cdot \mathbf{E}^* \\ &= 2\mathrm{iIm}\left\{(\mathbf{E}^* \cdot \nabla)\mathbf{E}\right\} + \mathbf{E} \nabla \cdot \mathbf{E}^* - \mathbf{E}^* \nabla \cdot \mathbf{E} \\ &= 2\mathrm{iIm}\left\{(\mathbf{E}^* \cdot \nabla)\mathbf{E}\right\} + 2\mathrm{iIm}\left\{\mathbf{E} \nabla \cdot \mathbf{E}^*\right\}. \end{aligned} \tag{2.43}$$

Then we can write the second item of Eq.(2.38) as

$$\frac{\sigma \varepsilon_0}{2k_0} \mathrm{Im}\left\{(\mathbf{E}^* \cdot \nabla)\mathbf{E}\right\} = \frac{c\sigma\varepsilon_0}{4i\omega} [\nabla \times \left(\mathbf{E} \times \mathbf{E}^*\right)] - \frac{c\sigma\varepsilon_0}{2\omega} \mathrm{Im}\left\{\mathbf{E} \nabla \cdot \mathbf{E}^*\right\}, \tag{2.44}$$

We can see the third term in Eq.(2.40) associated with the spin density of the electric field and the imaginary part of the divergence of the conjugate electric field. This derived equation demonstrates that the radiation pressure exerted on an electric dipole is not only proportional to the Poynting vector[13, 14]. This can be neglected for linear-polarized beams.

According to Eq.(2.40), optical trapping depends on many multiple parameters, such as the distribution of optical field gradients, the polarizability of the nanoparticle, and the corresponding total cross-section[15].

The depth of the optical potential well is often used to reflect the stiffness and efficiency of optical trapping. The trapping potential is normalized to $k_B T$, which is a measure of the energy of Brownian motion of the particle in an aqueous environment. Here, k_B is the Boltzmann constant and T is the absolute temperature of the environment, which is chosen to be equal to 300 K. A requirement for stable optical trapping is that the depth of the potential well is deeper than 10 $k_B T$ [16]. The radiation part of the force is not conservative; therefore, the definition of potential depends on the chosen curve C:

$$U(\mathbf{r}) = -\int_C \langle \mathbf{F}(\mathbf{r}) \rangle \, \mathrm{d}\mathbf{r}. \tag{2.45}$$

It is essential to remark that the formula is particularly suited for describing the behavior of dipolar nanoparticles. When a large particle cannot be approximated as a dipole, the optical force on a particle can be calculated with a rigorous electromagnetic model such as the Maxwell stress tensor (MST) method[17]. However, delving into the details of this method is beyond the scope of this thesis.

2.2.2. THE DIPOLE POLARIZABILITY OF A NANOPARTICLE

According to the equation derived in the previous section, we found that the polarizability α plays a vital role in the calculation of optical forces. It is important to take a close look at the dipole approximation process because our core theoretical model developed in this thesis for nonlinear optical trapping is based on it.

Let a homogeneous isotropic nanoparticle be illuminated by a plane wave. The electric field is given by $\mathbf{E}_0 = E_0 \hat{\mathbf{z}}$, as can be seen in Figure. 2.1. The radius of the spherical particle is r_0 and the distance to its center is r. ε_p denotes the permittivity of the nanoparticle and ε_h is the permittivity of the host medium (surrounding environment). The electric field inside and outside the nanosphere is $\mathbf{E}_1$ and $\mathbf{E}_2$, respectively. Provided the particle is small enough one may use the quasi-static approximation for which the

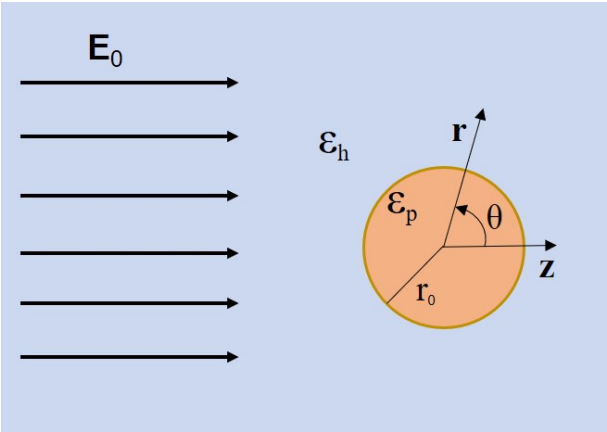

Figure 2.1: *A nanosphere in a uniform electric field.*

electric field is derived from electric potentials $\Phi_1(r,\theta)$ and $\Phi_2(r,\theta)$,

$$\mathbf{E}_1 = -\nabla\Phi_1, \quad \nabla^2\Phi_1 = 0 \quad (r < r_0), \tag{2.46}$$

$$\mathbf{E}_2 = -\nabla\Phi_2, \quad \nabla^2\Phi_2 = 0 \quad (r > r_0). \tag{2.47}$$

At the boundary of the sphere, the electric potential must satisfy the continuity equations:

$$\Phi_1 = \Phi_2, \quad \varepsilon_\mathrm{p}\frac{\partial\Phi_1}{\partial r} = \varepsilon_\mathrm{h}\frac{\partial\Phi_2}{\partial r} \quad (r = r_0). \tag{2.48}$$

At a large distance from the sphere r, we require that the potential gives the unperturbed incident field:

$$\lim_{r\to\infty}\Phi_2 = -E_0 r\cos\theta = -E_0 z. \tag{2.49}$$

It means the electric field is the unperturbed applied field and we have the functions to satisfy the boundary condition and partial differential equations above:

$$\Phi_1 = -\frac{3\varepsilon_\mathrm{h}}{\varepsilon_\mathrm{p}+2\varepsilon_\mathrm{h}}E_0 r\cos\theta, \tag{2.50}$$

$$\Phi_2 = -E_0 r\cos\theta + {r_0}^3 E_0\frac{\varepsilon_\mathrm{p}-\varepsilon_\mathrm{h}}{\varepsilon_\mathrm{p}+2\varepsilon_\mathrm{h}}\frac{\cos\theta}{r^2}. \tag{2.51}$$

Consider two opposite charges (q and – q) which are separated by distance d, as shown in Figure. 2.2. This configuration of charges is called a "*dipole*" with a "*dipole moment*" $\mathbf{p} = p\hat{\mathbf{z}}$, where $p = qd$. The two charges are inside the medium with permittivity ε_h. The two closely spaced opposite charges ±q have the potential at any point A (see Figure (2.2)):

$$\Phi = \frac{1}{4\pi\varepsilon_\mathrm{h}}\left(\frac{q}{|r-r_+|} - \frac{q}{|r-r_-|}\right), \tag{2.52}$$

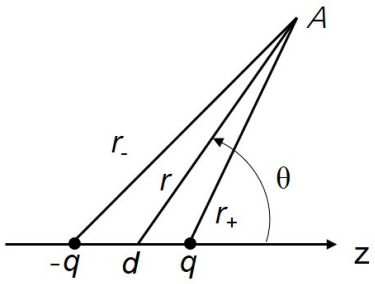

Figure 2.2: *The diagram of an electric dipole.*

In the $\lim(d \to 0)$, the potential becomes:

$$\Phi = \frac{p\cos\theta}{4\pi\varepsilon_h r^2}. \tag{2.53}$$

Let us compare this result with the potential Φ_2 in the exterior of the sphere as given by Eq. (2.51). Φ_2 is the sum of the applied uniform field and the field of an ideal dipole at the origin. with the dipole moment:

$$\mathbf{p} = 4\pi\varepsilon_0 r_0^3 \frac{\varepsilon_p - \varepsilon_h}{\varepsilon_p + 2\varepsilon_h}\mathbf{E}_0. \tag{2.54}$$

Combining with Eq. (2.23), the polarizability of the nanoparticle is

$$\alpha = 4\pi\varepsilon_0 r^3 \frac{\varepsilon_p - \varepsilon_h}{\varepsilon_p + 2\varepsilon_h}. \tag{2.55}$$

This equation can be used to analyze the response of a nanoparticle to an applied uniform electric field. Note that the field in the nanoparticle is uniform and we can replace this nanoparticle with an ideal dipole as long as it satisfies a constraint $2\pi n r_0/\lambda \ll 1$, where n is the imaginary part of the refractive index of the nanoparticle[11].

2.2.3. THE FOCAL FIELD WITH THE VECTORIAL DIFFRACTION THEORY

The equilibrium position of optical trapping in three orthogonal directions is established through the intricate interplay between the gradient force and the scattering force. Within the equation governing the time-averaged force, the focused optical field assumes a paramount role. This is because the gradient force is directly proportional to the gradients of the electric field intensity, while the scattering force correlates with the Poynting vector of the electromagnetic field, as outlined in Eq. (2.40). To achieve stable optical trapping of nanoparticles along all three dimensions, it is imperative to have a

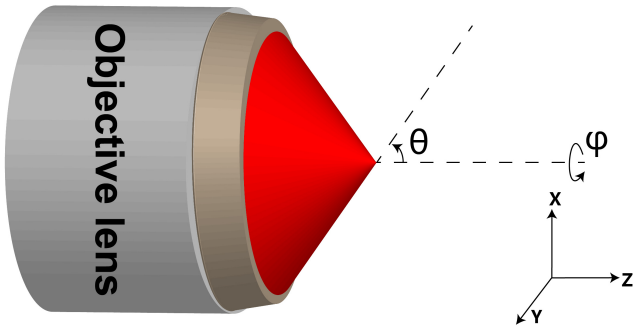

Figure 2.3: *The geometrical representation of the focused incident beam and definition of the coordinates system.*

steep distribution of field intensity gradients, which counters the scattering force[18]. This specific optical field configuration can be realized by employing an objective lens with a high numerical aperture (NA). Such a lens facilitates the formation of a focal spot with a diffraction-limited size, thereby ensuring the stringent conditions necessary for stable optical trapping.

In typical setups, the objective lens of a microscope has a relatively large pupil with a diameter of several millimeters. As a result of this large aperture, it is reasonable to only apply the paraxial approximation to describe the incident beam. In this approximation, we assume that the incident beam is entirely polarized along the x-direction, denoted as $\mathbf{E}_{\text{inc}} = E_{\text{inc}}\mathbf{n}_x$. Additionally, it's assumed that the lens used in the setup has a high transmission coating, and the Fresnel transmission coefficients equal 1.

The schematic diagram of the focus of the optical field is shown in Figure. 2.3. θ is the divergence angle of the conjugate ray. φ is the azimuthal angle on the XOY plane. f is the focal length of the lens. Assuming that the incident electric field has a fundamental Gaussian beam $E_{\text{inc}} = E_0 \exp(-f^2 \sin^2\theta / w_0^2)$, the size of the focal field $\mathbf{E}$ will depend on the radius of incoming beam w_0 relative to the size of the lens. We define the *filling factor* f_0 as

$$f_0 = w_0 / f \sin\theta_{\max}, \tag{2.56}$$

where $\theta_{\max}$ is determined by the NA of the objective lens and the real part of the refractive index of the composite material as $\theta_{\max} = \arcsin(\text{NA}/\text{Re}\{\mathbf{n}_{\text{h}}\})$. According to the vector diffraction theory, the angular spectrum expression of the focal field is in terms of cylindrical coordinates ($\rho = \sqrt{x^2 + y^2}$, φ, z) with origin at the focal point, given by

[19, 20]:

$$\mathbf{E} = E_{\text{inc}} \begin{bmatrix} I_{00} + I_{02}\cos(2\varphi) \\ I_{02}\sin(2\varphi) \\ -2iI_{01}\cos(\varphi) \end{bmatrix}, \tag{2.57}$$

$$\mathbf{H} = \frac{E_{\text{inc}}}{Z_{\mu\varepsilon}} \begin{bmatrix} I_{02}\sin(2\varphi) \\ I_{00} - I_{02}\cos(2\varphi) \\ -2iI_{01}\sin(\varphi) \end{bmatrix}, \tag{2.58}$$

where,

$$I_{00} = \int_0^{\theta_{max}} l(\theta)\sin\theta(1+\cos\theta)J_0(k\rho\sin\theta)\exp(ikz\cos\theta)d\theta, \tag{2.59}$$

$$I_{01} = \int_0^{\theta_{max}} l(\theta)\sin^2\theta J_1(k\rho\sin\theta)\exp(ikz\cos\theta)d\theta, \tag{2.60}$$

$$I_{02} = \int_0^{\theta_{max}} l(\theta)\sin\theta(1-\cos\theta)J_2(k\rho\sin\theta)\exp(ikz\cos\theta)d\theta, \tag{2.61}$$

with,

$$l(\theta) = \frac{ikf}{2\pi}\exp(-ikf)(\mathbf{n}_{\text{h}}\cos\theta)^{\frac{1}{2}}\exp\left(\frac{-f^2\sin^2\theta}{w_0^2}\right), \tag{2.62}$$

where $Z_{\mu\varepsilon}$ is the wave impedance of the medium: where $Z_{\mu\varepsilon} = \sqrt{(\mu_0\mu)/(\varepsilon_0\boldsymbol{\varepsilon}_{\text{h}})}$ and J_n is n^{th}-order of the Bessel function of the first kind. The relation between the average power of the incident light P and the amplitude of the incident light is $|E_{\text{inc}}|^2 = 4P/(\pi w^2\varepsilon_0 c)$. Therefore, we can analytically calculate the distribution of the focused electromagnetic field using the above equations.

According to the derived time-averaged optical force equation Eq. (2.40), stable optical trapping of a nanoparticle is the consequence of the interplay of different factors. When analyzing optical trapping, several factors are taken into account, including the size of gold nanoparticles, the wavelength of the incident light, and the impact of Brownian motion[21–23]. Take gold nanoparticles as an example, we are going to discuss the effect of variable factors on stable optical trapping. In addition to the factors mentioned earlier, we will also explore the effect of the volume fraction of the sample in a liquid environment on the optical trapping of gold nanoparticles.

Based on the vectorial diffraction theory and time-averaged force equation of Rayleigh nanoparticles, a simulation of the optical trapping of metallic nanoparticles is shown here. We fixed the average power of the incident light at 500 mW in the simulation. An objective with a high NA (NA = 0.9) is selected to focus the incident light. An x-polarized Gaussian beam is focused into a nanoparticle solution which is made of gold nanoparticles dispersed in water. The radius of the nanoparticle r_0 is set to 30 nm. The wavelength

of incident light λ is 800 nm in vacuum. $\theta_{\max}$ is determined by the NA of the objective lens as $\theta_{\max} = \arcsin(\mathrm{NA}/n_h)$, and that of the surrounding water is $n_h = 1.333$ [24]. We set the filling factor $f_w = 1$. At this wavelength, the relative permittivity of the gold nanoparticles is $\varepsilon_p = -24.061 + 1.5068\mathrm{i}$ [25].

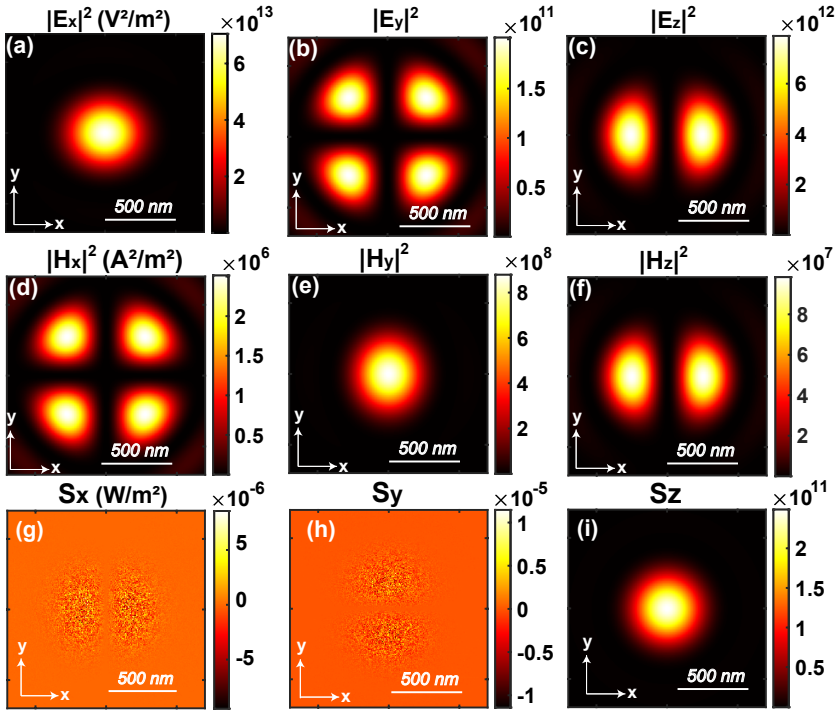

Figure 2.4: *Plots of three components of the electromagnetic field of an x-polarized focused Gaussian beam on the XOY plane. The wavelength of the incident beam is 800 nm. The NA of the objective is 0.9. The host medium is water (n_h = 1.33). (a) - (c) show the magnitudes of the individual field components $|E_x|^2, |E_y|^2, and |E_z|^2$ in the focal plane, respectively. (d)-(f) The intensities of individual components of the magnetic field $|H_x|^2, |H_y|^2, and |H_z|^2$ in the focal plane, respectively. (g)-(i) The three components of time-average Poynting vector $\langle S \rangle$ in the focal plane.*

Figure. 2.4 shows the distributions for the focused electromagnetic field on the focal plane (XOY plane). The vectorial focused electric field $\mathbf{E}$ is marked as $\mathbf{E} = (E_x, E_y, E_z)$ in Cartesian coordinates. The distribution of the squared moduli of the three components of the focused electric fields is calculated with the parameters in the caption shown in Figure. 2.4 (a), (b), and (c), respectively. The x-component of the electric field dominates the total electric field. As can be seen in Figure. 2.4 (c), $\mathrm{Max}|E_z|^2/\mathrm{Max}|E_x|^2 = 0.12$ which indicates that an appreciable amount of the electric field amplitude is in the longitudinal field. Using the Eq. (2.58), three magnetic field components focused on the focal plane

are also calculated and shown in Figure. 2.4 (d)-(f).

The Poynting vector in the focal plane (x-y plane) is also shown in Figure. 2.4. As can be seen in Figure. 2.4 (g) and (h), the magnitude of the Poynting vector along the x-direction and y-direction are almost zero in the focal plane. Figure. 2.4 (i) shows that the z component of the Poynting vector dominates the total Poynting vector. By substituting each set of $|\mathbf{E}|^2$ and $\mathbf{S}$ into Eq. (2.40), the time-averaged force exerted on the gold nanoparticle is obtained. For a comprehensive analysis, the three components of the optical forces on a dipole are discussed in the next section.

2.2.4. THE EFFECT OF VOLUME FRACTION ON OPTICAL TRAPPING

Optical trapping of gold nanoparticles in liquids has made significant progress since its first report in 1994 [6], including the extension of the nanoparticle size to diameters from 5 to 250 nm [22], and even controlling the orientation of nanorods [26, 27]. However, due to the strong scattering force and the unavoidable Brownian motion in the water, it is challenging to achieve stable optical trapping of gold nanoparticles with a radius ranging between 1 and 50 nm [28].

Quantitative analysis of the optical force is crucial for optimizing the stability of optical trapping. Stable optical trapping is the consequence of the interplay of different factors. The optical forces depend highly on the size of the particle. When the particle size is smaller than, or of the order of the skin depth of the gold, experiments show that the gradient force is proportional to the polarized volume of the particle [29]. When the radius is significantly larger than the skin depth of the gold for a given wavelength, the gradient force increases slowly because of the attenuation of the incident field in the particle. An increase in the size of the nanoparticle also leads to a larger extinction cross-section, which results in an enlargement of the radiation force.

In addition to the previously mentioned factors, there is an aspect that has not yet been explored in the optical trapping of gold nanoparticles: the effect of the sample's volume fraction, especially in aqueous environments. In practical biological experiments, it is common to encounter high-concentration aqueous solutions containing various biological samples. In practical biological experiments, the presence of aqueous solutions with high concentrations of bio-samples is inevitable[30, 31]. Therefore, it becomes essential to investigate the theoretical influence of the sample's volume fraction on the stability of optical trapping when dealing with gold nanoparticles in diverse solutions. This study includes various solutions such as gold nanoparticles, human serum albumin, and HIV-1 virus solutions.

The effective refractive index of the composite material is analyzed for three differ-

ent sample solutions. For the dispersal of metal Rayleigh nanoparticles in a liquid, the Maxwell-Garnett (MG) mixing rule can be used to describe the equivalent permittivity of a composite medium. The effective permittivity can be written as [32]

$$\boldsymbol{\varepsilon}_{\text{eff}} = \varepsilon_{\text{h}} \left[1 + 3f\Gamma \left(1 + \text{i}\frac{2}{3}(kr_0)^3\Gamma \right) \right], \tag{2.63}$$

$$\Gamma = \frac{\chi}{1-\chi f}, \quad \chi = \frac{(\varepsilon_{\text{p}} - \varepsilon_{\text{h}})}{(\varepsilon_{\text{p}} + 2\varepsilon_{\text{h}})}. \tag{2.64}$$

where $\boldsymbol{\varepsilon}_{\text{eff}}$ is the effective permittivity of the liquid containing the particles and f ($f = 4\pi N r_0^3/3V$) is the volume fraction of the gold nanoparticle in the solution and N is the number of nanoparticles in a volume V. Eq. (2.63) is called the MG mixing rule. The radius of the gold particle is 15 nm in our simulation.

HIV-1 virus with a radius of 50 nm [33] is selected as the large biosample (non-Rayleigh particle) in our simulations. The simple mixing rule is often used in biology applications without considering the shape of the inclusions and the topology of the composite material [34]. The effective refractive index can be obtained as a function of volume fraction f:

$$n_{\text{eff}} = n_{\text{p}} f + (1-f) n_{\text{h}}. \tag{2.65}$$

where n_{eff} is the effective refractive index of the composite material, n_p is the refractive index of the sample, n_h is the refractive index of the host medium.

Human serum albumin with a radius of 2.74 nm [35] is used as a biosample (dipole) in our simulation. For the composite medium consisting of a small sample and liquid, such as protein solution or DNA solution, we introduce the extended Lorenz-Lorenz equation[36]:

$$\frac{{n_{\text{eff}}}^2 - 1}{{n_{\text{eff}}}^2 + 2} = f\frac{{n_{\text{p}}}^2 - 1}{{n_{\text{p}}}^2 + 2} + (1-f)\frac{{n_{\text{h}}}^2 - 1}{{n_{\text{h}}}^2 + 2}, \tag{2.66}$$

f is the volume fraction of the dipole in the solution.

2.2.5. THE OPTICAL FORCE ON A DIPOLE EMBEDDED IN A MEDIUM

We have deduced the effective refractive index of the mixture. It is necessary to extend the force equation Eq.(2.40) from a vacuum to a general medium.

We limit our study to non-magnetic materials. It is customary to distinguish between primary and secondary sources. A primary source is located far from other sources and is not affected by them. It is assumed to have known charge and current densities. Charges within the matter in motion respond to the Lorentz force from other charges and external sources, making them generally secondary charges.

The total electromagnetic field inside medium is the superposition of the fields radiated by the primary sources and the fields radiated by the oscillating dipoles that are

induced inside matter. The latter fields (secondary sources) vary at an atomic scale. Inside the matter with a polarization density **P**, the electric displacement **D** is defined by:

$$\mathbf{D} = \varepsilon_0 \mathbf{E} + \mathbf{P}. \tag{2.67}$$

In vacuum, $\mathbf{P} = 0$. Inside matter, the current and charge densities that correspond to the dipole density induced in medium is call secondary (s) current and charge densities:

$$\mathbf{J}_s = -i\omega\mathbf{P}, \tag{2.68}$$

$$\rho_s = -\nabla \cdot \mathbf{P}. \tag{2.69}$$

Both bound and free electrons contribute to these current and charge densities. The total source is the sum of the primary (p) and secondary (s) sources.The total source and current densities are thus

$$\rho = \rho_p + \rho_s = \rho_p - \nabla \cdot \mathbf{P}, \tag{2.70}$$

and

$$\mathbf{J} = \mathbf{J}_p + \mathbf{J}_s = \mathbf{J}_p - i\omega\mathbf{P}. \tag{2.71}$$

The current and densities of the primary source connected the continuity equation Eq. (**??**) become

$$\nabla \cdot \mathbf{J}_p = i\omega\rho_p. \tag{2.72}$$

By substituting Eq. (2.70) and Eq. (2.71) into the Maxwell equations in vacuum Eq. (2.1) to (2.4). Combing with Eq,(2.67) and $\mathbf{B} = \mu_0\mu\mathbf{H}$, the electromagnetic fields in medium satisfy the Maxwell equations:

$$\nabla \times \mathbf{E} = i\omega\mu_0\mu\mathbf{H}, \tag{2.73}$$

$$\nabla \times \mathbf{H} = -i\omega\mathbf{D} + \mathbf{J}_p, \tag{2.74}$$

$$\nabla \cdot \mathbf{D} = \rho_p, \tag{2.75}$$

$$\nabla \cdot \mathbf{B} = 0, \tag{2.76}$$

where **D** denotes the electric displacement, **B** is the magnetic induction, **J** and ρ denote current density and charge density. ε_0 and μ_0 are the permittivity and permeability of the vacuum, respectively. μ is the relative permeability of the matter. Here we assure the matter is non-magnetic and $\mu = 1$.

Take a homogeneous isotropic nanoparticle as an example. The polarization **P** is the average dipole moment per unit volume of the medium, which means the sum of the dipole moment vectors in a region(region, divided by the volume of that region.)[11].

Commonly, it is equal to zero if there are no external fields. The susceptibility χ represents how easily the medium can be polarized under the excitation by the total field. For linear medium, we have the relation:

$$\mathbf{P} = \varepsilon_0 \chi \mathbf{E}, \tag{2.77}$$

where χ is the electric susceptibility tensor. The relative electric permittivity tensor is

$$\boldsymbol{\varepsilon} = 1 + \chi. \tag{2.78}$$

For simplicity, $\boldsymbol{\varepsilon}$ is the complex relative permittivity of the matter. Hence we can rewrite the Eq.(2.67) as:

$$\mathbf{D} = \varepsilon_0 \mathbf{E} + \mathbf{P} = \varepsilon_0 \mathbf{E} + \varepsilon_0 (\boldsymbol{\varepsilon} - 1)\mathbf{E} = \varepsilon_0 \boldsymbol{\varepsilon} \mathbf{E}, \tag{2.79}$$

which gives

$$\nabla \times \mathbf{E} = i\omega\mu_0 \mathbf{H}, \tag{2.80}$$

$$\nabla \times \mathbf{H} = -i\omega\varepsilon_0 \boldsymbol{\varepsilon} \mathbf{E} + \mathbf{J}_p. \tag{2.81}$$

Consider an electromagnetic field $\mathbf{E}$, $\mathbf{H}$ in a medium, we have the Lorentz force exerted by fields on a dipole inside a volume V is :

$$\mathbf{F} = \int_V \mathbf{f}, \tag{2.82}$$

$$\mathbf{f} = \rho_s \mathbf{E} + \mathbf{J}_s \times \mathbf{B}. \tag{2.83}$$

Combing with Eq.(2.68) and Eq.(2.69), we have

$$\mathbf{f} = -\mathbf{E}(\nabla \cdot \mathbf{P}) + \frac{\partial \mathbf{P}}{\partial t} \times \mathbf{B}. \tag{2.84}$$

To derive the electromagnetic force acting on a dipole located at $\mathbf{r}_0$, we can introduce the dipole approximation between the polarization density $\mathbf{P}$ and dipole moment $\mathbf{p}$:

$$\mathbf{P} = \mathbf{p}\delta(\mathbf{r} - \mathbf{r}_0), \tag{2.85}$$

into the Lorentz force density $\mathbf{f}$.

In a linear medium the dipole moment $\mathbf{p}$ that is induced in an atom or a molecule is directly proportional to the so-called local electric field $\mathbf{E}$. This is the electric field acting on an atom or molecule due to both external (primary) sources and all secondary sources within the matter, excluding the atom or molecule itself. So we have

$$\mathbf{p} = \boldsymbol{\alpha} \mathbf{E}, \tag{2.86}$$

$$\boldsymbol{\alpha} = 4\pi\varepsilon_0 r^3 \frac{\boldsymbol{\varepsilon}_\mathrm{p} - \boldsymbol{\varepsilon}_\mathrm{h}}{\boldsymbol{\varepsilon}_\mathrm{p} + 2\boldsymbol{\varepsilon}_\mathrm{h}}, \tag{2.87}$$

where $\boldsymbol{\varepsilon_p}$ and $\boldsymbol{\varepsilon_h}$ denotes the complex permittivity of dipole-like nanoparticle and the complex permittivity of the host medium. We can deduce the force exerted on a dipole embedded in a medium:

$$\langle \mathbf{F} \rangle = \frac{1}{2}\mathrm{Re}\{\boldsymbol{\alpha}\}\mathrm{Re}\{\mathbf{E}^* \nabla \mathbf{E}\} + \frac{1}{2}\mathrm{Im}\{\boldsymbol{\alpha}\}\mathrm{Im}\{\mathbf{E}^* \nabla \mathbf{E}\}. \tag{2.88}$$

This is the optical force on a dipole embedded in a medium with the complex notation. In this chapter, we will discuss only linear conditions. Metallic nanoparticles can exhibit nonlinear effects when exposed to high-intensity fields. We will investigate these nonlinear effects in subsequent sections of the thesis.

2.3. CALCULATION RESULTS AND DISCUSSION

To achieve stable optical trapping of small gold nanoparticles, it is essential to employ a high-intensity focused beam that can generate a force significant enough to counteract the Brownian motion within the host medium. In this study, we utilize an x-polarized Gaussian beam with an average power of 500 mW as a beam which is focused by the lens. The refractive index of the HIV-1 virus is 1.5 at λ = 633 nm[33]. According to the experimental measurement[36], the refractive index of human serum albumin (HSA) solution is 1.603 when the wavelength of incident light λ is 589 nm.

The trapped gold nanoparticles can be treated as a probe in the gold nanoparticle solution. The refractive index of the gold nanoparticle is 0.274+2.94i at 589 nm and 0.183+3.43i at 633 nm in the HSA solution and protein solution[25]. An objective with a high NA (NA = 1.2) is selected to focus the incident light. $\theta_{\max}$ is determined by the NA of the objective lens and the real part of the refractive index of the composite material as $\theta_{\max} = \arcsin(\mathrm{NA}/\mathrm{Re}\{\mathbf{n}_{\mathrm{eff}}\})$.

The effective refractive index (n_{eff}) of the composite material with a volume fraction from low to high is calculated using Eq.(2.63) - (2.65). Fig. 2.5 plots the real and imaginary parts of the refractive index of three composite materials colored blue and red, respectively. In practice, the gold nanoparticle solution is highly dilute in the optical trapping experiment. Therefore, the volume fraction of the gold nanoparticle f is set from 0 to 0.05 in our simulation, as shown in Fig. 2.5 (a). The blue line represents the real part of the refractive index of the gold nanoparticle solution below the red line (imaginary part). Note that our force equation for a dipole is derived in a non-absorbing environment. The red line in Fig. 2.5 (a) represents an environment with an absorption property at an order of magnitude of ten to the power of minus 2. Therefore, we can disregard the minor difference. The refractive index of the virus and protein solution are real. Both the volume fraction of the virus solution f_1 and the protein solution f_2 are set from 0 to 0.5,

as shown in Fig. 2.5 (b) and (c).

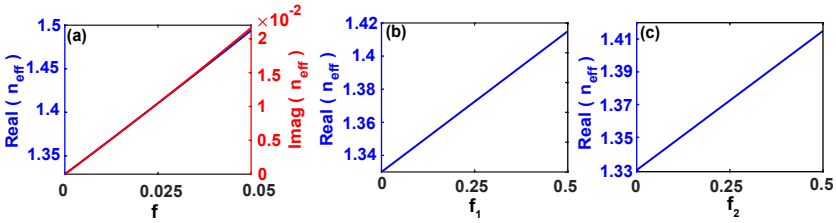

Figure 2.5: *Comparison in the effective refractive index of three composite media: (a) gold nanoparticle solution at λ = 633 nm, (b) Virus solution (HIV-1 virus) at λ = 633 nm, and (c) protein solution (human serum albumin) at λ =589 nm. The real and imaginary parts of the refractive index are plotted by the blue line and red line. The surrounding environment is water.*

Fig. 2.6 shows the distribution of optical forces along the x-axis on the gold sphere with a radius of 15 nm in three different solutions and for three volume fractions. The first solution investigated is the gold nanoparticle solution itself with an incident wavelength of 633 nm. Fig. 2.6 (a), (d), and (g) show the gradient force, scattering force, and potential, respectively, along the x-axis with volume fractions of $f = 0.000$, $f = 0.025$, and $f = 0.05$ (black, red, and blue colors, respectively). In Fig. 2.6 (a), gradient forces along the x-axis are shown as an odd function of x for different values of the volume fraction, while the scattering forces are negligible on the focal plane, as shown in Fig. 2.6 (d). The positive sign indicates force toward the x-axis, while the negative sign indicates force away from the x-axis. Fig. 2.6 (g) shows the potential with four-volume fractions along the x-axis. Although all the depth of the potential well exceeds 10 $k_B T$, the decrease in the depth of the potential well shows the reduction of the stability of optical trapping as the volume fraction is increased. Next, the optical trapping in the virus solution is investigated based on the gold nanoparticle solution, as shown in Fig. 2.6 (b), (e), and (h) with volume fractions of $f_1 = 0$, $f_1 = 0.25$, and $f_1 = 0.5$ (black, red, and blue colors, respectively). The calculation results show that the optical forces and potentials of a gold nanoparticle in the virus solution decrease along the x-axis as the volume fraction increases. Finally, the optical forces and potential depth of the potential wells in the protein solution are shown for the optical trapping of a gold nanoparticle with an incident wavelength of 589 nm in Fig. 2.6 (c), (f), and (i) with volume fractions of $f_2 = 0$, $f_2 = 0.25$, and $f_2 = 0.5$ (black, red, and blue colors, respectively).

The optical forces which its direction along the y-axis are shown in Fig. 2.7 (a)-(f). The gradient forces on a gold nanoparticle in the gold nanoparticle solution, virus solution, and protein solution are plotted with different volume fractions, as shown in Fig. 2.7 (a), (b), and (c). In the virus solution and the protein solution, the black, red, and blue color

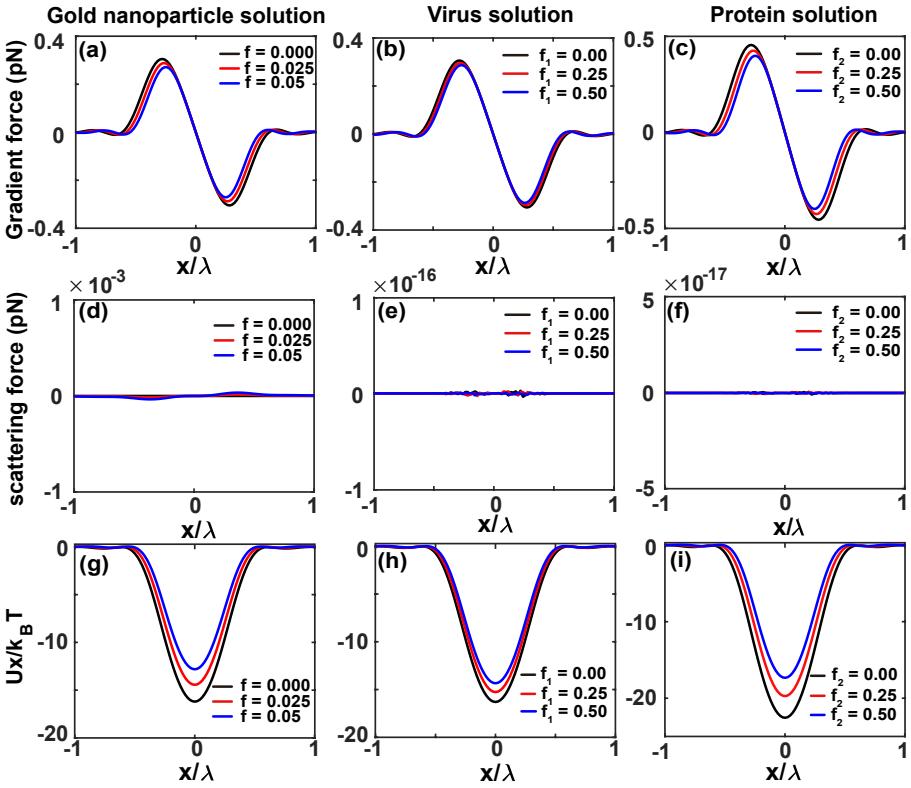

Figure 2.6: *Distribution of optical forces and potentials on a gold particle with 15 nm radius along the x-axis. (a) the gradient force in the gold nanoparticle solution, (d) the scattering force, and (g) the corresponding optical potential. The black, red, and blue denote the volume fraction of the gold nanoparticle $f = 0.000$, $f = 0.025$, and $f = 0.05$, respectively. (b), (e) and (h) plot the gradient force, the scattering force, and the potential in the virus solution. The black, red, and blue colors denote the volume fraction $f_1 = 0$, $f_1 = 0.25$, and $f_1 = 0.5$. For the protein solution, the optical force and potentials are illustrated in (c), (f), and (i). Its volume fraction f_2 is set to 0, 0.25, and 0.5, respectively.*

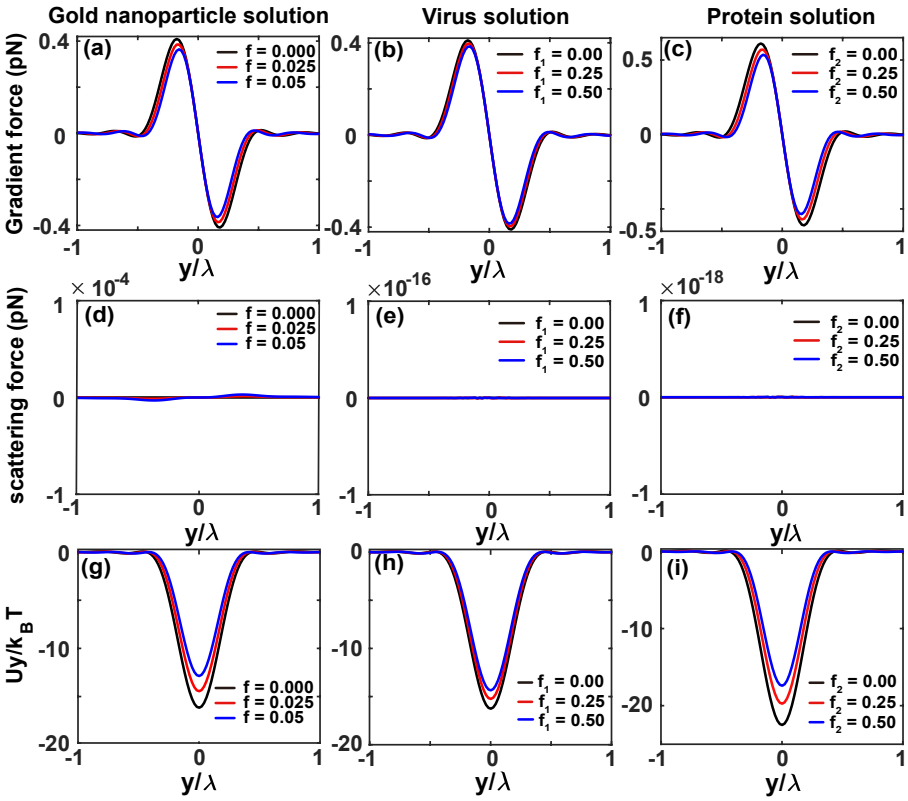

Figure 2.7: *The optical force and the potential along the y-axis for a gold nanoparticle with a radius of 15nm. (a), (b) and (c) show the gradient force for different values of the volume fraction along the y-axis in gold nanoparticle solution, virus solution, and protein solution, respectively. (d), (e), and (f) plot the scattering force. The corresponding potential along the y-axis in three composite materials is shown in (g), (h), and (i).*

indicate the volume fraction f = 0, f = 0.25, and f = 0.5, respectively. The scattering forces in three composite materials are plotted in (d), (e), and (f). The potential along the *y*-axis is shown in Fig. 2.7 (g), (h), and (i). All optical forces and potentials decrease along the *y*-axis with an increasing volume fraction. Fig. 2.6 and Fig. 2.7 demonstrate that the focal point (0,0) is a position for the stable trapping of a gold nanoparticle in the transverse plane.

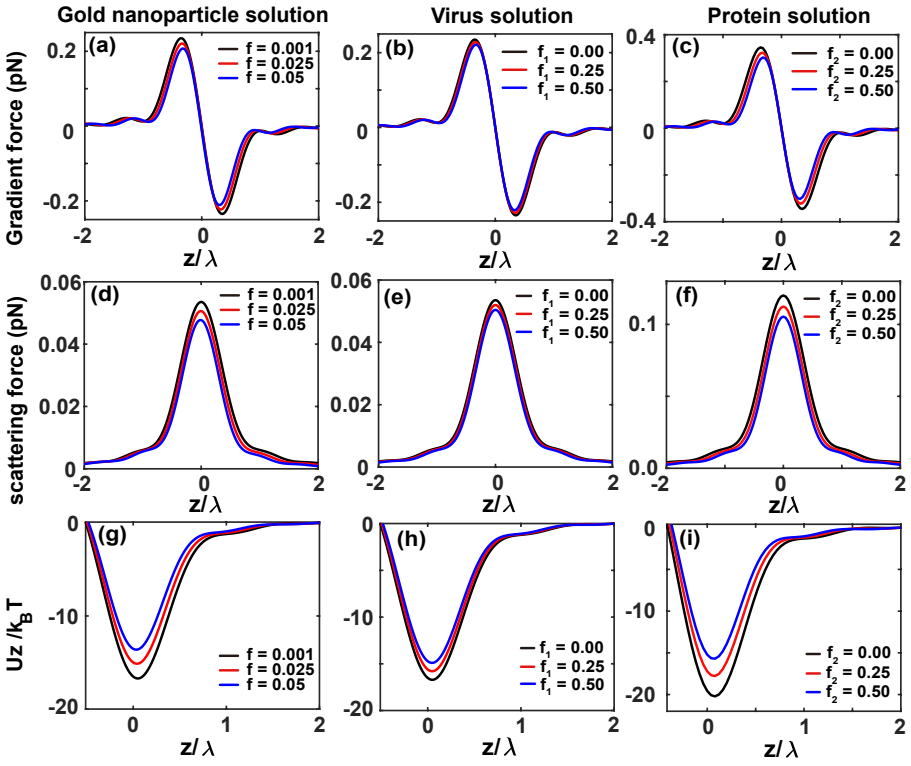

Figure 2.8: *Distribution of gradient, scattering forces, and potentials along the z-axis in three composite materials. (a)-(c) Gradient forces in gold nanoparticle solution, virus solution, and protein solution. (d)-(f) Scattering forces in three solutions. (g)-(i) Optical potentials along the z-axis in three solutions.*

For the forces whose direction along the optical axis (*z*- axis), $\langle \mathbf{F} \rangle_{\text{grad}}$ and $\langle \mathbf{F} \rangle_{\text{scatter}}$ are calculated. The positive sign indicates the force towards the *z*-axis, while the negative sign indicates the force away from the *z*-axis. In Fig. 2.8 (a)-(c), the magnitude of the gradient force decreases as the volume fraction increases from low to high. Similarly, the scattering force also decreases when the volume fraction increases, but always points toward the positive direction of the *z*-axis, as shown in (d), (e), and (f). The magnitude of

the radiation force along the z-axis is several orders larger than the force along the x- and y-axes because the energy flux mainly propagates along the z-axis, as shown in Fig. 2.4. $\langle \mathbf{F} \rangle_{\text{total}}$ is the sum of the gradient force and scattering force. The optical potential well is obtained by Eq. (2.45) for three volume fractions and are shown along the z-axis, as can be seen in Fig. 2.8 (g), (h), and (i). The equilibrium position of the optical trapping is only slightly away from the focal plane, as shown in Fig. 2.8 (g), (h), and (i). Therefore, the impact of this displacement of the particle away from the focal point on the trapping stiffness is negligible. Based on the calculations presented in Fig. 2.6, Fig. 2.7, and Fig. 2.8, it is evident that stable optical trapping can be effectively achieved in three dimensions. This is supported by the depth of the potential well exceeding 10 $k_B T$ along the x-, y-, and z-axis. Furthermore, these results emphasize the critical role played by the sample's volume fraction in influencing the stability of optical trapping within the composite medium. As the volume fraction increases, both the gradient force and potential depth decrease, resulting in reduced stability of optical trapping. Therefore, when optimizing conditions for optical trapping, careful consideration of the sample's volume fraction is essential.

2.4. CONCLUSION

To summarize, our approach in this chapter begins with an introduction to the classical method used to calculate the time-averaged optical force acting on a dipole, without involving nonlinear effects. We combine Maxwell's equations with the Lorentz force law and provide a comprehensive step-by-step derivation of the time-averaged force equation. We also apply the concept of the polarizability of a dipolar sphere to characterize how the dipole responds to an external optical field, employing the dipole approximation theory. Additionally, we delve into the calculation of the tightly focused field generated by an x-polarized beam, employing the vectorial diffraction theory.

In Section 2.3, we obtain the distribution of optical field gradients of the tightly focused field. The effect of volume fraction on optical force and potential is also analytically investigated based on dipole-approximation of the nanoparticle. The correlation between the effective refractive index of the composite material and the volume fractions from low to high is presented for the gold nanoparticle solution, the HIV-1 solution, and the human serum albumin solution. The time-averaged force is calculated on a gold nanoparticle with a radius of 15 nm along three orthogonal directions at three different volume fractions. The optical potential is studied comparatively for a given incident power. The stability of the optical trapping is strong enough to allow a gold nanoparticle to remain trapped in three composite materials for a long time.

Remarkably, the results of our calculations show robust stability in optical trapping, indicating that the gold nanoparticles could remain trapped within the three composite materials for extended durations. We observe that as the volume fraction increases, the depth of the potential well decreases. Consequently, achieving stable optical trapping became more challenging at higher volume fractions within the sample solution. The insights gained from this model offer valuable theoretical support for enhancing the efficiency of optical trapping techniques involving gold nanoparticles in a wide range of applications.

REFERENCES

[1] K. Dholakia and T. Čižmár, *Shaping the future of manipulation,* Nature photonics **5**, 335 (2011).

[2] C. Keir, Neuman, Attila, and Nagy, *Single-molecule force spectroscopy: optical tweezers, magnetic tweezers and atomic force microscopy.* Nature methods (2008), https://doi.org/10.1038/nmeth.1218.

[3] Y. Yu, T.-H. Xiao, Y. Wu, W. Li, Q.-G. Zeng, L. Long, and Z.-Y. Li, *Roadmap for single-molecule surface-enhanced raman spectroscopy,* Advanced Photonics **2**, 014002 (2020).

[4] E. J. Bjerneld, F. Svedberg, and M. Käll, *Laser-induced growth and deposition of noble-metal nanoparticles for surface-enhanced raman scattering,* Nano Letters **3**, 593 (2003).

[5] X. Huang, P. K. Jain, I. H. El-Sayed, and M. A. El-Sayed, *Gold nanoparticles: interesting optical properties and recent applications in cancer diagnostics and therapy,* Nanomedicine **2**, 681 (2007).

[6] K. Svoboda and S. M. Block, *Optical trapping of metallic Rayleigh particles,* Optics Letters **19**, 930 (1994).

[7] S.-J. Park, T. A. Taton, and C. A. Mirkin, *Array-based electrical detection of dna with nanoparticle probes,* Science **295**, 1503 (2002).

[8] J. S. Lee, P. A. Ulmann, M. S. Han, and C. A. Mirkin, *A dna-gold nanoparticle-based colorimetric competition assay for the detection of cysteine.* Nano Letters **8**, 529 (2008).

[9] P. Yupapin, Aziz, N. Suwanpayak, Ma, Jalil, Saktioto, and Ali, *Gold nanoparticle trapping and delivery for therapeutic applications,* International Journal of Nanomedicine **7**, 11 (2012).

[10] N. Wangoo, C. R. Suri, and G. Shekhawat, *Interaction of gold nanoparticles with protein: A spectroscopic study to monitor protein conformational changes,* Applied Physics Letters **92**, 1323 (2008).

[11] C. F. Bohren and D. R. Huffman, *Absorption and scattering of light by small particles* (John Wiley & Sons, 2008).

[12] J. P. Gordon, *Radiation forces and momenta in dielectric media,* Phys. Rev. A **8**, 14 (1973).

[13] S. Albaladejo, M. I. Marqués, M. Laroche, and J. J. Sáenz, *Scattering forces from the curl of the spin angular momentum of a light field,* Phys. Rev. Lett. **102**, 113602 (2009).

[14] O. Maragò, P. H. Jones, P. G. Gucciardi, G. Volpe, and A. C. Ferrari, *Optical trapping and manipulation of nanostructures,* Nature Nanotechnology **8**, 807 (2013).

[15] P. C. Chaumet and M. Nieto-Vesperinas, *Time-averaged total force on a dipolar sphere in an electromagnetic field,* Opt. Lett. **25**, 1065 (2000).

[16] A. Devi and A. K. De, *Theoretical investigation on nonlinear optical effects in laser trapping of dielectric nanoparticles with ultrafast pulsed excitation,* Optics Express **24**, 21485 (2016).

[17] C. Min, Z. Shen, J. Shen, Y. Zhang, H. Fang, G. Yuan, L. Du, S. Zhu, T. Lei, and X. Yuan, *Focused plasmonic trapping of metallic particles,* Nature communications **4**, 1 (2013).

[18] K. C. Neuman and S. M. Block, *Optical trapping,* Review of Scientific Instruments **75**, 2787 (2004).

[19] J. Braat and P. Török, *V. s. ignatowsky: Diffraction by a lens of arbitrary aperture,* in *Imaging Optics* (Cambridge University Press, 2019) p. 919–944.

[20] B. Richards and E. Wolf, *Electromagnetic diffraction in optical systems, ii. structure of the image field in an aplanatic system,* Proceedings of the Royal Society of London. Series A. Mathematical and Physical Sciences **253**, 358 (1959).

[21] P. V. Ruijgrok, N. R. Verhart, P. Zijlstra, A. L. Tchebotareva, and M. Orrit, *Brownian Fluctuations and Heating of an Optically Aligned Gold Nanorod,* Phys. Rev. Lett. **107**, 037401 (2011).

[22] F. Hajizadeh and S. S.Reihani, *Optimized optical trapping of gold nanoparticles,* Opt. Express **18**, 551 (2010).

[23] L. Huang, H. Guo, J. Li, L. Ling, B. Feng, and Z.-Y. Li, *Optical trapping of gold nanoparticles by cylindrical vector beam,* Optics Letters **37**, 1694 (2012).

[24] G. M. Hale and M. R. Querry, *Optical constants of water in the 200-nm to 200-µm wavelength region,* Appl. Opt. **12**, 555 (1973).

[25] P. B. Johnson and R. W. Christy, *Optical Constants of the Noble Metals,* Phys. Rev. B **6**, 4370 (1972).

[26] Y. Qin, L.-M. Zhou, L. Huang, Y. Jin, H. Shi, S. Shi, H. Guo, L. Xiao, Y. Yang, C.-W. Qiu, *et al.*, *Nonlinearity-induced nanoparticle circumgyration at sub-diffraction scale,* Nature communications **12**, 1 (2021).

[27] L.-M. Zhou, Y. Shi, X. Zhu, G. Hu, G. Cao, J. Hu, and C.-W. Qiu, *Recent progress on optical micro/nanomanipulations: Structured forces, structured particles, and synergetic applications,* ACS Nano **16**, 13264 (2022).

[28] O. M. Maragò, P. H. Jones, P. G. Gucciardi, G. Volpe, and A. C. Ferrari, *Optical trapping and manipulation of nanostructures,* Nature nanotechnology **8**, 807 (2013).

[29] P. M. Hansen, V. K. Bhatia, N. Harrit, and L. Oddershede, *Expanding the Optical Trapping Range of Gold Nanoparticles,* Nano Letters **5**, 1937 (2005).

[30] M. Friebel and M. C. Meinke, *Determination of the complex refractive index of highly concentrated hemoglobin solutions using transmittance and reflectance measurements,* Journal of Biomedical Optics **10**, 064019 (2005).

[31] V. V. Tuchin *et al.*, *Tissue optics,* (Society of Photo-Optical Instrumentation Engineers (SPIE) Bellingham, WA, USA, 2015).

[32] A. Acevedo-Barrera and A. Garcia-Valenzuela, *Analytical approximation to the complex refractive index of nanofluids with extended applicability,* Opt. Express **27**, 28048 (2019).

[33] O. Block, A. Mitra, L. Novotny, and C. Dykes, *A rapid label-free method for quantitation of human immunodeficiency virus type-1 particles by nanospectroscopy,* Journal of virological methods **182**, 70 (2012).

[34] T. Vo-Dinh, *Biomedical photonics handbook: biomedical diagnostics* (CRC press, 2014).

[35] M. Kiselev, G. IuA, G. Dobretsov, and M. Komarova, *Size of a human serum albumin molecule in solution,* Biofizika **46**, 423 (2001).

[36] T. L. McMeekin, M. L. Groves, and N. J. Hipp, *Refractive indices of amino acids, proteins, and related substances,* (ACS Publications, 1964) pp. 54–66.

3

THE OPTICAL TRAPPING OF METALLIC NANOPARTICLES IN NONLINEAR REGIME

How many roads must a man walk down;
Before they call him a man.

Bob Dylan

Some original content of this chapter has been submitted in *Chinese Optics Laser*.

Chapter 2 serves as an introduction to the classical theory extensively employed for calculating the optical force acting on Rayleigh metallic particles within a linear regime. However, in 2010, a groundbreaking discovery emerged in the field of optical trapping, known as the "trap split" phenomenon. This discovery posed a formidable challenge to our established understanding of physics [1]. The "trap split" phenomenon is an intriguing and enigmatic occurrence that holds the potential to revolutionize the manipulation of nanoparticles. It surpasses the constraints imposed by the diffraction limit, opening up exciting new possibilities for scientific exploration within the nonlinear realm of optical trapping.

Yet, the scalar method, which has proven to be both convenient and effective in traditional optical trapping, can not adequately represent the nonlinear response of metal nanoparticles to external optical fields. Consequently, there arises a need to extend our theoretical framework to accommodate the nonlinear regime.

In response to this challenge, in this chapter, we propose a theoretical model that elucidates the nonlinear optical trapping effects through the application of the vector method. By amalgamating the principles of vectorial diffraction theory with optical nonlinear effects, we derive a vectorial method for calculating the nonlinear response of the nanoparticle to the tightly focused field. This model facilitates a quantitative analysis of optical force equations and optical potential wells. Furthermore, we undertake a comparative analysis between the results obtained using the scalar method and those derived through the vector method, ultimately revealing that the latter demonstrates superior alignment with experimental observations. In light of these findings, we conclude that this vector method offers a promising avenue for studying deeper into the quantitative analysis of nonlinear optical force and optical potential.

3.1. INTRODUCTION

A widely accepted consensus in the field of optical trapping was that when subwavelength particles were trapped just using a single linear-polarized focused beam, only one optical potential well could be observed. This understanding has persisted for several decades since the invention of optical tweezers [2–4]. Nonlinear optical trapping introduces an intriguing and unconventional phenomenon known as the "trap split." This phenomenon defies traditional optical trapping expectations by allowing the observation of two distinct trapping sites. It occurs when the third-order nonlinear effect of dipolar gold nanoparticles is stimulated, leading to this remarkable "trap split" phenomenon [1]. The adjustable distance between two spaced trapping positions can reach beyond the diffraction limit of the focus field without any other complex opti-

cal instruments [5–8]. The tunable gap of trapped particles and stable manipulation of multiple nanoparticles thereby provide new opportunities for the application in atomic and molecular trapping [9], micro-fluid mechanics [10] and bio-medicine[11] at the sub-diffraction-limit scale. Therefore, a comprehensive and quantitative analysis of nonlinear optical trapping is urgently needed.

For particles with radii much smaller than the wavelength of the incident light, they can effectively be represented as dipoles. [12, 13].The dipole approximation theory is a commonly employed framework for calculating both radiation and gradient forces in such scenarios [14–18]. Considering a homogeneous and isotropic dipolar particle immersed in an aqueous medium and illuminated by an electromagnetic field, scalar polarizability can be used to describe the response of the dipole to the external optical field in the linear regime[12].

In the linear regime, the gradient force arises due to the interaction between the electric dipole moment of the particle and the gradients in optical intensity and this force is proportional to the real part of the polarizability[14]. Conversely, the radiation force, which results from the radiation and absorption of light by the particle, is proportional to the imaginary part of the polarizability.[15]. However, the scalar method is insufficient to fully comprehend the nonlinear effects in the gradient force and potential well. This raises questions about whether scalar polarizability can adequately reflect the nonlinear response of the dipole to the external field. To address these questions and challenges, we expand upon the traditional approach and demonstrate that employing the vector method offers a more accurate and complete description of nonlinear optical trapping effects. This vector method is better suited to unravel the intricacies of nonlinear interactions between particles and optical fields.

In this chapter, we embark on a comprehensive analysis of nonlinear gradient forces and radiation forces that come into play when a nanoparticle interacts with tightly focused laser pulses. Our approach utilizes a focused linear-polarized pulse laser as the light source to achieve high optical intensity and a 30 nm radius gold nanoparticle as the modeled particle. When subjected to illumination from a high-NA objective lens, this configuration triggers the optical Kerr effect at a corresponding excitation level[19–21]. To describe the behavior of the gold nanoparticles accurately, we calculate their complex refractive index as a function of the incident electric field's intensity, relying on the Kerr-effect equations.

In our analysis, we take advantage of vectorial diffraction theory to dissect the tightly focused optical field into its individual three-dimensional components, each corresponding to one of the three orthogonal directions[22]. The vectorial polarizability of the

dipole emerges from the intricate interplay between the nonlinear optical properties of the dipole and the three components of the tightly focused field. Capitalizing on the principle of vectorial superposition, we formulate traditional gradient force equations along specific directions, utilizing the polarizability vector and the vectorial optical field. By integrating the total optical force in the focal plane, we obtain the corresponding nonlinear optical potential, which serves as a precise indicator of the equilibrium trapping position of the dipole.

A notable disparity becomes evident when comparing the potential well obtained through the scalar method with that derived through the vector method. While the model employing the scalar method fails to yield a definitive conclusion, the optical potential calculated using the vector method consistently situates the trapped particles along the axis parallel to the direction of linear polarization. The calculation results unequivocally establish that the vector approach closely aligns with experimental observations. This innovative method is effective not only in nonlinear optical trapping but also in the traditional method. It represents a significant stride towards achieving a deeper understanding of nonlinear optical trapping.

3.2. THE NONLINEAR OPTICAL PROPERTIES OF THE GOLD NANOPARTICLE

Supposing the incident laser is an x-polarized Gaussian beam, α is the polarizability of the nanosphere given by[14],

$$\alpha_0 = 4\pi\varepsilon_0 r_0^3 \frac{\mathbf{n}_p^2 - \mathrm{n}_h^2}{\mathbf{n}_p^2 + 2\mathrm{n}_h^2}, \quad \alpha = \frac{\alpha_0}{1 - i\alpha_0 k^3/(6\pi\varepsilon_h)}, \tag{3.1}$$

where the complex number $\mathbf{n}_p$ is the complex refractive index of the gold nanoparticle and $\mathrm{n_h}$ is the refractive index of the host medium. ε_0 is the relative permittivity of the vacuum. ε_h is the relative permittivity of the host medium. r_0 is the radius of the particle. c is the speed of light in a vacuum. k is the wave number of the incident optical field in the host medium. Here, σ is the extinction cross-section ($\sigma = \omega n_h \mathrm{Im}\{\alpha\}/c\varepsilon_0$)[23], with ω is the optical frequency of the incident light.

For metallic nanoparticles, especially, the absorption of light by the particle contributes significantly to the radiation force[24]. It is meaningful to discuss the absorption and the localized surface plasmon resonance (LSPR) effect during the optical trapping process. Here, we take the gold nanoparticle with a radius of 30 nm as an example. Its absorption (σ_{abs}), scattering (σ_{sca}), and extinction ($\sigma_{\mathrm{ext}} = \sigma_{\mathrm{abs}} + \sigma_{\mathrm{sca}}$) cross sections are calculated and plotted in Fig. 3.1(a). Clearly, the cross-sections mentioned above

exhibit a peak at approximately the Surface Plasmon Resonance (SPR) wavelength, typically around 510 nm for gold nanoparticles. It is noteworthy that close to the SPR wavelength, the absorption cross-section is much larger than the scattering cross-section. This means that the absorption of light caused by the SPR can create heating problems that may interfere with optical manipulation, which can disrupt optical manipulation processes[25]. This is especially problematic when working with gold nanoparticles and other metallic nanoparticles.

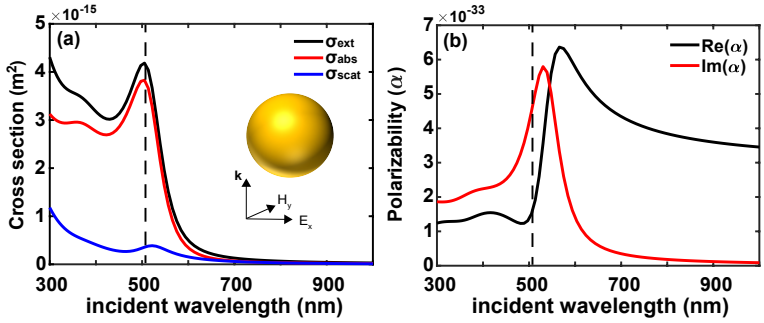

Figure 3.1: *(a) The cross-section of a gold nanoparticle with a 30 nm radius. The extinction cross-section (σ_{ext}), absorption cross-section (σ_{abs}), and scattering cross-section (σ_{sca}) are plotted as black, red, and blue lines, respectively. (b) The complex polarizability of the gold nanoparticle as a function of the incident wavelength.*

The gradient and radiation force follow the behavior of the real and imaginary parts of the polarizability, respectively. The magnitude of Im$\{\alpha\}$ is much larger than the magnitude of the real part Re$\{\alpha\}$ at the SPR wavelength, as shown in Fig. 3.1 (b). The gradient force exerted on the gold nanoparticle is comparatively smaller than the radiation force at the SPR wavelength [17], leading to a weak trapping stiffness of the gold nanoparticle. Therefore, we chose the near-infrared pulsed laser as the light source to stimulate the nonlinear optical effect and avoid the LSPR effect on the traps.

Gold nanoparticles have many nonlinear optical properties that generate great interest in applications, such as optical switches [26, 27], optical limiting devices [28], and nanoprobes [29]. The changes in the complex refractive index of the gold nanoparticle are described by the Kerr-effect equation: ($\mathbf{n} = \mathbf{n}_p + \mathbf{n}_2 \mathrm{I}$) [21, 30, 31], where I is the peak intensity of the focused field and $\mathbf{n}_2$ is the nonlinear complex refractive index.

To excite the nonlinear effect of the particle, it is highly desirable to focus the incident pulse laser with a high NA objective lens. In this work, we consider the incident optical field as an x-polarized femtosecond laser pulse. For a femtosecond laser pulse, the peak

power of a pulse is estimated from the pulse duration τ and the pulse energy $\mathcal{E}_{\text{pulse}}$.

$$P_{\text{peak}} \approx \gamma \frac{\mathcal{E}_{\text{pulse}}}{\tau} = \gamma \frac{P_{\text{ave}}}{\upsilon \tau}, \tag{3.2}$$

where γ is the factor depending on the temporal shape of the pulse and υ is the repetitive frequency of the pulse laser. P_{ave} is the average power of the pulsed laser. For the Gaussian shape pulse and soliton pulse, the factor is 0.94 and 0.88, respectively[32]. In this thesis, we assign the incident pulse in our analytical model to a rectangular temporal envelope and $\gamma = 1$. In this scenario, the strength of the pulse will remain steady over the pulse duration. The peak intensity of the incident beam can be expressed as $\mathrm{I} = 2P_{\text{peak}}/\pi r^2$ where the radius of the focal spot $r_{\text{spot}} = 0.82\lambda/\mathrm{NA}$ [33]. The maximum value of the modulus square of the total electric field $|E|^2 = 2\mathrm{I}/(\varepsilon_0 \mathrm{c} \mathrm{n_h})$, ε_0 is the permittivity of the vacuum. Then we will discuss the nonlinear optical properties of gold nanoparticles under such an incident optical field.

Supposing the incident average power P_{ave} increases gradually from 0 W to 0.5 W, the peak intensity of the focused field I_{peak} is plotted as a function of incident average power P_{ave} in Fig.3.2 (a). Here, the imaginary part of $\mathbf{n}_2$ is set as $-1.6i \times 10^{-16}\mathrm{m}^2/\mathrm{W}$ when the center wavelength of pulsed light λ is 800 nm, while the real part of $\mathbf{n}_2$ is much smaller than the imaginary part and is set to be zero in our simulations [34, 35]. The linear refractive index of gold nanoparticles $\mathbf{n}_{\mathrm{p}} = 0.41661 + 5.2347i$ when $\lambda = 800\mathrm{nm}$.[36]. By combing the optical Kerr-effect equation $\mathbf{n} = \mathbf{n}_p + \mathbf{n}_2\mathrm{I}$ [31, 37], We can rewrite the polarizability of the nanoparticle into a form that depends on intensity:

$$\alpha = \frac{4\pi\varepsilon_0 r_0^3 [(\mathbf{n}_p + \mathbf{n}_2\mathrm{I})^2 - \mathrm{n}_h^2]/[(\mathbf{n}_p + \mathbf{n}_2\mathrm{I})^2 + 2\mathrm{n}_h^2]}{1 - \frac{i2\varepsilon_0 k^3 r_0^3}{3\varepsilon}[(\mathbf{n}_p + \mathbf{n}_2\mathrm{I})^2 - \mathrm{n}_h^2]/[(\mathbf{n}_p + \mathbf{n}_2\mathrm{I})^2 + 2\mathrm{n}_h^2]}. \tag{3.3}$$

The calculation results of the nonlinear polarizability which determines the optical force are plotted as a function of the optical intensity in Fig.3.2 (b). From Eq.(**??**), the sign change of the real part of polarizability indicates the reversal of the direction of the gradient force. With the incident power increasing, a peak of the imaginary part of polarizability appears because of the nonlinear effects. The extinction cross-section depends on the imaginary part of polarizability plotted in Fig.3.2 (c).

The focused electromagnetic field can be calculated using vectorial diffraction theory [22]. The total electric field $\mathbf{E}$ is divided into three-dimensional components E_x, E_y, and E_z. Using Eq.(3.3), the response of the dipole to each component of the electric field can be calculated individually and formed into a polarizability vector. Following the principle of vector superposition, the expression of the polarizability vector can be

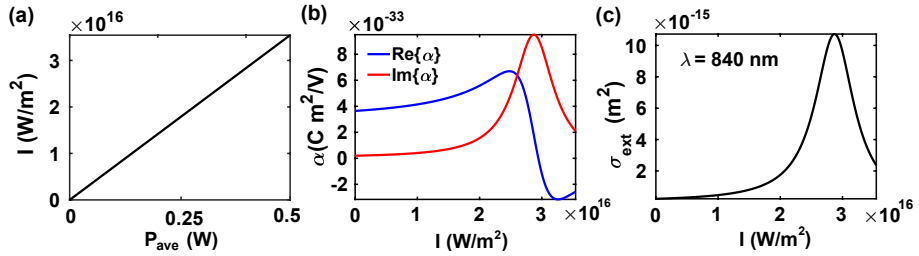

Figure 3.2: *(a) The optical intensity of the focused field is plotted as a function of the average power P_{ave} increasing from 0 to 0.5W. (b) The real and imaginary parts of the nonlinear polarizability change with the increasing average power P_{ave}. (c) The extinction cross-section σ_{ext} of gold nanoparticles varies with the increasing of the average power; a peak value of σ_{ext} occurs for the nonlinear sphere.*

written as

$$\alpha_i = \frac{4\pi\varepsilon_0 r_0^3[(\mathbf{n}_p+\mathbf{n}_2\mathrm{I}_i)^2-\mathrm{n}_h^2]/[(\mathbf{n}_p+\mathbf{n}_2\mathrm{I}_i)^2+2\mathrm{n}_h^2]}{1-\frac{i2\varepsilon_0 k^3 r_0^3}{3\varepsilon}[(\mathbf{n}_p+\mathbf{n}_2\mathrm{I}_i)^2-\mathrm{n}_h^2]/[(\mathbf{n}_p+\mathbf{n}_2\mathrm{I}_i)^2+2\mathrm{n}_h^2]}, \quad i=x,y,z. \tag{3.4}$$

Here α_i denotes the Cartesian components of the polarizability vector $\boldsymbol{\alpha}=\{\alpha_x,\alpha_y,\alpha_z\}$. Combined with the distribution of the electric field, we can obtain the distribution of the polarizability in the focal plane.

3.3. THE NONLINEAR OPTICAL FORCE ON A METALLIC NANOPARTICLE

The pulsed light consists of superimposed monochromatic plane waves. Let's consider an x-polarized electromagnetic wave packet, which is a combination of waves with different frequencies, and its propagation along the z-axis[38],

$$\boldsymbol{\mathcal{E}}(z,t)=\mathrm{Re}\left\{\frac{1}{2\pi}\int_0^{\infty}\mathbf{E}(\Omega)e^{i(\Omega t-\mathbf{k}(\Omega)z)}\cdot\hat{e}_x d\Omega\right\}, \tag{3.5}$$

where $\mathbf{E}(\Omega)=|E|e^{i\phi(\Omega)}$ is the complex amplitude of the electric field at frequency Ω and complex wave number $\mathbf{k}=\mathbf{n}\Omega/c$. Here, $\mathbf{n}$ is the complex refractive index, and c is the velocity of light in vacuum, respectively. In general, the refractive index is a function of frequency and we are concerned with the propagation of a pulse created by a combination of monochromatic waves centered around a center carrier frequency ω_0. We can separate an optic pulse into a carrier wave and an envelope $\boldsymbol{\mathcal{A}}(z,t)$ with a center

frequency ω_0:

$$\boldsymbol{\mathcal{E}}(z,t) = \mathrm{Re}\left\{\boldsymbol{\mathcal{A}}(z,t)e^{i(\omega_0 t - \mathbf{k}(\omega_0)z)}\right\}, \tag{3.6}$$

$$\boldsymbol{\mathcal{A}}(z,t) = \frac{1}{2\pi}\int_{-\omega}^{\infty}\mathbf{A}(\omega)e^{i(\omega t - \mathbf{k}(\omega)z)}d\omega. \tag{3.7}$$

where we introduce offset wave vector

$$k(\omega) = k(\Omega) - k(\omega_0), \quad \omega = \Omega - \omega_0. \tag{3.8}$$

If the full width at half maximum (FWHM) of the pulse spectrum is significantly smaller than the carrier frequency, the pulse envelope changes slowly over time. The phase shift of the pulse is linear with respect to frequency and does not cause distortion of the pulse.

The Lorentz law describes the instantaneous force exerted on an electric dipole by general real electromagnetic fields $\boldsymbol{\mathcal{E}}$, $\boldsymbol{\mathcal{H}}$[39]:

$$\boldsymbol{\mathcal{F}} = (\boldsymbol{\mathcal{P}}\cdot\nabla)\boldsymbol{\mathcal{E}} + \mu_0\frac{\partial\boldsymbol{\mathcal{P}}}{\partial t}\times\boldsymbol{\mathcal{H}}. \tag{3.9}$$

The electric dipole $\boldsymbol{\mathcal{P}} = \mathrm{Re}\{\mathbf{p}\}$ is fixed at position $\mathbf{r}$ in a medium. The complex dipolar moment $\mathbf{p}$ is relate to the electric field and a complex polarization $\boldsymbol{\alpha}$ in SI units. Substituting the complex field and complex dipole moment into Eq.(3.9), we have the time-average force[15, 39]:

$$\langle\boldsymbol{\mathcal{F}}\rangle = \frac{1}{2}\mathrm{Re}\{\boldsymbol{\alpha}\}\,\mathrm{Re}\left\{\mathbf{E}^*\cdot\nabla\mathbf{E}\right\} + \frac{1}{2}\mathrm{Im}\{\boldsymbol{\alpha}\}\,\mathrm{Im}\left\{\mathbf{E}^*\cdot\nabla\mathbf{E}\right\}. \tag{3.10}$$

The time-averaged optical force on the particle over a pulse duration can be derived by an integral of the force over one pulse cycle $\tau = 1/\nu$:

$$\langle\mathbf{F}(\mathbf{r})\rangle = \frac{1}{T}\int_{-\tau/2}^{-\tau/2}\langle\boldsymbol{\mathcal{F}}\rangle\,\mathrm{d}\,t. \tag{3.11}$$

This is the final expression of the time-averaged optical force during the pulse duration. The optical force in the focal plane ($x-$y plane) can be considered as the sum of the $x-$ and $y-$components. Let $\tau = 1/\nu$ be the period of the laser pulses with duration τ, then the we can rewrite time-averaged gradient force $\langle\mathbf{F}\rangle_{\mathrm{grad}}$ as

$$\langle\mathbf{F}_x\rangle_{\mathrm{grad}} = \frac{1}{T}\int_{-\tau/2}^{\tau/2}\frac{1}{4}\sum_i\mathrm{Re}\{\boldsymbol{\alpha}_i\}\frac{\partial|{E_i}^2|}{\partial x}dt, \tag{3.12}$$

$$\langle\mathbf{F}_y\rangle_{\mathrm{grad}} = \frac{1}{T}\int_{-\tau/2}^{\tau/2}\frac{1}{4}\sum_i\mathrm{Re}\{\boldsymbol{\alpha}_i\}\frac{\partial|{E_i}^2|}{\partial y}dt, \tag{3.13}$$

$$\langle\mathbf{F}_z\rangle_{\mathrm{grad}} = \frac{1}{T}\int_{-\tau/2}^{\tau/2}\frac{1}{4}\sum_i\mathrm{Re}\{\boldsymbol{\alpha}_i\}\frac{\partial|{E_i}^2|}{\partial z}dt, \tag{3.14}$$

with $i = (x, y, z)$. The radiation force in Eq.(2.40) can be rewritten as follows,

$$\langle \mathbf{F}_x \rangle_{\text{rad}} = \frac{1}{T} \int_{-\tau/2}^{\tau/2} \frac{1}{2} \text{Im}\{\alpha_i\} \text{Im}\{E_i^* \frac{\partial E_i}{\partial x}\} dt, \tag{3.15}$$

$$\langle \mathbf{F}_y \rangle_{\text{rad}} = \frac{1}{T} \int_{-\tau/2}^{\tau/2} \frac{1}{2} \text{Im}\{\alpha_i\} \text{Im}\{E_i^* \frac{\partial E_i}{\partial y}\} dt, \tag{3.16}$$

$$\langle \mathbf{F}_z \rangle_{\text{rad}} = \frac{1}{T} \int_{-\tau/2}^{\tau/2} \frac{1}{2} \text{Im}\{\alpha_i\} \text{Im}\{E_i^* \frac{\partial E_i}{\partial z}\} dt. \tag{3.17}$$

After calculating the sum of all the individual optical forces along a path **C**, we can calculate the optical potential of the particle in the focused field as

$$U(\mathbf{r}) = -\int_{\mathbf{C}} \langle \mathbf{F}(\mathbf{r}) \rangle \, d\mathbf{r}. \tag{3.18}$$

It is worth noting that the gradient force is conservative and the radiation force is a non-conservative force. The integral path from $\mathbf{r}$ to ∞ is limited to a certain area in the focal plane where the net force is a conservative vector field. After carrying out the integration of net force, we obtain the comparison result between the use of the scalar method and the vector method.

3.4. RESULTS AND DISCUSSION

Supposing the average power $P_{\text{ave}} = 0.5$W, Fig. 3.3 (a)-(c) show the distribution and magnitude of the three components of the electric field in the Cartesian coordinate in the focal plane. The $x-$ component of the electric field dominates the total electric field. The real part of individual polarizability components $\text{Re}\{\alpha_x\}$, $\text{Re}\{\alpha_y\}$, and $\text{Re}\{\alpha_z\}$ are shown in Fig. 3.3 (d) - (f), respectively. The sign inversion of $\text{Re}\{\alpha_x\}$ indicates the reversal of the direction of gradient forces. As shown in Fig. 3.3 (e) and (f), the sign inversion of the $y-$ and $z-$components polarizability does not occur due to the relatively low intensity of the $y-$ and $z-$ components of the electric field. The magnitude of the changes in α_y and α_z is not significant compared to α_x, but their contribution to the optical forces in the focal plane should not be ignored.

3.4.1. CALCULATION RESULTS

The $x-$component gradient force $\langle \mathbf{F}_x \rangle_{\text{grad}}$ generated by the interaction of the $x-$ component of the field intensity gradients $\partial |E_x|^2 / \partial x$ and $\text{Re}\{\alpha_x\}$ is shown in Fig. 3.4 (a). The red color indicates that the particle experiences a force along the positive $x-$axis, while blue indicates a force along the negative $x-$axis. The magnitude of $\langle \mathbf{F}_x \rangle_{\text{grad}}$ resulting

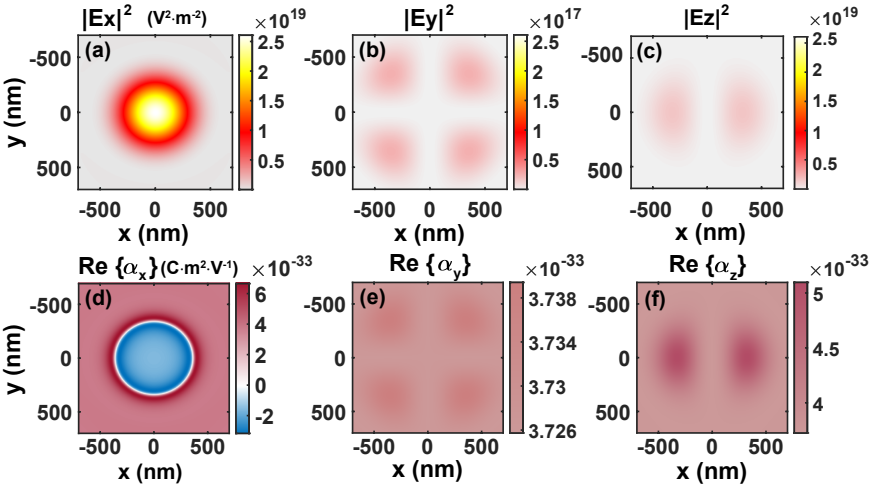

Figure 3.3: *Distribution of the focused electric field intensity in the focal plane and the corresponding polarizability of the dipolar sphere. (a)-(c) The peak value of the individual field components* $|E_x|^2$, $|E_y|^2$, *and* $|E_z|^2$, *respectively. (d)- (f) The real part of the individual components* $\mathrm{Re}\{\alpha_x\}$, $\mathrm{Re}\{\alpha_y\}$, *and* $\mathrm{Re}\{\alpha_z\}$, *respectively.*

from the $y-$ and $z-$ components of the electric field are comparatively small, as shown in Fig. 3.4 (b) and (c). Fig. 3.4 (d) - (f) show the results of the $y-$component of the gradient forces derived from the $x-$, $y-$, and $z-$component of the electric field using Eq. (3.12), respectively. Fig. 3.4 (g) and (h) show that the radiation force is negligible and can be omitted in the focal plane. This is because the energy of the light propagates mainly along the $z-$direction in the focal plane [22]. After the sum of all the individual optical force vectors, we can obtain the total optical force in the focal plane, as shown in Fig. 3.4 (i). The dark blue color indicates that the optical force is pointing towards the center point, which is the same as that in a linear regime. Due to the nonlinear effect, the optical force is reversed in a certain region marked in brown color. The position of the optical trapping is not evident from the distribution of optical force, as shown in Fig. 3.4 (i). A comparison of optical forces along the $x-$ and $y-$axis calculated by the scalar and vector methods is made to better understand the difference between the two methods.

A comparison of total forces calculated by the scalar and vector methods is made to further understand the difference between the two methods. The red color indicates that the particle experiences a force towards the center point, while blue indicates that a force is away from the center of the circle. The total force obtained by the scalar method is shown in Fig. 3.5 (c). Fig. 3.5 (a) shows the vector results as the sum of forces in Fig. 3.4 (a)- (f). The distribution and magnitude of the forces obtained by these

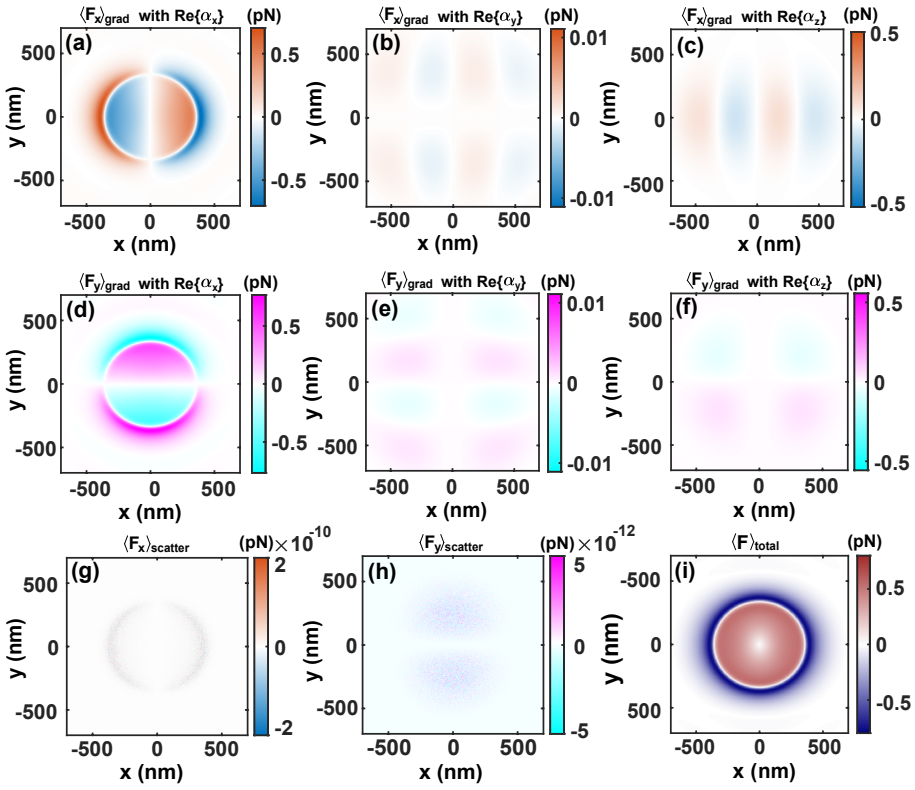

Figure 3.4: *The nonlinear optical force in the focal plane. (a)-(c) The plot of $x-$component of gradient forces derived from* $\mathrm{Re}\{\alpha_x\}$, $\mathrm{Re}\{\alpha_y\}$, *and* $\mathrm{Re}\{\alpha_z\}$, *respectively. The red indicates that the direction of the gradients is along the $x-$axis and the force value is positive; while the blue denotes that the negative force is in the opposite direction of the $x-$axis. (d)-(f) The plot of the $y-$component of gradient forces calculated with the vector method. The positive value means the direction of force is pointing to the $y-$axis and vice versa for the negative force. (g) and (h) The $x-$ and $y-$ components of radiation forces. (i) The total optical force in the focal plane. Dark blue indicates that the optical force is towards the center point, while brown indicates that the optical force direction is away from the center.*

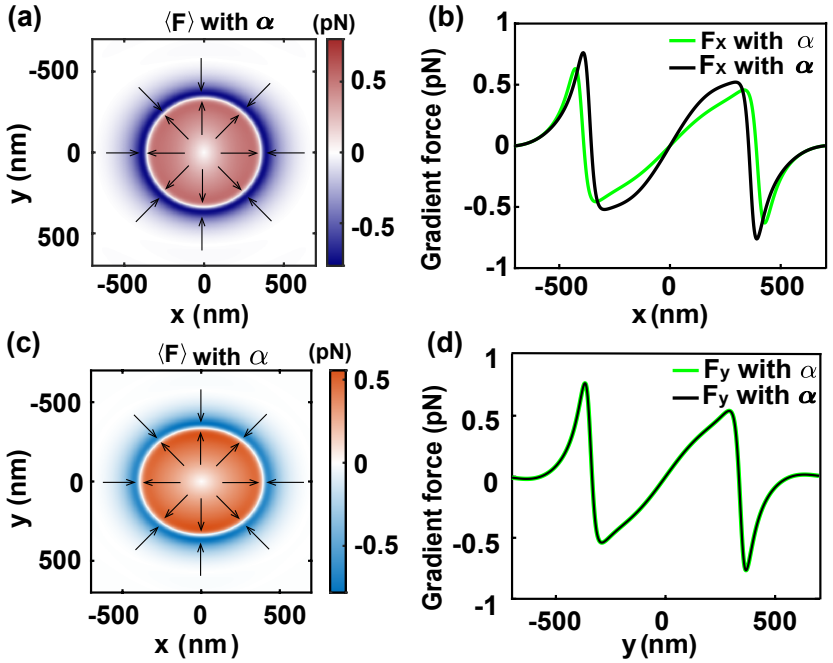

Figure 3.5: *The total optical forces obtained by scalar and vectorial methods. (a) The total gradient forces are calculated with the scalar method. (b) Plots of gradient forces along the x−axis for the comparison of the two methods. The green line means the gradient force is calculated by the scalar method; the black line for the calculation results based on the vectorial method. (c) The total gradient forces are calculated using vectorial polarizability. (d) y−component of gradient forces calculated with scalar polarizability and vectorial polarizability.*

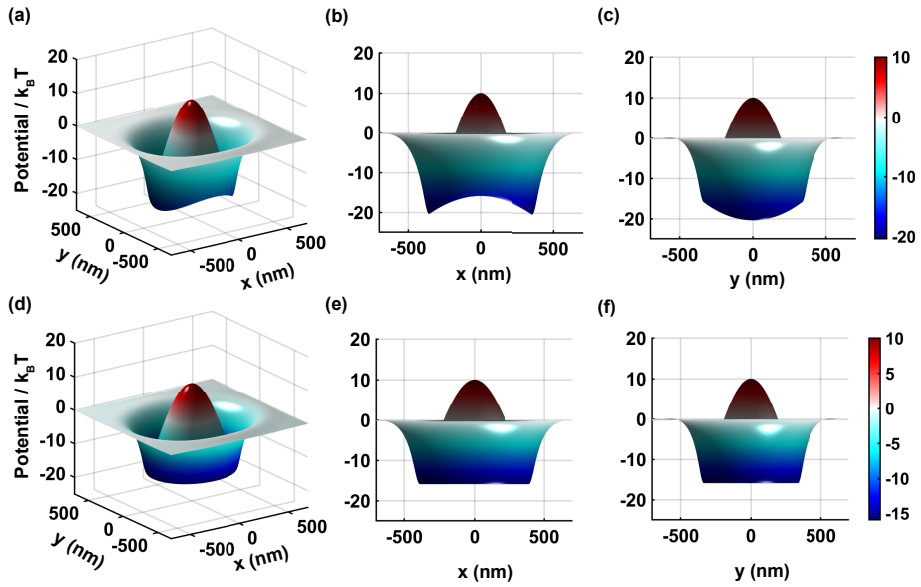

Figure 3.6: *The nonlinear optical potential well in the focal plane. (a) The nonlinear optical potential well with the vector method in the focal plane. (b) The parallel projection of the potential well to the direction of the $y-$axis. (c) The parallel projection of the potential well to the direction of the $x-$axis. (d) The potential well with the scalar method. (e) and (f) Parallel projections to the $y-$axis and $x-$axis, respectively.*

two methods are different and the distribution of the force with scalar method is not spherical. The black line computed by the vectorial polarizability has a larger maximum value than those calculated by the scalar polarizability in the $x-$axis, as shown in Fig. 3.5 (b). Fig. 3.5 (d) shows the results of total forces using the scalar method and the vector method on the $y-$axis, respectively. The total force with α coincides exactly with the results using αin the $y-$axis. The difference in the results of the $x-$component of forces in Fig. 3.5 (b) can be attributed to the use of the vectorial model. In the scalar method, the scalar polarizability is calculated using the total electric field, which approximates the real part of the polarizability along the dominant electric field component (e.g., the $x-$component for the $x-$polarized field). However, the scalar method cannot explicitly calculate the contributions of the other components (e.g., y and z) of the electric field and their corresponding polarizabilities (Re$\{\alpha_y\}$ and Re$\{\alpha_z\}$). In contrast to the scalar method, the vectorial model calculates the interaction between Re$\{\alpha_y\}$ and$\left|E_y\right|^2$ on the $x-$axis, as well as the interaction between Re$\{\alpha_z\}$and $|E_z|^2$ on the $x-$axis individually. Although the $x-$component of the electric field dominates the total electric field, the $y-$ and $z-$components of the electric field also contribute to the force along the $x-$axis.

The nonlinear optical potential well in the focal plane can be obtained by the vectorial method as shown in Fig. 3.6 (a). Here, the positive and negative values of the potential indicate that the particle experiences a repulsive and attractive potential in this plane. The coordinate of the minimum potential represents the position of the stable optical trapping. Fig. 3.6 (b) and (c) show that the minimum potential is located at two points along the $x-$axis, indicating the presence of two equilibrium positions for the optical trapping. To illustrate the difference between the scalar method and the vector method, the potential wells calculated using the scalar method are plotted in the second row. The two different methods can both achieve the "trap split" of the optical potential well, as shown in Fig. 3.6 (a) and (d). However, parallel projections of the optical potential well reveal the difference between them. The potential well deduced from the scalar method has a “ring-like” depth in the lower part which means the particle will be trapped in a ring shape, as shown in Fig. 3.6 (e) and (f). In contrast, the vector method considers the response of the dipolar particle to each individual component of the vectorial optical field, providing a different description, as shown in Fig. 3.6 (a).

3.4.2. EXPERIMENTAL RESULTS AND DISCUSSION

The schematic diagram of the experimental setup based on our simulation parameters is shown in Fig. 3.7 (a). We used an $x-$polarized pulsed laser with a center wavelength of 800 nm, 100 fs pulse duration and 80 MHz repetitive frequency as a light source. Then it is focused by an objective lens with NA = 0.75 inside a glass tube that contains water with gold nanoparticles of 30 nm radius. The light emitted by the green illuminator is used to illuminate the fluid. The images of the focal region are collected by the CCD. The direction of polarization of a pulsed laser can be rotated by using a half-wave plate. When the polarization direction is rotated by 90 degrees using a half-wave plate, the two trapped nanoparticles are reoriented from being parallel to the $x-$axis to being parallel to the $y-$axis, as demonstrated in Fig. 3.7 (b) (*see supplementary videos S1*). This result is consistent with the prediction of the vectorial model, as shown in Fig. 3.6 (a). Therefore, it can be concluded that the scalar method is not able to accurately describe the dipole's response to the tightly focused optical field in nonlinear optical trapping, while the vectorial method provides a more precise description.

In the nonlinear regime, it's crucial to recognize that when the peak intensity of each individual component of the electric field is sufficiently high, it can induce third-order nonlinear optical effects, causing changes in the dielectric function of the metal nanoparticle. When dealing with a tightly focused field, the nonlinear optical response to each component of the electric field can vary. Therefore, to accurately describe non-

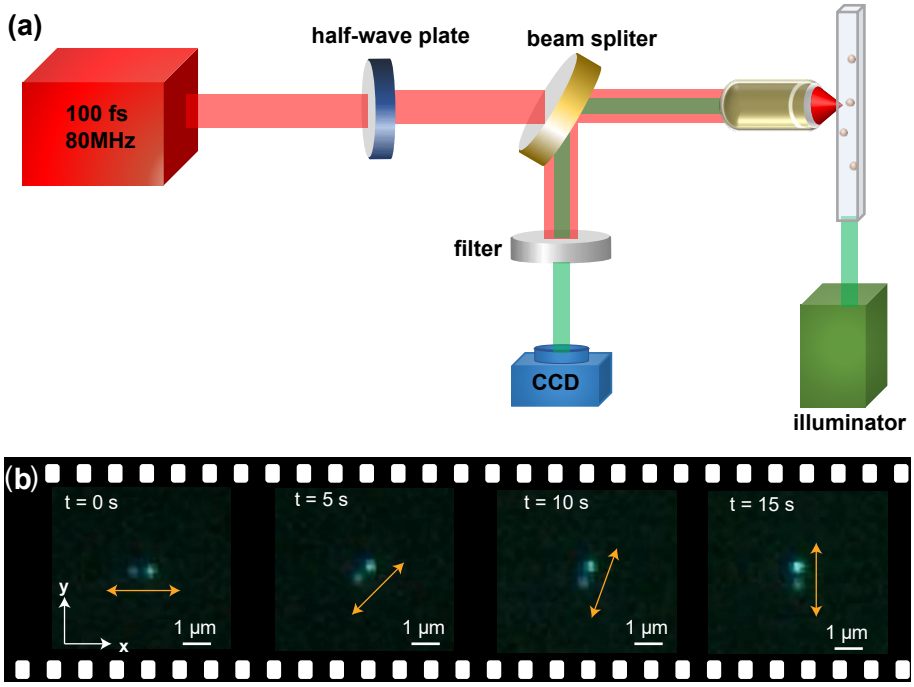

Figure 3.7: *(a) The schematic diagram of the experimental setup. An x−polarized pulsed laser propagates through a half-wave plate. The incident beam is focused by an objective with 0.75 NA. The sample in a glass tube consists of gold nanoparticles with a radius of 30 nm. A Green illuminator is used to illuminate the trapped particles. The filter is a lower pass plate for passing the green light and blocking the pulsed light. The image of the optical trapping is recorded by a CCD. (b) Yellow arrows indicate the direction of the polarization of the pulsed laser. The two trapped- nanoparticles are also rotated along with the half-wave plate.*

linear optical trapping, it becomes necessary to analyze optical forces using the vectorial method. In contrast, in the linear regime, where the optical properties of the metal nanoparticle remain unchanged, there is no distinction between the scalar method and the vectorial method.

3.4.3. DISCUSSION

In this chapter, we have provided a detailed analysis of the nonlinear optical forces acting on the transverse plane. However, 3-D experimental results are observed in the actual experiment. In addition to the detection of the results on the transverse plane, we also placed an objective lens of 0.2 NA on the side for observing the results on the longitudinal plane, as shown in Fig. 3.8 (a). Fig. 3.8 (b) and (c) demonstrate a stable nonlinear optical trapping on the transverse plane and longitudinal plane (*see supplementary videos S2*). Hence, to achieve a comprehensive understanding of the observed 3-D nonlinear optical trapping, it is essential to extend our discussion to include the optical forces along the longitudinal plane.

By using Eq.(3.14) and Eq.(3.17), the gradient forces and radiation forces along the z-axis can be calculated. The real part of the nonlinear polarizability of the three components is depicted in Fig. 3.9. (a), (b), and (c). The negative value of the real part of polarizability demonstrates the alteration of the optical response raised by the nonlinear optical effect. In the longitudinal plane, the gradient forces exerted on the particles are described in the second row, as can be seen in Fig. 3.9 (d), (e), and (f). The red color signifies the direction of the gradient force along the positive direction of the z-axis, while the blue represents the force along the negative direction. The radiation forces can not be neglected because the energy flux mainly propagates in the longitudinal direction in the focal region. The imaginary components of nonlinear polarizability are plotted in Fig. 3.10 (a), (b), and (c). The z-component of radiation forces associated with the corresponding three components of imaginary polarizabilities are calculated and illustrated in Fig. 3.10 (d), (e), and (f). The calculations indicate that the magnitude of the radiation force in the z-direction is significantly larger, approximately one order of magnitude greater, than the gradient force on z- direction. This significant difference in force magnitudes suggests that the radiation force dominates in the z-direction.

The total optical forces along the z-direction are obtained by the sum of each individual gradient force and radiation force, as shown in Fig. 3.11. Based on the calculations, it appears that there is no optical force in the negative z-axis direction to counterbalance the optical force along the positive z-axis. Consequently, there are no stable equilibrium positions in the z-direction for the trapped nanoparticle. However, this is controversial

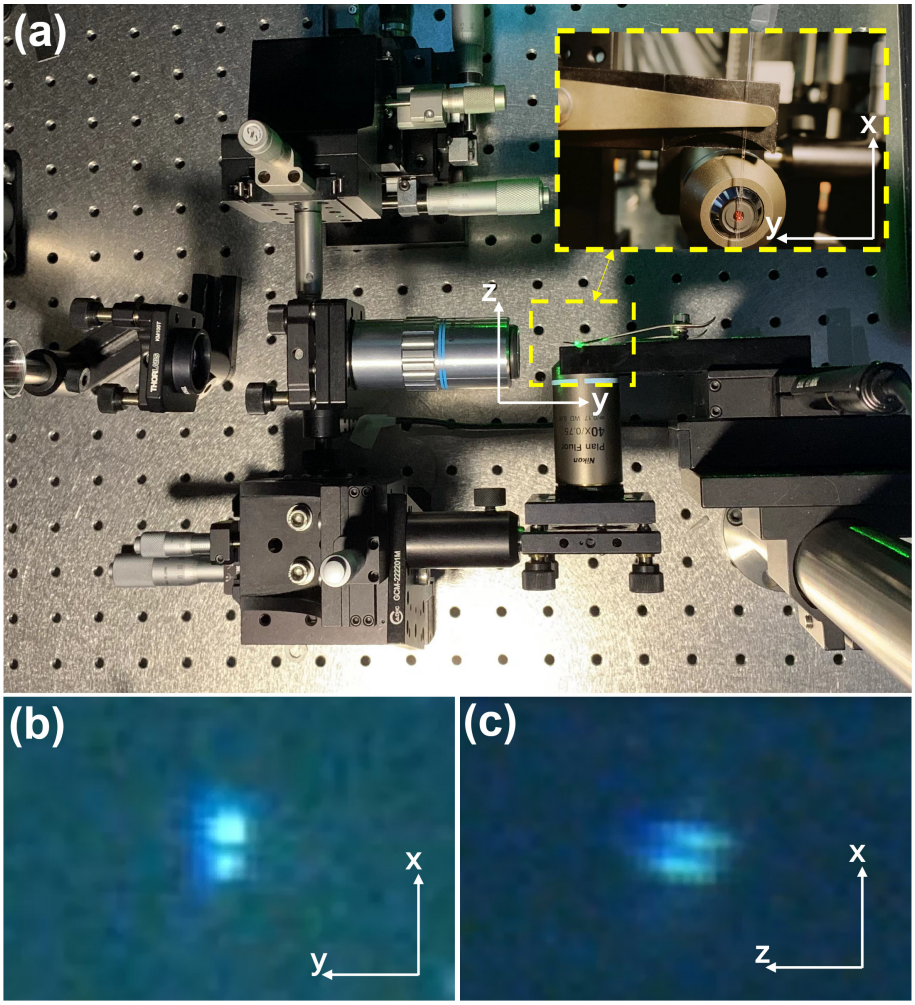

Figure 3.8: *(a) Experimental setup diagram. In the experiment, the optical axis was set as the z-axis. We used an objective lens of 0.75 NA to achieve the nonlinear optical trapping and observe experimental results in the transverse plane. Additionally, we used a 0.2 NA objective lens to observe results in the longitudinal plane. (b) Nonlinear optical trapping results in the transverse plane. (c) Light capture results in the longitudinal plane.*

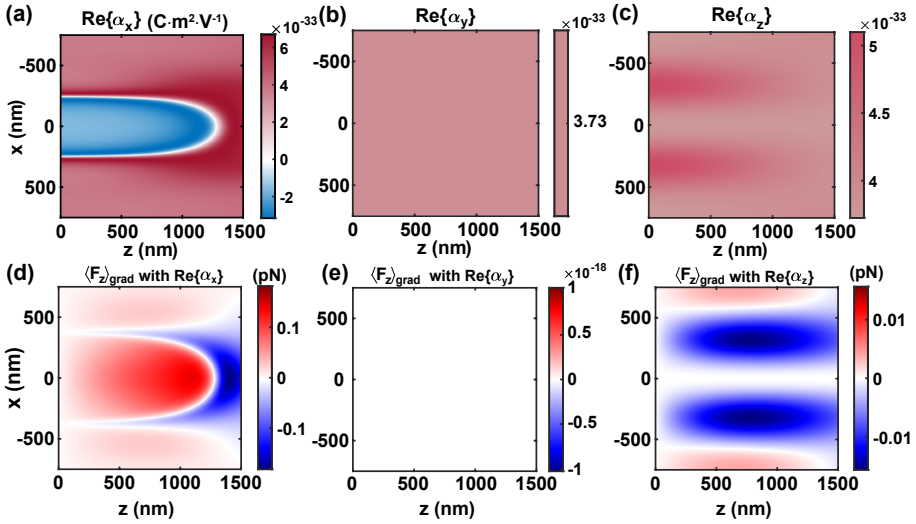

Figure 3.9: *(a), (b), and (c) Distribution of the three components of the real part of the polarizability in the longitudinal plane for P_{ave} = 0.5 W, respectively. (d) - (f) The z-component of the gradient force is plotted in the second row.*

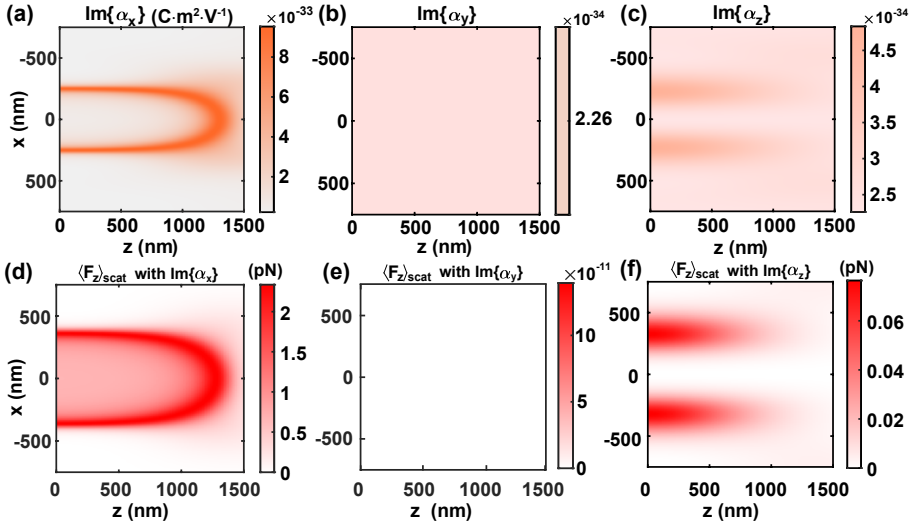

Figure 3.10: *(a), (b), and (c) Distribution of the three components of the imaginary part of polarizability in the longitudinal plane for P_{ave} = 0.5 W, respectively. (d) - (f) The three components of the radiation force along the z-direction.*

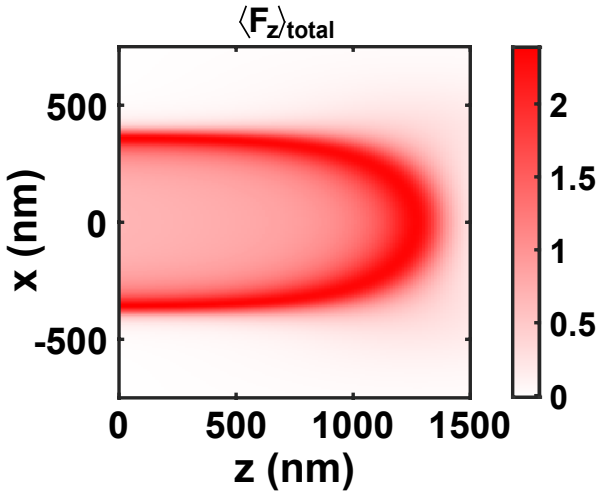

Figure 3.11: *The distribution of total optical forces along the z-direction. The red color denotes the direction of force towards the positive direction of the z-axis.*

with our observation that the nanoparticle is stably trapped in the z-axis. Although we successfully analyzed the nonlinear optical force and the nonlinear optical potential well in the transverse plane, it is limited in the z-component optical force.

3.5. CONCLUSION

In summary, we have introduced an enhanced vectorial model for the quantitative analysis of nonlinear optical forces using the dipole's polarizability vector. This nonlinear polarizability, contingent upon optical intensity and incorporating the Kerr effect, has been derived. The nonlinear response of a dipolar gold nanoparticle to the tightly focused field is comprehensively described utilizing vector diffraction theory, culminating in the determination of a polarizability vector. With the vectorial approach, we have elucidated the individual gradient forces generated by each component of the electric fields in the focal plane, as well as the radiation forces. By integrating the total optical force at the focal plane, the nonlinear potential well has been determined and compared with experimental results. In the longitudinal plane (along the $z-$ direction), the calculation results using the vectorial method reveal that there is no equilibrium position. However, this lack of equilibrium positions in the $z-$ direction does not impact the analysis performed in the focal plane. The "trap split" in the focal plane remains consistent with the theoretical framework and experimental observations.

Our study incontrovertibly demonstrates the inadequacy of the scalar method in an-

alyzing nonlinear optical trapping, while the vectorial model significantly enhances our understanding of these phenomena. This transition from a scalar to a vector model not only expands the traditional methodology but also holds promise for advancing the development of nonlinear optical tweezers and their associated applications.

REFERENCES

[1] Y. Jiang, T. Narushima, and H. Okamoto, *Nonlinear optical effects in trapping nanoparticles with femtosecond pulses,* Nature Physics **6**, 1005 (2010).

[2] A. Ashkin, J. M. Dziedzic, J. E. Bjorkholm, and S. Chu, *Observation of a single-beam gradient force optical trap for dielectric particles,* Opt. Lett. **11**, 288 (1986).

[3] A. Ashkin and J. M. Dziedzic, *Optical Levitation by Radiation Pressure,* Applied Physics Letters **19**, 283 (2003).

[4] A. Ashkin and J. P. Gordon, *Stability of radiation-pressure particle traps: an optical earnshaw theorem,* Opt. Lett. **8**, 511 (1983).

[5] Y. Zhang, J. Shen, C. Min, Y. Jin, Y. Jiang, J. Liu, S. Zhu, Y. Sheng, A. V. Zayats, and X. Yuan, *Nonlinearity-induced multiplexed optical trapping and manipulation with femtosecond vector beams,* Nano letters **18**, 5538 (2018).

[6] L. Gong, B. Gu, G. Rui, Y. Cui, Z. Zhu, and Q. Zhan, *Optical forces of focused femtosecond laser pulses on nonlinear optical rayleigh particles,* Photonics Research **6**, 138 (2018).

[7] L. Huang, Y. Qin, Y. Jin, H. Shi, H. Guo, L. Xiao, and Y. Jiang, *Spheroidal trap shell beyond diffraction limit induced by nonlinear effects in femtosecond laser trapping,* Nanophotonics **9**, 4315 (2020).

[8] Y. Qin, L.-M. Zhou, L. Huang, Y. Jin, H. Shi, S. Shi, H. Guo, L. Xiao, Y. Yang, C.-W. Qiu, *et al.*, *Nonlinearity-induced nanoparticle circumgyration at sub-diffraction scale,* Nature Communications **12**, 3722 (2021).

[9] S. Chu, J. Bjorkholm, A. Ashkin, and A. Cable, *Experimental observation of optically trapped atoms,* Physical review letters **57**, 314 (1986).

[10] R. W. Applegate, J. Squier, T. Vestad, J. Oakey, and D. W. Marr, *Optical trapping, manipulation, and sorting of cells and colloids in microfluidic systems with diode laser bars,* Optics express **12**, 4390 (2004).

[11] S. Grover, R. C. Gauthier, and A. Skirtach, *Analysis of the behaviour of erythrocytes in an optical trapping system,* Optics express **7**, 533 (2000).

[12] C. F. Bohren and D. R. Huffman, *Absorption and scattering of light by small particles* (John Wiley & Sons, 2008) Chap. 5.

[13] U. Kreibig and M. Vollmer, *Optical properties of metal clusters*, Vol. 25 (Springer Science & Business Media, 2013) Chap. 1.

[14] L. Novotny and B. Hecht, *Principles of nano-optics* (Cambridge university press, 2012) Chap. 14.

[15] P. C. Chaumet and M. Nieto-Vesperinas, *Time-averaged total force on a dipolar sphere in an electromagnetic field,* Optics letters **25**, 1065 (2000).

[16] V. Wong and M. A. Ratner, *Gradient and nongradient contributions to plasmon-enhanced optical forces on silver nanoparticles,* Physical Review B **73**, 075416 (2006).

[17] J. R. Arias-González and M. Nieto-Vesperinas, *Optical forces on small particles: attractive and repulsive nature and plasmon-resonance conditions,* JOSA A **20**, 1201 (2003).

[18] S. Albaladejo, M. I. Marqués, M. Laroche, and J. J. Sáenz, *Scattering forces from the curl of the spin angular momentum of a light field,* Physical review letters **102**, 113602 (2009).

[19] G. Wang, A. A. Baker-Murray, and W. J. Blau, *Saturable absorption in 2d nanomaterials and related photonic devices,* Laser & Photonics Reviews **13**, 1800282 (2019).

[20] L. De Boni, E. L. Wood, C. Toro, and F. E. Hernandez, *Optical saturable absorption in gold nanoparticles,* Plasmonics **3**, 171 (2008).

[21] R. W. Boyd, *Nonlinear optics* (Academic press, 2020).

[22] L. Novotny and B. Hecht, *Principles of nano-optics* (Cambridge university press, 2012) Chap. 3.

[23] U. Kreibig and M. Vollmer, *Optical properties of metal clusters*, Vol. 25 (Springer Science & Business Media, 2013).

[24] S. Yadav, A. Devi, and A. K. De, *Synergistic effect of fano resonance and optical nonlinearity in laser trapping of silver nanoparticles,* Phys. Rev. A **102**, 043511 (2020).

[25] T. Iida and H. Ishihara, *Theoretical study of the optical manipulation of semiconductor nanoparticles under an excitonic resonance condition,* Phys. Rev. Lett. **90**, 057403 (2003).

[26] X. Zhang, B. Sun, J. M. Hodgkiss, and R. H. Friend, *Tunable ultrafast optical switching via waveguided gold nanowires,* Advanced Materials **20**, 4455 (2008).

[27] Y. H. Lee, Y. Yan, L. Polavarapu, and Q.-H. Xu, *Nonlinear optical switching behavior of au nanocubes and nano-octahedra investigated by femtosecond z-scan measurements,* Applied Physics Letters **95**, 023105 (2009).

[28] R. West, Y. Wang, and T. Goodson, *Nonlinear absorption properties in novel gold nanostructured topologies,* The Journal of Physical Chemistry B **107**, 3419 (2003).

[29] S. A. Maier, P. G. Kik, H. A. Atwater, S. Meltzer, E. Harel, B. E. Koel, and A. A. Requicha, *Local detection of electromagnetic energy transport below the diffraction limit in metal nanoparticle plasmon waveguides,* Nature materials **2**, 229 (2003).

[30] R. Del Coso and J. Solis, *Relation between nonlinear refractive index and third-order susceptibility in absorbing media,* JOSA B **21**, 640 (2004).

[31] F. Hache, D. Ricard, C. Flytzanis, and U. Kreibig, *The optical kerr effect in small metal particles and metal colloids: the case of gold,* Applied Physics A **47**, 347 (1988).

[32] R. Paschotta, *Field guide to lasers*, Vol. 12 (SPIE press Bellingham, WA, 2008).

[33] A. Devi and A. K. De, *Theoretical investigation on nonlinear optical effects in laser trapping of dielectric nanoparticles with ultrafast pulsed excitation,* Optics Express **24**, 21485 (2016).

[34] R. W. Boyd, Z. Shi, and I. De Leon, *The third-order nonlinear optical susceptibility of gold,* Optics Communications **326**, 74 (2014).

[35] K. Wang, H. Long, M. Fu, G. Yang, and P. Lu, *Size-related third-order optical nonlinearities of au nanoparticle arrays,* Optics express **18**, 13874 (2010).

[36] H.-J. Hagemann, W. Gudat, and C. Kunz, *Optical constants from the far infrared to the x-ray region: Mg, al, cu, ag, au, bi, c, and al 2 o 3,* JOSA **65**, 742 (1975).

[37] R. del Coso and J. Solis, *Relation between nonlinear refractive index and third-order susceptibility in absorbing media,* J. Opt. Soc. Am. B **21**, 640 (2004).

[38] A. M. Weiner, *Ultrafast optics* (John Wiley & Sons, 2011).

[39] S. Stenholm, *The semiclassical theory of laser cooling,* Rev. Mod. Phys. **58**, 699 (1986).

4

NONLINEAR OPTICAL TRAPPING WITH SATURABLE AND REVERSE SATURABLE ABSORPTION EFFECT

When you want knowledge like you want air under water

then you will get it.

—— Socrates

Some original content of this chapter published in *Advanced Photonics*

We have observed that the direction of the gradient force can be reversed in nonlinear optical trapping, a phenomenon whose underlying physical mechanisms have remained elusive. In this chapter, we shed light on the intricate processes responsible for this phenomenon. We attribute the nonlinear optical force to a combination of factors, including the third-order nonlinear effect of the metallic nanoparticle, optical saturable absorption (SA), and reverse saturable absorption (RSA) under high-intensity irradiance. Our investigation focuses on the change in gradient forces acting on a gold nanoparticle when subjected to a femtosecond pulse laser with circular polarization. We have discovered that the gradient force initially diminishes and reverses its direction as the light power increases due to the SA effect. Subsequently, under even higher intensities, the gradient force reverses once more because of the RSA effect. Our quantitative calculations also reveal alterations in potential wells induced by these nonlinear effects. Encouragingly, experimental results align closely with our theoretical predictions, providing empirical validation for our findings.

4.1. INTRODUCTION

The stable optical trapping of nano-objects is based on the interaction between the scattering and the gradient force[1]. The scattering force is exerted on a nanoparticle in the direction of light propagation while the gradient force is in the direction of the tightly focused optical field gradient[2]. This classical principle is convenient and intuitive in a discussion of normal optical trapping. However, in nonlinear optical trapping of the gold nanoparticle, the gradient forces are not in the direction of the spatial light gradient and become tunable by introducing the intensity-dependent nonlinear processes: optical saturable absorption (SA) and reverse saturable absorption (RSA).

Ample works show that gold nano-objects exhibit SA and RSA effect[3–5]. The SA is excited with a relatively low excitation intensity, whereas the RSA is excited with a higher optical intensity. In the SA process, the electrons are pumped from the ground-state to the excited-state leading to ground-state bleaching during the short pulse duration. The nonlinear absorption coefficient of the gold nanoparticle is observed to be negative, and the transmittance of the material increases under this circumstance. The nonlinear process changes from SA to RSA at a higher laser intensity and the nonlinear absorption coefficient becomes positive, and the value of transmittance begins to decrease due to excited-state absorption [6, 7]. The idea behind our theoretical approach is to investigate the gradient forces on the gold nanoparticle with a reversal of the nonlinear coefficient sign in these two nonlinear processes as the increase of input laser power.

In the Rayleigh regime (radius $\ll$ wavelength), a nanoparticle can be modeled as an

electric dipole in response to the incident optical field. The gradient force depends on the polarizability of the dipole and on the inhomogeneous electric field. To stimulate the SA and RSA processes, a tightly focused circularly-polarized femtosecond pulsed laser beam is applied as the incident optical field using Debye vectorial diffraction theory[8]. The complex refractive index of the gold nanoparticles is calculated as a function of the modulus of the incident electric field. As the incident electric field increases, the transmittance of the material increases as a consequence of the SA effect and reduces because of the RSA effect. Combining the incident optical field and polarizability with the time-averaged force equation, we found that gradient forces reduce and reverse when the incident electric field exceeds a threshold value during the SA process in a certain region of the focused field. In the RSA process, the magnitude of gradient forces becomes smaller and another reversal of the direction of gradient forces appeals. After calculating the potential well of optical trapping, the potential well changes from a concave to a convex type in the SA process. As the input power increases, the potential well changes from a convex to a concave type in the RSA process. The results of the calculation indicate that ring-shaped particles can be trapped in the nonlinear optical trapping, which is in good agreement with the reported experiments[9].

4.2. THE THEORETICAL METHOD

Numerous works have indicated that gold nanoparticles exhibit distinct responses in the SA and RSA regimes[3–7, 10]. Physically, the rate of change in the coefficient of nonlinear absorption for a gold nanoparticle remains negative during SA but switches to being positive within the RSA regime. This reversal of sign produces significant changes in physical properties. The dependence on the intensity of the coefficient of nonlinear absorption κ for gold nanoparticles is calculated from [11].

$$\kappa = \frac{\lambda}{4\pi}\left(\frac{a_0}{1+I/I_s}+\beta I\right), \tag{4.1}$$

where I_s is the saturable optical intensity, β is the two-photon absorption coefficient, and a_0 is the linear absorption coefficient of the gold nanoparticle.

The nonlinear absorption coefficients of the gold nanoparticles are summarized and compared in Table 4.1. All of the experimental results are obtained with two-dimensional gold nanoparticle arrays. The magnitude of saturable intensity I_s is $10^{13}\mathrm{W/m^2}$ and the nonlinear absorption coefficient β is $10^{-11}\mathrm{m/W}$.

Plenty of works have demonstrated the enhancement of field intensity on the closely spaced gold nanoparticle arrays[12, 13]. So the saturable intensity for a single nanoparticle is higher than the arrays. For optical trapping, accurate values of the saturable

intensity I_s of a single nanoparticle are desirable and different from the values of gold nanoparticle arrays. However, we can estimate a reasonable value of saturable intensity I_s of a single gold nanoparticle based on the previous results of gold nanoparticle arrays in table.4.1. The nonlinear parameters of the gold nanostructures are summarized and compared here.

Table 4.1: Comparison of the absorption coefficient values of gold from different articles.

Sample	λ(nm)	τ(fs)	I_s(W/m^2)	β(m/W)
nanorods [4]	780	220	7×10^{13}	15×10^{-11}
triangular nanoparticles [10]	800	50	55×10^{13}	29×10^{-11}
nanocubes [14]	800	60	12.8×10^{13}	16.1×10^{-11}
nano-octahedras [14]	800	60	25.3×10^{13}	24.4×10^{-11}

In the above cases, the magnitude of saturable intensity I_s is in the order of 10^{13}W/m^2. It should be noted that the experimental results are obtained with two-dimensional nano particle arrays. For optical trapping in our work, however, the saturable intensity I_s in the above table should be lower than that of a single nanoparticle. For scientific rigor, here, we should use a reasonable value of saturable intensity I_s for a single gold nanoparticle.

Numerous experimental works have demonstrated that the field intensities are enhanced in closely spaced gold nanoparticle arrays due to the field hybridization effect[13, 15–18]. Consequently, to stimulate the nonlinear effect, the requirement of optical intensity for arrays is lower than for a single nanoparticle, due to the absence of interference among particles. Hence, we can estimate a reasonable value based on the previous results of measurement, which is one order higher than that in the arrayed cases. Given this, the saturable optical intensity of a single gold nanoparticle I_s is set to a reasonable estimated value which is 55×10^{14} W/m^2 and $\beta = 29\times10^{-11}$ m/W[10] in our simulation.

It is known that the real part of n_2 is much smaller than the imaginary part, and thus, as an approximation, we set the real part equal to zero. The complex refractive index of the gold nanoparticle can be obtained with the intensity-dependent nonlinear absorption coefficient by $\boldsymbol{n_p} = n_0 + i a\lambda/(4\pi)$[19]. The linear refractive index of gold nanoparticles $\boldsymbol{n_p}$ is = 0.41661 + 5.2347i and $a_0 = 7.8311\times10^7$ m^{-1}[20].

The incident electric field **E** plays an essential role in determining the direction and magnitude of the gradient force. To excite the nonlinear effect of samples, the tightly focused optical field with a high NA object lens is beneficial. At the excitation wavelength λ = 840nm, the wave number in the host medium (water) is k ($k = 2\pi n_h/\lambda$). The focal length in the host medium F = 6.5 mm and the filling factor of the lens is $f_w = 1$. The maximum focal angle θ_{max} is determined by the NA of the lens and the host medium as $\theta_{max} = \arcsin(\mathrm{NA}/n_h)$. We use cylindrical coordinates in the focal region, given by ρ (ρ =

$\sqrt{x^2+y^2}$), φ, and z with φ the azimuthal angle and z the coordinate along the optical axis with z=0 corresponding to the focal plane. According to vectorial diffraction theory, the focused electromagnetic field **E** and **H** with circular-polarization is given by[8]:

$$\mathbf{E} = E_{00}\begin{bmatrix} I_{00} + I_{02}(\cos(2\varphi) + i\sin(2\varphi)) \\ iI_{00} - I_{02}(\cos(2\varphi) - i\sin(2\varphi)) \\ 2I_{01}(\sin(\varphi) - i\cos(\varphi)) \end{bmatrix}, \tag{4.2}$$

$$\mathbf{H} = \frac{E_{00}}{Z_{\mu\varepsilon}}\begin{bmatrix} iI_{00} + I_{02}(\sin(2\varphi) + i\cos(2\varphi)) \\ I_{00} - I_{02}(\cos(2\varphi) - i\sin(2\varphi)) \\ 2I_{01}(\cos(\varphi) - i\sin(\varphi)) \end{bmatrix}, \tag{4.3}$$

where
$$I_{00} = \int_0^{\theta_{max}} l(\theta)\sin\theta(1+\cos\theta)J_0(k\rho\sin\theta)\exp(ikz\cos\theta)d\theta, \tag{4.4}$$
$$I_{01} = \int_0^{\theta_{max}} l(\theta)\sin^2\theta J_1(k\rho\sin\theta)\exp(ikz\cos\theta)d\theta, \tag{4.5}$$
$$I_{02} = \int_0^{\theta_{max}} l(\theta)\sin\theta(1-\cos\theta)J_2(k\rho\sin\theta)\exp(ikz\cos\theta)d\theta, \tag{4.6}$$
and
$$l(\theta) = \exp(-ikF)\frac{ikF}{2\pi}(n_h\cos\theta)^{\frac{1}{2}}\cdot\exp\left(\frac{-\sin^2\theta}{f_w^2\sin^2\theta_{max}}\right), \tag{4.7}$$

where E_{00} is the amplitude of the circular-polarised electric field in the pupil of the lens, J_n is the n$^{\text{th}}$ order of the Bessel function of the first kind. $Z_{\mu\varepsilon}$ is impedance of the host medium. E_{00} is the amplitude of the incident electric field. Compared with the continuous wave (CW) source, an ultrafast pulsed laser has a much higher peak power. The peak power of the pulsed laser P_{peak} can be expressed in the incident average power P_{ave}, the pulse duration τ, and the repetition frequency f_{rep} : $P_{\text{peak}} = P_{\text{ave}}/(\tau f_{\text{rep}})$[21]. The peak optical intensity in the focal point is then given by $I_{\text{peak}} = 2P_{\text{peak}}/\pi R^2$ where R is the radius of the Airy spot. The peak intensity of the focused pulsed laser is high enough to excite the nonlinear effect and leads to stable optical trapping of the particles [22].

By substituting the I_{peak} into Eq.(4.1), we can get the polarizability α of nonlinear gold nanoparticles from Eq.(3.1). Then, the time-averaged gradient forces in the presence of the nonlinear effect can be obtained. Let $T = 1/f$ be the period of the laser pulses with duration τ, then the time-averaged gradient force $\langle\mathbf{F}\rangle_{\text{grad}}$ is

$$\langle\mathbf{F}\rangle_{\text{grad}} = \frac{1}{T}\int_{-\tau/2}^{\tau/2}\langle\mathbf{F}\rangle_{\text{grad}}\,dt. \tag{4.8}$$

Here, the pulse has a rectangular temporal envelope, which means that the peak power is constant during the pulse duration. Furthermore, by integrating the gradient

force over a path we obtain the force potential:

$$U(\mathbf{r}) = -\int_{\infty}^{r} \langle \mathbf{F}(\mathbf{r}') \rangle_{\text{grad}} \, d\mathbf{r}'. \tag{4.9}$$

Supposing the incident average power P_{ave} increases gradually from 0 W to 2.0 W, the peak electric field amplitude $|\mathbf{E}_{\text{peak}}|$ of the focused field can be calculated with the relation $|\mathbf{E}_{\text{peak}}|^2 = 4P_{\text{peak}}/(\pi R^2 \varepsilon c n_h)$[21].

4.3. EXPERIMENTAL SETUP

The schematic diagram of the experimental setup is based on our simulation parameters, as shown in Fig. 4.1. We used an x-polarized pulsed laser with a pulse duration of 100 fs and 80 MHz repetitive frequency as a light source. The laser beam from a Ti: sapphire laser is firstly linearly polarized by a polarizer, and its polarization direction is then regulated by rotating a half-wave $(\lambda/2)$ plate. After passing through the second polarizer, the laser power can be changed by rotating the $(\lambda/2)$ plate with the controller. The circularly polarized beam is obtained by a quarter-wave $(\lambda/4)$ plate.

Then it is focused by an objective lens with NA = 0.65 inside a glass micro-tube, and the sample solution with gold nanoparticles of 60 nm diameter is filled in the micro-tube. The light emitted by the illuminator indicated in green is used to illuminate the sample solution. The illumination and the trapping beam incident orthogonally into the sample tube; thus, only the scattered illuminating beam can be collected by the objective. This design works like the dark-field illumination and helps to improve the motion presentation of the gold nanoparticles on the CCD.

4.4. RESULTS AND DISCUSSION

4.4.1. CALCULATION RESULTS

The peak value of the electric field and the magnetic field of the focused circularly polarized femtosecond laser pulse are displayed in Fig.4.2. Here, all numerical calculations in this paper are performed under the conditions that $F = 4.5$mm, $NA = 0.65$, $f_w = 1$, $n_h = 1.33$, $\tau = 100fs$, and $\upsilon = 80$ MHz, according to the experiments.

The values of $|\mathbf{E}_{\text{peak}}|$ are plotted as a function of incident average power P_{ave} in Fig.4.3 (a). The calculation results of the nonlinear absorption coefficient κ are plotted as a function of the modulus of the peak electric field in Fig.4.3 (b). The decrease in κ with low excitation refers to the saturable absorption (SA). When the value of the maximum electric field reaches high excitation, the growth in κ indicates that the nonlinear effect turns into reverse saturable absorption (RSA), as shown in Fig.4.3 (b). The extinction cross-section σ_{ext} is calculated with the increasing input power. When the incident field

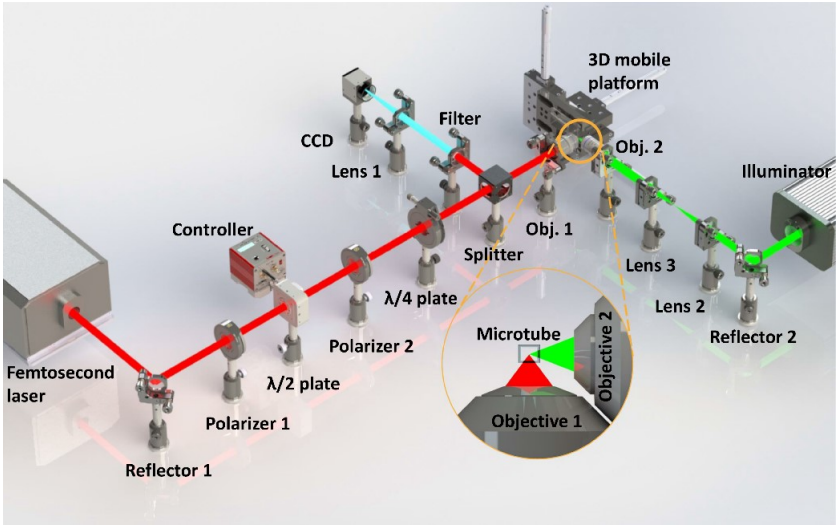

Figure 4.1: *The schematic diagram of the experimental setup. An x-polarized pulse laser propagates through a quarter wave plate to generate a circular polarization beam. The laser beam is focused by an objective with 0.65 NA. The sample solution consisting of 60 nm gold nanoparticles is filled in the glass micro-tube. An additional green beam is used to illuminate the sample. The experimental manipulation process is observed through the objective and imaged on the CCD.*

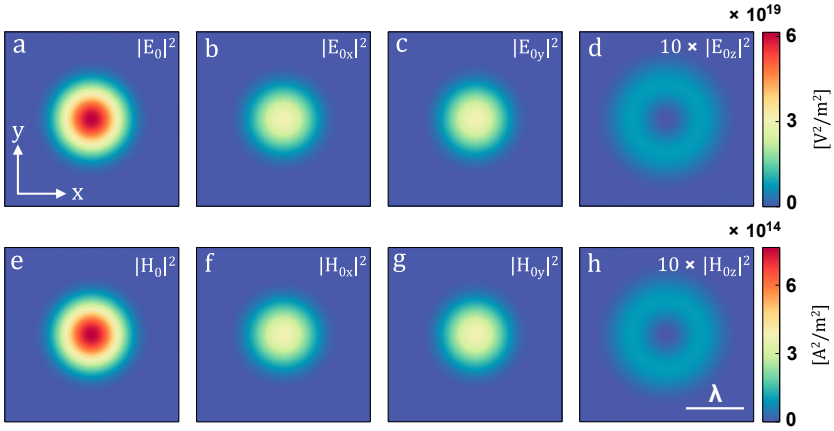

Figure 4.2: *Focal field distributions of a circularly-polarized femtosecond laser pulse with an averaged power Pave = 1.54 W (i.e., the maximal power used in the experiment). (a–d) The square of the modulus of the peak electric field in the focal plane (a) The square of the modulus of the total electric field (b-d) The x, y, and z components of the electric field. (e–h) The magnetic field in the focal plane.*

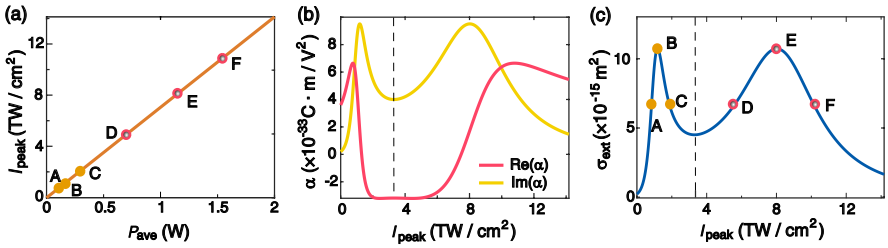

Figure 4.3: *(a) The amplitude of the peak electric fields of the focused field is plotted as a function of the average power P_{ave} increasing from 0 to 2.0W. (b) Nonlinear absorption coefficients are plotted as a function of the peak electric field. (c) The extinction cross-section σ_{ext} of gold nanoparticles varies with the increase of the peak electric field. The peak of σ_{ext} appears in the SA process (A, B, and C) and in the RSA process (D, E, and F), respectively.*

is zero, the extinction cross-sections are determined by the localized surface plasmon resonance (LSPR)[23]. As the incident optical intensity increases from low to high, the peak of the cross-section appears with a certain wavelength due to the nonlinear effects, as shown in Fig.4.3 (c). We investigate the processes of change of the optical force and potential well at three points (A, B, and C) in the SA process and at another three points (D, E, and F) in the RSA process below.

Fig.4.4 shows the optical forces and potential well during the SA process in the focal plane $(x, y, 0)$. The blue color indicates the direction and magnitude of the gradient force toward the center point. Note that the scattering forces are neglected because the magnitude of the scattering force is very small in the focal plane. Combined with the vectorial diffraction theory Eq.(4.2), the direction and distribution of the gradient force are calculated using Eq.(4.8).

Fig.4.4 (a) and (d) shows the distribution of the gradient force in the focal plane for the average power P_{ave}= 110 mW. The distribution of the optical force is circularly symmetry because of the circular polarization beam. The gradient force points to the center of the focal spot similar to that for the case without a nonlinear effect. Fig.4.4 (b) shows the corresponding optical force along the x-axis. The extinction cross-section σ_{ext} reaches a peak value at P_{ave} = 170 mW marked as point B in the SA process. At the B point, the magnitude of the gradient force is close to zero in a certain region, as shown in Fig.4.4 (b) and (e). The curve of the optical force becomes flat in a certain region when the extinction cross-section reaches a peak during the SA process. At C point in Fig.4.3, Fig.4.4 (c) shows a reversed gradient force, whose direction points away from the center point in a certain region for the average power P_{ave}= 300 mW. According to Fig.4.4 (f), the maximum of this opposing force is 0.45 pN and the length of the region of the opposing

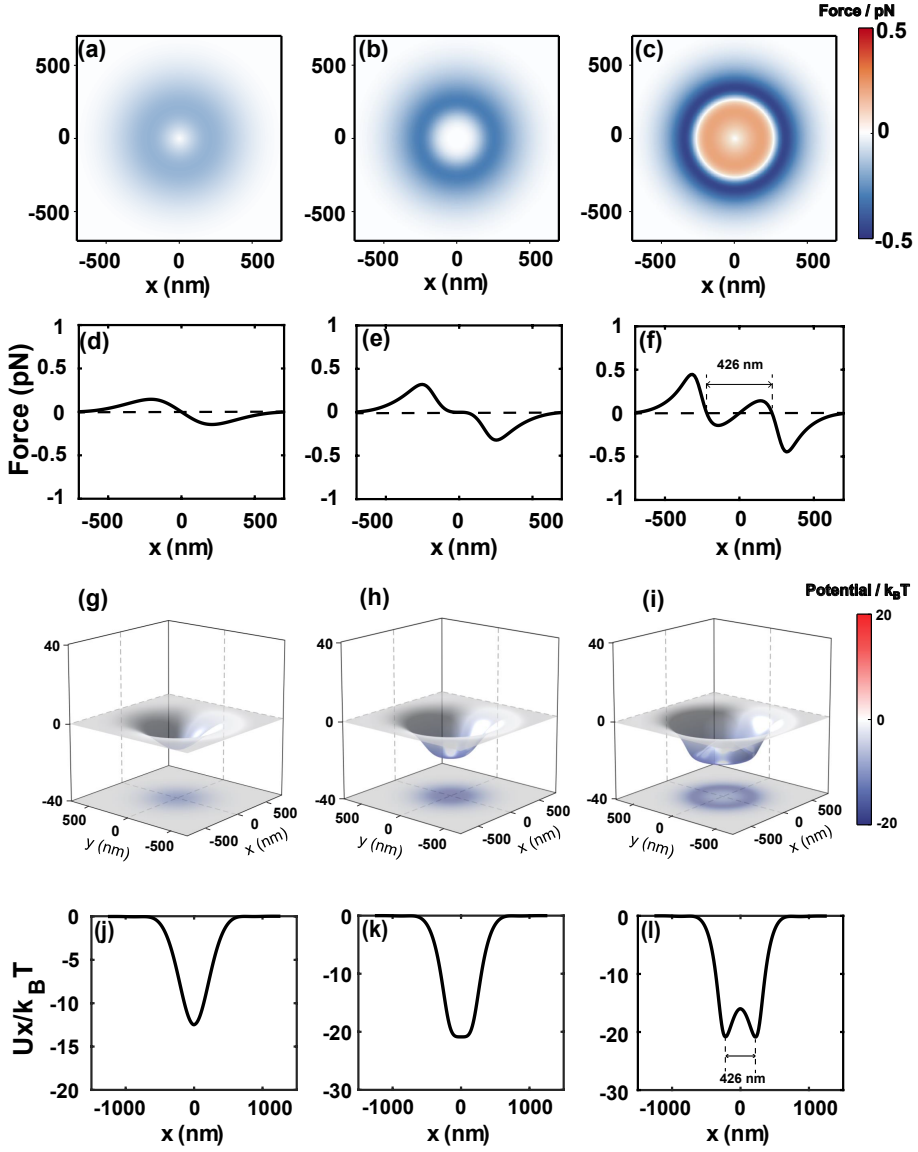

Figure 4.4: *The gradient force and potential well in the SA process. (a) The gradient forces in the focal plane are plotted for P_{ave} = 110mW. (d) The gradient force along the x-axis. (g) The potential well normalized to k_BT on the focal plane. (j) The potential well along the x-axis for P_{ave} = 110 mW. (b) and (c) The gradient forces in the focal plane are plotted for P_{ave} = 170 mW and 300 mW, respectively. The blue color indicates the direction towards the center of the focal plane and the red color indicates the force backwards the center point. (e) and (f) The corresponding optical forces along the x-axis (g) - (i) The corresponding potential wells in the focal plane for P_{ave} = 170mW and 300mW. (h) - (l) The distribution of potential well along the x-axis.*

force along the x-axis is 426 nm.

The trapping potential is normalized to $k_B T$, where k_B is the Boltzmann constant, and $T(T = 300\text{K})$ is the absolute temperature of the environment. The corresponding potentials for $P_{\text{ave}} = 110$ mW are calculated and shown in Fig.4.4 (g). The potential well has a conventional concave surface at the bottom part. The depth of the potential well is -13 $k_B T$, as shown in Fig.4.4 (g) and (j). The shape of the bottom part of the potential becomes flat in a certain region for $P_{\text{ave}} = 170$ mW, which indicates that the optical force starts to reverse with increasing input power, as can be seen in Fig.4.4 (h). The depth of the potential well is -20 $k_B T$ at 170 mW. In Fig. 4.4 (k), the shape of the bottom part of the potential well changes from a flat plane to a convex plane in a certain region. The minimal potential is -20 $k_B T$ and the potential on the top of the convex plane is -16 $k_B T$. The radius of the region is 426 nm in Cartesian coordinate, as shown in Fig. 4.4 (l). The region of the convex shape is in accordance with the region of the reversed gradient force. Therefore, the particle will be trapped in a ring shape between the conventional gradient force and the reversed force. This theoretical prediction of nonlinear optical trapping is in good agreement with the result of the reported experiment[9].

At D point in the RSA process, the incident average power P_{ave} is 0.7 W. The optical force and potential well are plotted in Fig.4.5 (a), (d), (j), and (h). The region of the reversed gradient force has a radius of 376 nm, as shown in Fig.4.5 (a) and (d). The potential in this region has an inverted shape of the well. The maximum potential is 12 $k_B T$ for $P_{\text{ave}} = 1.15$ W. The minimal value of the potential is -20 $k_B T$, which is the same as the minimal value at the B and C points in the SA process, as can be seen in Fig.4.4 (k) and (l). The particle can be trapped in the ring shape between the conventional gradient force region and the reversed gradient force region. At the peak point of the extinction cross-section in the RSA process, namely the E point, the average power P_{ave} is 1.15 W. The curve of the gradient force becomes flat and the magnitude of the gradient forces is close to zero near the focal point, as can be seen in Fig.4.5 (e) and (f). The region of the first reversed gradient force becomes larger with a radius of 430 nm. The maximum potential is 35 $k_B T$ for $P_{\text{ave}} = 1.15$ W. The top part of the potential well is flat, as shown in Fig. 4.5 (h) and (k). The average power P_{ave} is 1.54 W at the F point in the RSA process. The radius of the region of the first reversed gradient force is 465 nm which is larger than the radius in case E. The gradient forces reverse again from the focal point with the increasing of incident power, as shown in Fig. 4.5 (i) and (j). The top part of the potential well changes from a flat plane to a concave shape, which generates a conventional potential well in the center region. There are two possible regions for optical trapping of a particle according to Fig.4.5 (k) and (l). One is a ring shape of the potential well with

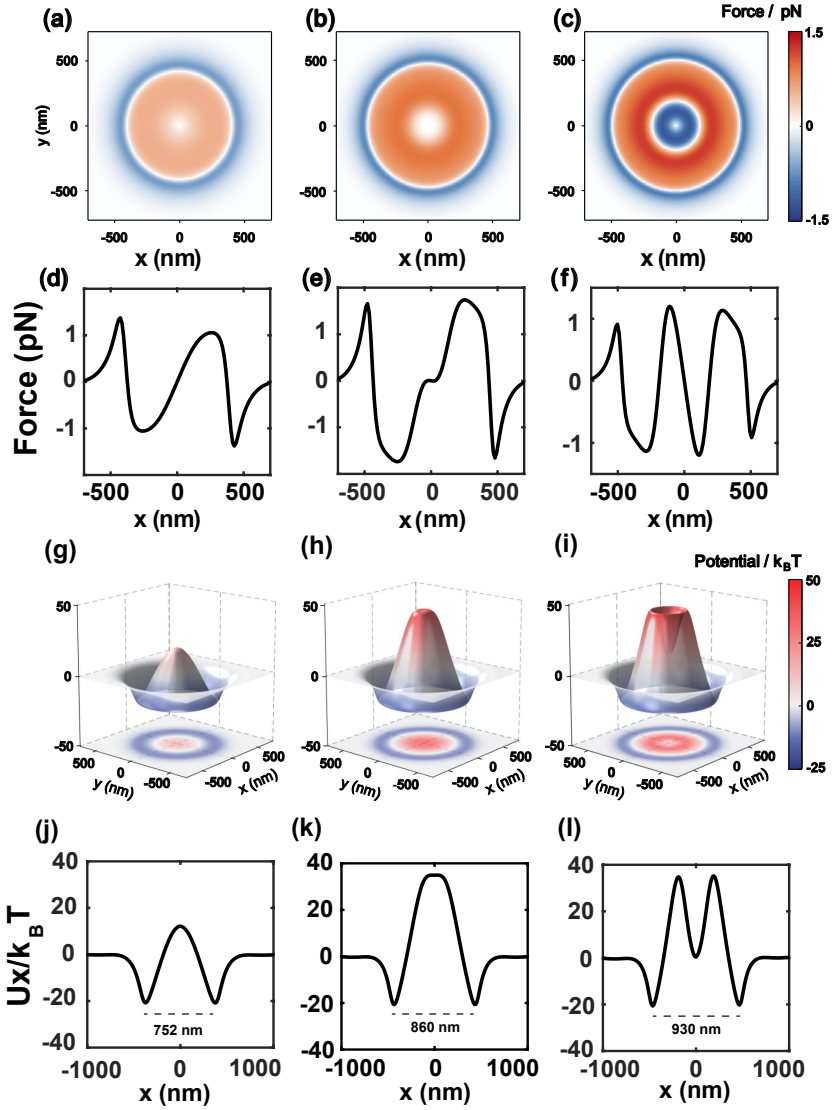

Figure 4.5: *The optical force and potential well in the RSA process. (a) Distribution of the gradient force on the focal plane at D point in the RSA process (d) A curve of the gradient force along the x-axis for P_{ave} = 0.7 W. (g) and (j) The optical potential well in the focal plane and its profile along the x-axis for P_{ave} = 0.7 W, respectively. (b), (e), (h), and (k) the gradient forces in the focal plane, the gradient forces along the x-axis, the optical potential well in the focal plane and its profile along the x-axis for P_{ave} = 1.15 W at the E point in the RSA process, respectively. (c) and (f) For P_{ave} = 1.54 W, the gradient forces and the corresponding potential on the focal plane, respectively. (i) and (l) the gradient forces and the corresponding potential along the x-axis, for an average power of 1.54 W, respectively.*

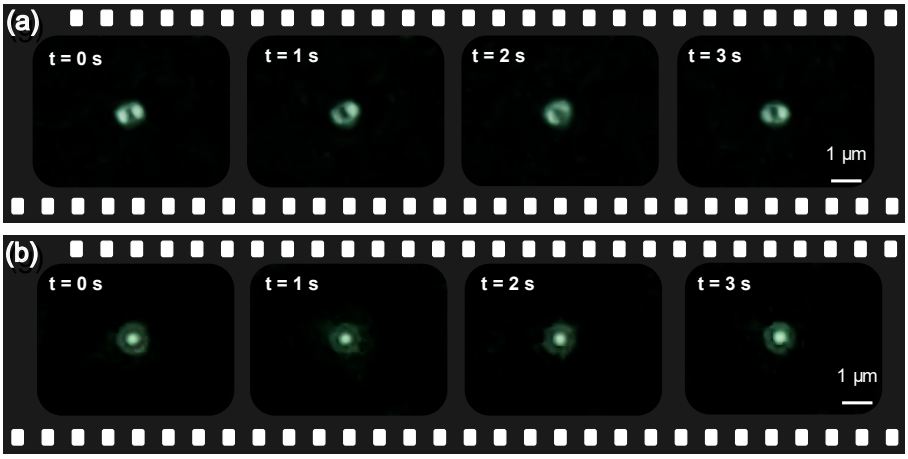

Figure 4.6: *(a) and (b) are experimental screenshots of gold nanoparticles trapped under incident powers of 1.15 W and 1.54 W, respectively. Because of the distinctive trapping potential formed within the deep RSA regime, a gold nanoparticle is constrained stably at the center while another performs an outer circumgyration.*

a radius of 460 nm has a depth of -20 $k_B T$. In this circumstance, the central potential barrier flattens out, and a maximum positive potential barrier of 34 $k_B T$.

4.4.2. EXPERIMENTAL RESULTS

Fig. 4.6 (a) and (b) present successive frames of the video of optical trapping (*see supplementary videos S3 and S4*). In the early RSA regime, the optical force and trapping potential well retained a similar circumgyrating motion to that for the SA regime at P_{ave} = 1.15 W, as shown in Fig. 4.6 (a). For the experiments at P_{ave} = 1.54 W, in addition to a circumgyrating nanoparticle, another particle is trapped at the center point inside the path of circumgyration. The bright flare at the center verifies the high stability of the central trapped nanoparticle, whereas the fall in brightness in the outer ring results from the particle being in a state of circumgyration of high speed. We conclude that circumgyration originally arising in the SA regime holds steady, and another trap is formed through the deep RSA effect.

Although our camera's sampling rate is lower at 30 fps compared to the 1500 fps used in the previous work Ref. [9], we have maintained consistent experimental conditions, for example, the NA of the objective lens, size of nanoparticles, central wavelength, and the repetition frequency of the trapping laser. The only different parameter is the pulse duration, which results in different input peak power. According to the measurements provided in Ref. [9], there is a strong correlation between the rotation speed and the in-

Table 4.2: Rotation speeds under different input powers.

	Ref.[9]			This work			
				point C	point D	point E	point F
P_{ave} (W)	0.35	0.5	0.65	0.3	0.7	1.15	1.54
P_{peak} $\times 10^5$(W)	6.25	8.93	11.6	3.75	8.76	14.38	18.76
Rotation speed (r/s)	220	235	250	200	230	260	290

put peak power. Therefore, by carefully comparing the peak power of the incident pulse in our work with that in the reported experiment, we can draw a reasonable conclusion for the rotation rate, as shown in Table.4.2.

According to the results in Ref. [9], the rotation speed is nearly a linear function with the incident laser. Thus, we can approximately estimate the rotation speed with an average power of 0.7 W, 1.15 W, and 1.54 W, which refer to the points D to F in our work, respectively. The estimated rotation speeds are shown in the right half part of Table. 4.2.

4.4.3. DISCUSSION

The optical force originates from the physical properties of the trapped objects and their interactions with the optical field. The consensus is that stable optical trapping is achieved through the balance of optical forces. The nonlinear response of the gold material excited in an ultra-high electric field, however, disturbs the established balance. Its transmittance increases as a consequence of SA and diminishes under RSA. With an incident femtosecond pulse of circularly polarized light, the optical forces exerted thereby on a gold nanoparticle reduce and reverse in the SA regime. The potential profile changes from concave to convex at the central position. Consequently, at relatively low intensities in the nonlinear optical tweezers, a ring-shaped potential well can be formed and nanoparticles can be driven to circumgyrate along the orbital energy flux.

As input power increases, nonlinear RSA comes into effect and the convex energy barrier strengthens gradually. When the incident intensity reaches a specific threshold value, the magnitude of the optical forces becomes smaller and another reversal in the direction of the optical forces appears at the center. From a potential energy perspective, a neo-subsidence appears at the original convex vertex within a larger excitation, indicating that an additional particle is trapped at the center, encircled by the original circumgyrating nanoparticle(s). Hereto, a completed nonlinear optical trapping mechanism is established in theory and demonstrated in experiments. Implementing nonlinear composite optical manipulation phenomena now becomes possible with the poten-

tial for an expansion in applications.

THE HEATING PROCESS UNDER THE ILLUMINATION OF FEMTOSECOND PULSES

Since we used a large laser fluence to stimulate the third-order nonlinear effect, it is needed to discuss the induced thermal problem in our experimental environment. We note that femtosecond-pulsed illumination can lead to a sharp and transient increase in the temperature of the nanoparticle. This effect can confine the heat to the close vicinity of the nanoparticle, preventing extended heating of the surrounding environment[24]. Compared to the absorption coefficient of the gold NP ($a_{\mathrm{Au}} = 8.2053 \times 10^5 \mathrm{cm}^{-1}$) [25], the absorption coefficient of water ($a_{\mathrm{water}} = 1.9639 \times 10^{-2} \mathrm{cm}^{-1}$)[26] is extremely small at the wavelength of 800 nm. The temperature increase is mainly caused by gold nanoparticle absorption. The absorption of laser pulse energy by a gold nanoparticle can be described as a three-step process [27, 28], each of these steps involving different time scales as follows:

1. electronic absorption: During the SA and RSA process, part of the incident laser pulse is absorbed by free electrons of the gold NP. The electronic gas thermalizes over a time scale $\tau_{e-e} \approx 220 fs$[27]. The temperature of the electron (T_e) is increased but the temperature of the phonon (T_{ph}) remains unchanged.
2. Electron-phonon thermalization: The hot electronic gas relaxes through an electron-phonon interaction ($\tau_{e-ph} \approx 1.7 ps$) [28]. The ion of the gold lattice is heated due to the electron–phonon interaction and this step is independent of the size of the nanoparticle. At this step, the nanoparticle is in internal equilibrium at a uniform temperature ($T_e = T_{ph}$) but is not in equilibrium with the initial ambient temperature.
3. External heat diffusion: The energy diffusion from the nanoparticle to the surrounding environment (water) usually occurs at a longer time scale and leads to a cooling of the nanoparticle and the heating of the surroundings. The time scale of this step depends on the size of the NP and ranges from 100 picoseconds to a few nanoseconds[29].

In the ideal case, the heat source (the gold nanosphere) can be modeled as a dipole, the heat power density can be calculated by a Dirac distribution:[30]

$$\rho_w c_w \partial_t T(d,t) = k_w \nabla^2 T(d,t) + \sigma_{abs} I_{ave} \delta(d)\delta(t)/f_{\mathrm{rep}}, \tag{4.10}$$

where ρ_w is the mass density of water, c_w is the specific heat capacity at constant pressure, and k_w is the thermal conductivity of the system at the time t and distance d from the dipole, σ_{abs} is the absorption cross-section of the nanoparticle, I_{ave} is time average optical intensity, and f_{rep} is the repetition rate of the pulsed laser. The ideal problem has an analytical solution with the thermal diffusivity of water a_w which can be

written as[31]

$$T(d,t) = \frac{\sigma_{abs} I_{ave}}{\rho_w c_w f} \frac{1}{(4\pi a_w t)^{3/2}} \exp(-\frac{d^2}{4\pi a_w t}). \tag{4.11}$$

Considering a realistic spherical nanoparticle (r = 30 nm), there is no analytical solution but the approximation can be done according to the above equation. The initial temperature can be obtained by calculating the time t for $\partial_t T(d,t) = 0$ at the original point ($d \approx 0$). Then the temperature increase of the gold nanoparticle reaches its maximum value at its center point which can be written as[30]

$$T_{NP\_max} = \frac{1}{3\sqrt{3}} \frac{\sigma_{abs} I_{ave}}{V \rho_{Au} c_{Au} f}, \tag{4.12}$$

where ρ_{Au} is the mass density of gold, c_{Au} is the specific heat capacity of gold at constant pressure, and V is the volume of the nanosphere. The time evolution of the temperature in the nanoparticle can be conveniently fitted using a stretched exponential function [30]

$$T_{NP}(t) = T_{NP\_max} \exp\left[-\left(\frac{a_w t}{\tau_0 r^2}\right)^n\right]. \tag{4.13}$$

Then we use this function to fit the evolution of the temperature, as plotted in Fig.4.7. The optimized fit parameters are $n = 0.39$ and $\tau_0 = 0.041$. Note that the pulse repetition f = 80MHz and pulse duration is 100 fs. The average power is 1.54 W. These parameters correspond to those configured at point F. The sampling time is 50 ns. The room temperature is 23 °C. Fig.4.7 illustrates the temperature gain and loss as a function of time under the pulsed illumination. The temperature of the nanoparticle rises instantaneously to the maximum value and then drops back to room temperature after a few hundred picoseconds.

Next, we then discuss the subsequent spatial evolution of the temperature in the surrounding environment. Firstly, the initial temperature $T(d,0)$ remains uniform inside the sphere ($0 < r \leq 30nm$) because the thermal conductivity of the gold k_{Au} is much higher than k_w. Then it generates a temperature envelope[30],

$$\text{Initial temperature:} \quad T(d,t) = T_{NP}(t), \qquad \text{for } 0 < \text{d} < r; \tag{4.14}$$

$$\text{Boundary conditions:} \quad k_w 4\pi r^2 \partial_r T(r,t) = V \rho_{Au} c_{Au} \frac{dT_{NP}(t)}{dt}, \qquad \text{for d = r;} \tag{4.15}$$

$$\text{Diffusion equation:} \quad \rho_w c_w \partial_t T(d,t) = k_w \frac{1}{d^2} \partial_r t[d^2 \partial_r T(d,t)], \qquad \text{for d < r.} \tag{4.16}$$

The Eq. 4.16 is the boundary condition at the interface from the energy conservation law. Similarly, when considering a finite-size nanoparticle, a stretched exponential function

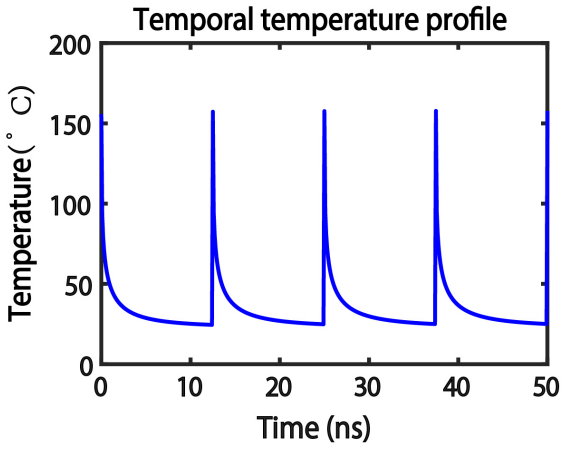

Figure 4.7: *The temporal temperature profile at the original point of the GNP. The repetition rate of a pulsed laser is 80 MHz. The total time scale is 50 ns.*

can also be used to fit the envelope of the spatial temperature profile in the surrounding water [31]:

$$T_{\text{spatial}}(d,t) = T_{NP}(t)\exp\left[-\left(\frac{d/r-1}{\rho_0}\right)^n\right]. \tag{4.17}$$

The fit parameters are n = 0.45 and ρ_0 = 0.06 [31]. The result is presented in Fig. 4.8 with the spatial temperature of the nanoparticle. For a large interface resistivity [32, 33], the heating of the surrounding fluid can be highly inefficient. The spatial temperature profile reveals that the temperature outside of the nanoparticle rapidly returns to room temperature over a short distance. Therefore, the temperature rising is completely ignorable in this work.

4.5. CONCLUSION

Using a circular polarization femtosecond beam, we performed intensive research on the evolution of nonlinear properties and responses of gold nanoparticles, as well as the nonlinear optical forces that accompany the process. Within the deep RSA regime, a composite trapping state, i.e., a state in which an additional static trap encircled by the original circumgyration appears at the very center, is demonstrated. The results from experiments match well with those from theory. The demonstration proves that the switching of trap states stems from a reversal of the optical forces, which is induced through the reversal in sign of the rate of change in the coefficient of nonlinear absorption. The results fill gaps in knowledge of the existing nonlinear optical tweezers and help in perfecting a relatively complete physical system. Our understanding of the mechanism under-

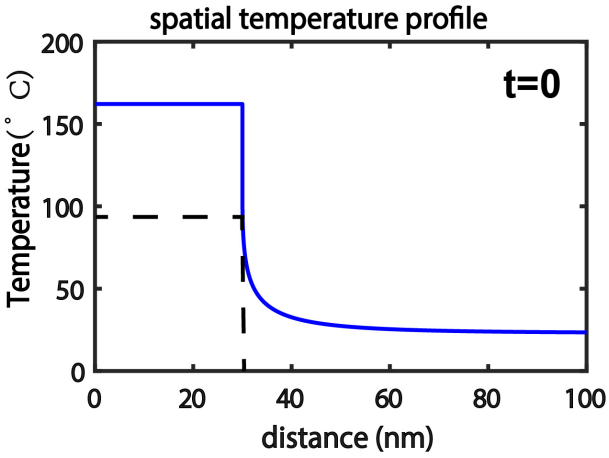

Figure 4.8: *The temperature envelope of the spatial evolution for the system consisting of a particle (r = 30 nm) in water.*

scoring nonlinear optical trapping is improved thus paving the way for a broader study of nonlinear metallic materials. Furthermore, the novel nonlinear optical trapping effect has the potential to synergize with diverse structured light beams and other nonlinear materials, including quantum dots and nonlinear nanocrystals. More novel trap phenomena binding with other nanotechnologies are expected to be discovered for the extension of the physical significance of nonlinear optical trapping, as well as conductive to further developments in practical applications.

REFERENCES

[1] A. Ashkin, J. M. Dziedzic, J. E. Bjorkholm, and S. Chu, *Observation of a single-beam gradient force optical trap for dielectric particles,* Optics Letters **11**, 288 (1986).

[2] K. C. Neuman and S. M. Block, *Optical trapping,* Review of scientific instruments **75**, 2787 (2004).

[3] Y. Gao, X. Zhang, Y. Li, H. Liu, Y. Wang, Q. Chang, W. Jiao, and Y. Song, *Saturable absorption and reverse saturable absorption in platinum nanoparticles,* Optics communications **251**, 429 (2005).

[4] H. I. Elim, J. Yang, J.-Y. Lee, J. Mi, and W. Ji, *Observation of saturable and reverse-saturable absorption at longitudinal surface plasmon resonance in gold nanorods,* Applied physics letters **88**, 083107 (2006).

[5] L. De Boni, E. L. Wood, C. Toro, and F. E. Hernandez, *Optical saturable absorption in gold nanoparticles,* Plasmonics **3**, 171 (2008).

[6] U. Gurudas, E. Brooks, D. M. Bubb, S. Heiroth, T. Lippert, and A. Wokaun, *Saturable and reverse saturable absorption in silver nanodots at 532 nm using picosecond laser pulses,* Journal of Applied Physics **104**, 073107 (2008).

[7] K. Wang, H. Long, M. Fu, G. Yang, and P. Lu, *Intensity-dependent reversal of nonlinearity sign in a gold nanoparticle array,* Optics Letters **35**, 1560 (2010).

[8] L. Novotny and B. Hecht, *Principles of nano-optics,* Cambridge University Press, (2007).

[9] Y. Qin, L.-M. Zhou, L. Huang, Y. Jin, H. Shi, S. Shi, H. Guo, L. Xiao, Y. Yang, C.-W. Qiu, *et al.*, *Nonlinearity-induced nanoparticle circumgyration at sub-diffraction scale,* Nature communications **12**, 1 (2021).

[10] K. Wang, H. Long, M. Fu, G. Yang, and P. Lu, *Size-related third-order optical nonlinearities of au nanoparticle arrays,* Optics express **18**, 13874 (2010).

[11] Y. H. Lee, Y. Yan, L. Polavarapu, and Q.-H. Xu, *Nonlinear optical switching behavior of au nanocubes and nano-octahedra investigated by femtosecond z-scan measurements,* Applied Physics Letters **95**, 023105 (2009).

[12] Y. Huang, X. Zhang, E. Ringe, M. Hou, L. Ma, and Z. Zhang, *Tunable lattice coupling of multipole plasmon modes and near-field enhancement in closely spaced gold nanorod arrays,* Scientific reports **6**, 1 (2016).

[13] T. Schumacher, K. Kratzer, D. Molnar, M. Hentschel, H. Giessen, and M. Lippitz, *Nanoantenna-enhanced ultrafast nonlinear spectroscopy of a single gold nanoparticle,* Nature communications **2**, 1 (2011).

[14] Y. H. Lee, Y. Yan, L. Polavarapu, and Q.-H. Xu, *Nonlinear optical switching behavior of au nanocubes and nano-octahedra investigated by femtosecond z-scan measurements,* Applied Physics Letters **95**, 023105 (2009).

[15] Y. Huang, X. Zhang, E. Ringe, M. Hou, L. Ma, and Z. Zhang, *Tunable lattice coupling of multipole plasmon modes and near-field enhancement in closely spaced gold nanorod arrays,* Scientific reports **6**, 23159 (2016).

[16] T. Cesca, P. Calvelli, G. Battaglin, P. Mazzoldi, and G. Mattei, *Local-field enhancement effect on the nonlinear optical response of gold-silver nanoplanets,* Optics Express **20**, 4537 (2012).

[17] R. Harrison and A. Ben-Yakar, *Role of near-field enhancement in plasmonic laser nanoablation using gold nanorods on a silicon substrate,* Optics Express **18**, 22556 (2010).

[18] D. Wu and X. Liu, *Optimization of silica–silver–gold layered nanoshell for large near-field enhancement,* Applied Physics Letters **96** (2010).

[19] R. Del Coso and J. Solis, *Relation between nonlinear refractive index and third-order susceptibility in absorbing media,* JOSA B **21**, 640 (2004).

[20] H.-J. Hagemann, W. Gudat, and C. Kunz, *Optical constants from the far infrared to the x-ray region: Mg, al, cu, ag, au, bi, c, and al 2 o 3,* JOSA **65**, 742 (1975).

[21] L. Gong, B. Gu, G. Rui, Y. Cui, Z. Zhu, and Q. Zhan, *Optical forces of focused femtosecond laser pulses on nonlinear optical rayleigh particles,* Photonics Research **6**, 138 (2018).

[22] A. Maheshwari and A. De, *Theoretical investigation on nonlinear optical effects in laser trapping of dielectric nanoparticles with ultrafast pulsed excitation,* Optics Express **24**, 21485 (2016).

[23] X. Fan, W. Zheng, and D. J. Singh, *Light scattering and surface plasmons on small spherical particles,* Light: Science & Applications **3**, e179 (2014).

[24] R. R. Anderson and J. A. Parrish, *Selective photothermolysis: precise microsurgery by selective absorption of pulsed radiation,* Science **220**, 524 (1983).

[25] K. M. McPeak, S. V. Jayanti, S. J. Kress, S. Meyer, S. Iotti, A. Rossinelli, and D. J. Norris, *Plasmonic films can easily be better: rules and recipes,* ACS photonics **2**, 326 (2015).

[26] M. Daimon and A. Masumura, *Measurement of the refractive index of distilled water from the near-infrared region to the ultraviolet region,* Applied optics **46**, 3811 (2007).

[27] H. I. Elim, J. Yang, J.-Y. Lee, J. Mi, and W. Ji, *Observation of saturable and reverse-saturable absorption at longitudinal surface plasmon resonance in gold nanorods,* Applied physics letters **88** (2006).

[28] W. Huang, W. Qian, M. A. El-Sayed, Y. Ding, and Z. L. Wang, *Effect of the lattice crystallinity on the electron- phonon relaxation rates in gold nanoparticles,* The Journal of Physical Chemistry C **111**, 10751 (2007).

[29] M. Hu and G. V. Hartland, *Heat dissipation for au particles in aqueous solution: relaxation time versus size,* The Journal of Physical Chemistry B **106**, 7029 (2002).

[30] G. Baffou and H. Rigneault, *Femtosecond-pulsed optical heating of gold nanoparticles,* Physical Review B **84**, 035415 (2011).

[31] G. Baffou and R. Quidant, *Thermo-plasmonics: using metallic nanostructures as nano-sources of heat,* Laser & Photonics Reviews **7**, 171 (2013).

[32] A. J. Schmidt, J. D. Alper, M. Chiesa, G. Chen, S. K. Das, and K. Hamad-Schifferli, *Probing the gold nanorod- ligand- solvent interface by plasmonic absorption and thermal decay,* (2008).

[33] Z. Ge, D. G. Cahill, and P. V. Braun, *Thermal conductance of hydrophilic and hydrophobic interfaces,* Physical review letters **96**, 186101 (2006).

5

CONCLUSIONS AND OUTLOOK

In the Introduction (Chapter 1) we introduce traditional optical trapping and its wide applications in physics and biology. Each step of exploiting optical trapping in the nonlinear regime is also introduced at the end of the chapter.

With regard to the time-averaged optical force exerted on the metallic nanoparticle in the Rayleigh regime, we conclude:(Chapters 2)

1. The deduction of the time-averaged optical forces equation and the dipole approximation theory for the Rayleigh nanoparticle. The vectorial diffraction theory for the focused optical field.

2. The simulation results of optical trapping are affected by the sample's size and the volume fraction. The stable optical trapping is affected

With regard to the nonlinear effect involved in the optical trapping, we conclude (Chapter 3):

3. The changes in the nonlinear optical properties of the gold nanoparticle under the stimulation of tightly-focused pulsed-laser.

4. The changes of the nonlinear gradient forces and optical potentials with the nonlinear effect. We also discussed the nonlinear scattering forces along the optic axis in the discussion. The experimental results coincided with the theoretical prediction.

Then regarding the mysteries behind the nonlinear optical trapping, we conclude (Chapter 4):

5. The stimulation of the saturable absorption effect via the circular polarization pulsed beam. The nonlinear polarizability and the nonlinear refractive index of the gold nanoparticle are also explored and calculated.

6. The derivation of the nonlinear optical force exerted on the gold nanoparticle in the

Reverse saturable absorption (RSA) regime. The changes in the optical potential well are also developed and demonstrated. The experimental results are also presented in the chapter. After combining the third-order nonlinear effects and the changes in nonlinear optical properties of the gold nanoparticles, we analytically present a quantitative analysis for the nonlinear optical trapping.

In this thesis, we present an updated and comprehensive theoretical framework for the optical trapping of metallic nanoparticles. This versatile method is applicable to both linear and nonlinear optical trapping scenarios, accommodating arbitrary polarization states. Our quantitative analysis of nonlinear optical trapping has wide-ranging applications and implications.

In the nonlinear regime, we unlock the potential for achieving sub-diffraction-limit control over the rotation of gold nanoparticles. This breakthrough allows for a detailed understanding of the underlying physics of light-matter interactions in these intricate systems. The newfound capability to manipulate nonlinear composite optical phenomena opens the door to diverse applications.

For instance, these advanced optical tweezers can serve as optically-driven sensors and microfluidic devices, offering unprecedented control over particle speed, rotation radius, and direction. Such capabilities have immense value in metrology and various other fields. This thesis marks a significant step forward in the study and application of optical trapping, particularly in the nonlinear regime, expanding the boundaries of what is achievable with this technology.

These nonlinear optical trapping effects and the creation of the analysis method open up exciting possibilities for synergizing with other nonlinear materials, such as quantum dots and nonlinear nanocrystals. Additionally, when combined with various structured light beams, these effects have the potential to yield even more remarkable trapping phenomena. We anticipate the discovery of novel trap behaviors and their integration with other nanotechnologies, extending the physical significance of nonlinear optical trapping and catalyzing further advancements in practical applications. This represents a promising frontier in the realm of optical manipulation and nanotechnology.

APPENDIX

.1. APPENDIX

$$A \times (\nabla \times B) = \nabla(A \cdot B) - (A \cdot \nabla)B. \tag{A1}$$

$$\nabla \times (A \times B) = -(A \cdot \nabla)B + A\nabla \cdot B + (B \cdot \nabla)A - B\nabla \cdot A. \tag{A2}$$

ACKNOWLEDGEMENT

To everyone who reads this, at first glance, it might seem like I did this all on my own. However, this dissertation, which I needed to obtain my doctorate, was definitely not a solo effort. Many individuals have supported me throughout this journey, and I wish to express my deep gratitude to them here.

First, I would like to thank my promoter at Delft University of Technology, Prof. H. Paul Urbach, and my co-promoter, Dr. Aurèle Adam. Paul, thank you for your guidance in tackling complex problems and for helping me develop strong academic standards. Your emphasis on rigorous mathematics has deeply impacted me and will continue to benefit me in the future. Aurèle, thank you for your extensive help in many aspects. You participated in all my research work, provided abundant assistance, always encouraged me, and responded promptly to my needs.

I also wish to extend my gratitude to my promoter, Prof. Xiaocong Yuan, and my other supervisors, Prof. Changjun Min and Prof. Yuquan Zhang at Shenzhen University. Prof. Yuan, you have been not just a promoter but also a sponsor. I deeply appreciate all your support. Your insightful views greatly helped me address my questions, particularly in resolving a longstanding issue that had troubled me for years. I would like to express my gratitude to Prof. Min and Prof. Zhang for their guidance and support. Your guidance has strengthened both my theoretical understanding and experimental skills. Your guidance has significantly enriched the quality of my work. This dissertation could not have been completed without your help.

I am also grateful to all the other members of the Optic research group: Yvonne, Lidija, Silvania, Omar, Gao, Joseph, Florian, Roland, Thim, Peter, and the late Jeff. It was always a pleasure to chat with you during coffee breaks. I would also like to thank my PhD fellows: Andreas, Boling, Daniel, Dmytro, Fellipe, HouZhe, Kefei, Lei, Luca, Matthias, Paolo, Peiwen, Poju, Posheng, Sander, Xiujie, Xukang, Yifeng, YingTang, and Yuxin. Thanks for all the enjoyable activities inside and outside the office.

I extend my thanks to the thesis committee for their careful consideration and evaluation of this thesis.

Lastly, I want to thank my family, who have always supported me, especially Anqi and Emma, who encouraged me and stood by me through the toughest moments. Your support and encouragement were crucial in the completion of this dissertation. Thank

you, everyone!

ZhengZhu

CURRICULUM VITÆ

ZHENG ZHU

27-04-1990 Born in Shandong, China.

EDUCATION

2008–2012 Undergraduate in Computer science
Nanchang University

2012–2015 Undergraduate in Optics engineer
Chinese Petrolum University

2016 PhD. Applied Physics
Technische Universiteit Delft
Thesis: Nonlinear optical trapping of metallic nanoparticles
Promotor: Prof. dr. H.P. Urbach & Prof. dr. Xiaocong. Yuan

AWARDS

2015 National scholarship of Master student

2015 Outstanding graduates

LIST OF PUBLICATIONS

Refereed Publications

6. **Z. Zhu**, Y. Zhang, C. Min,A.J.L Adam, H.P. Urbach, and X. Yuan *An improved method to calculate propagation of light field into multi-layer structure*, (In preparation).

5. **Z. Zhu**, Y. Zhang,C. Min, A.J.L Adam, H.P. Urbach, and X. Yuan *Relocation of field enhancement in the nanostructure via nonlinear plasmonics*, (In preparation).

4. Y. Zhang, **Z. Zhu**, S. Zhang, W. Zhang, Z. Man, A.J.L Adam, C. Min, H.P. Urbach, A.V. Zayats, and X. Yuan *Bistable nonlinear optical tweezers*, (In preparation).

3. **Z. Zhu**, Y. Zhang, A.J.L Adam, C. Min, H.P. Urbach, and X. Yuan *A vectorial model for the nonlinear gradient force exerted on metallic Rayleigh nanoparticles*, Chinese Optics Letter, Vol. 22, Issue 2, (2024).

2. **Z. Zhu**, Y. Zhang, S. Zhang, A.J.L Adam, C. Min, H.P. Urbach, and X. Yuan *Nonlinear optical trapping effect with reverse saturable absorption*, Advanced Photonics **5(4)**, pp.046006-046006 (2023).

1. **Z. Zhu**, Y. Zhang, A.J.L Adam, C. Min, H.P. Urbach, and X. Yuan *Theoretical investigation on the effect of volume fraction in the optical trapping of gold nanoparticles*, Optics Communications **541**, p.129572 (2023).

Conference Proceedings

2. Y. Zhang, **Z. Zhu** W. Zhang, C. Min, H.P. Urbach, and X. Yuan *Nonlinear effects in femtosecond optical tweezers*, Proc. SPIE **11558**, Quantum and Nonlinear Optics VII, 1155806 (10 October 2020).

1. **Z. Zhu**, A.J.L Adam, Y. Zhang, C. Min, H.P. Urbach, and X. Yuan *A New Method to Calculate the Propagation of an Arbitrary Plane Wave into a Multi-layer Structure*, Photonics Electromagnetics Research Symposium Fall (2019).